UNIVERSITY OF SOUTHAMPTON

FACULTY OF PHYSICAL AND APPLIED SCIENCES

School of Physics and Astronomy

Southampton High Energy Physics Group

Holographic Descriptions of Chiral Phase Transitions

by

Maria Magou

Presented for the degree of

Doctor of Philosophy

November 2012

UNIVERSITY OF SOUTHAMPTON

ABSTRACT

FACULTY OF PHYSICAL AND APPLIED SCIENCES

SCHOOL OF PHYSICS AND ASTRONOMY

SOUTHAMPTON HIGH ENERGY PHYSICS GROUP

DOCTOR OF PHILOSOPHY

HOLOGRAPHIC DESCRIPTIONS OF CHIRAL PHASE TRANSITIONS

by Maria Magou

Quantum Chromodynamics (QCD) poses a challenge in calculating physical phenomena in low energy scales due to its strongly coupled character. The tools available for understanding this region of QCD are limited. One such tool is gauge/gravity duality which promises to attack strongly coupled related phenomena, at least in a qualitative level, by using the conjectured equivalence between string theory and some classes of quantum field theories (gauge/gravity duality). In this thesis strongly coupled 3+1d and 2+1d field theories are explored by using D3/D7 and D3/D5 brane systems respectively. These theories exhibit some QCD-like characteristics like chiral symmetry breaking and confinement. The main focus of the following chapters is understanding chiral phase transitions in those theories and constructing their phase diagrams in finite temperature and chemical potential. Chiral symmetry breaking is induced in these holographic brane setups by turning on a background magnetic field or by choosing an appropriate running dilaton profile. The phase diagrams for each field theory considered are mapped, giving a rich structure of first, second and BKT holographic transitions. Some successful attempts where made to reproduce the standard QCD phase diagram, in the running dilaton scenario. Also, in the running dilaton case wrapped D5 branes where used to introduce holographic baryons. The baryonic phase, for some range of the parameter space, participates in the phase diagram and it is found in the regime expected from QCD. Finally, chiral phase transitions with energy scale where explored as well as their holographic effective potentials for various D3/D7 and D3/D5 systems.

Contents

List of Figures

List of Tables

Declaration of Authorship

I, Maria Magou, declare that this thesis, entitled "Holographic descriptions of chiral phase transitions" and the work presented in it are my own. I confirm that

- This work was done wholly or mainly while in candidature for a research degree at this university.
- Where any part of this thesis has previously been submitted for a degree or any other qualification at this university or any other institution, this has been clearly stated.
- Where I have consulted the published work of others, this is always clearly attributed.
- Where I have quoted the work of others, the source is always given. With the exception of such quotations, this thesis is entirely my own work.
- I have acknowledged all main sources of help.
- Where the thesis is based on work done by myself jointly with others, I have made clear exactly what was done by others and what I have contributed myself.
- Work contained in this thesis has previously been published as stated in the following list:
  - Chapter 4 : In collaboration with N.Evans, A.Gebauer and K.Y.Kim published as *"Holographic Description of the Phase Diagram of a Chiral Symmetry Breaking Gauge Theory, " JHEP* ***03*** *(2010) 132* [arXiV:1002.1885 [hep-th]]

– Chapter 5 : In collaboration with N.Evans, A.Gebauer and K.Y.Kim published as *"Phase diagram of the D3/D5 system in a magnetic field and a BKT transition , "* ***Phys.Lett. B 698*** *(2011) 91-95* [arXiV:1003.2694 [hep-th]]

– Chapter 6 : In collaboration with N.Evans, A.Gebauer and K.Y.Kim published as *"Towards a Holographic Model of the QCD Phase Diagram , "* ***J. Phys. G : Nucl. Part. Phys. 39*** *(2012) 054005* [arXiV:1109.2633 [hep-th]]

– Chapter 7 : In collaboration with N.Evans, K.Y.Kim, Y. Seo and S.J. Sin published as *"The Baryonic Phase in Holographic Descriptions of the QCD Phase Diagram , "* ***JHEP 09*** *(2012) 045* [arXiV:1204.5640 [hep-th]]

– Chapter 8 : In collaboration with N.Evans and K.Y.Kim published as *"Holographic Wilsonian Renormalization and Chiral Phase Transitions , "* ***Phys. Rev. D 84*** *(2011) 126016* [arXiV:1107.5318 [hep-th]]

No claims for originality are made for the material in chapters 2 and 3 which were compiled from a variety of sources. Also chapters 4,5,6 were reviewed in the thesis "Chiral Symmetry Breaking Transitions in Holographic Duals" by Astrid Gebauer.

Signed:

Date:

Acknowledgements

I would like to thank my supervisor Nick Evans for the help and guidance he provided during these four years. I would also like to thank my collaborators Astrid Gebauer, Keun-Young Kim, Yunseok Seo and Sang-Jin Sin for good collaboration and discussions. I would especially like to thank Keun-Young Kim for all the help he so kindly offered during this time.

I am also grateful to all the members of the Theory Group for creating a friendly atmosphere and especially my fellow students Maria Dimou, Iain Cooper, David Jones and Raul Alvares. I am also thankful to the University of Southampton for the finacial support, without which I wouldn't have been able to complete this thesis.

I would like to thank my fiancee Lambros for his moral support, encouragement and love. I owe the most to my parents for their love and support to all my decisions in life.

To my family

Chapter 1

Overview

Quantum chromodynamics (QCD) is the current most successful theory describing the strong nuclear interactions in nature. Although it is a part of the standard model of particle physics, the strongly coupled regime of the theory remains until today a challenging problem. That regime of QCD involves the physics related to the bound states of the theory, the hadrons e.g proton.

From the methods available at the moment, lattice QCD is probably the most successful tool available for dealing with strong coupling. Numerical methods are employed to probe physics related to the strong coupling phenomena like chiral symmetry breaking, confinement e.t.c. Although lattice is very successful in some respects, it fails to explore dynamical quantities and also physics at finite chemical potential. Other models are available as well but none of them provides an analytic and systematic method for dealing with the physics of the strong coupling.

Gauge/gravity duality is an alternative tool, which gives access to the strongly coupled regime of quantum field theory. It has been widely used the last fourteen years and it is based on the conjecture that ten dimensional string theory living on some manifold is an equivalent way of formulating some classes of quantum field theories. This conjecture (or duality) implies that field theory knowledge can be used to understand more about string theory and vice versa. One version of the duality states that strongly coupled field theories are dual to the low energy effective description of string theory, supergravity. Supergravity is a tractable

theory, unlike string theory, and supergravity calculations are possible in contrast to its dual strongly coupled field theory. This is the exact feature of the duality we intend to apply in this thesis. Using the knowledge we have of supergravity, we will try and gain some lessons on strongly coupled field theories, with a particular interest in their phase structure.

In principle to describe QCD the knowledge of its dual description is necessary. The dual of QCD is not known, mainly because QCD is weakly coupled in large energies and full string theory is required to describe this weakly coupled sector. Nevertheless, many useful lessons can be derived from studying other strongly coupled field theories. The reason for that is that strongly coupled field theories generally share some common features which can be universal in all those theories, or at least in some classes of them. Although, the results gained from holography are only qualitative, it does provide a way of studying phenomena that cannot be accessed differently.

In this thesis, examples of strongly coupled field theories are considered which exhibit some QCD-like characteristics like quark fields in the fundamental representation, confinement and chiral symmetry breaking. D3/D7 and D3/D5 brane systems are used in order to study chiral symmetry breaking in non abelian gauge theories. These systems allow a geometric interpretation of the chiral condensate, which is the order parameter for the chiral transition, and of confinement.

In order to follow this thesis, a short introduction regarding QCD is given in 2, focusing only on the concepts which are necessary to understand this thesis. In chapter 3, basic string theory and D branes are introduced which will lead into the introduction of gauge/gravity duality with a specific interest in the introduction of flavour in the duality.

In chapters 4-7 the phase structure of various strongly coupled field theories are considered. All these chapters are based on D3/D7 and D3/D5 systems, which correspond to 3+1d and 2+1d field theories with fields in the fundamental representation (quarks). The main focus of these chapters is chiral symmetry

breaking with temperature and chemical potential. In chapters 4-5 chiral symmetry breaking is induced by the introduction of a magnetic field in the theory, which provides the chiral symmetry breaking scale. The work done in chapters 4,5 is based on top down approaches.

In chapters 6-7 the chiral symmetry breaking is accomplished by using a phenomenologically chosen running dilaton profile, which is equivalent to the running of the gauge coupling in the field theory. This dilaton profile is introduced by hand and therefore in these two chapters a bottom up logic is combined with the top down approach of the D3/D7 and D3/D5 systems. Specifically, in chapter 6 various phase diagrams are calculated which capture many aspects of the QCD phase diagram and hint on their dependence on the running coupling. In chapter 7 the existence of holographic baryons is explored, as well as the existence of a baryonic phase transition in the phase diagram. Furthermore, confinement in the geometry used in chapters 6 and 7 is studied, with the help of holographic Wilson loops, in order to investigate a possible connection between the baryon phase and confinement.

In chapter 8 chiral transitions are explored for varying Wilsonian cut-offs. Chiral transitions in different setups are considered and low energy effective potentials are produced. The setups used are in the spirit of chapters 4 and 5. Finally, in chapter 9 conclusions are given.

Chapter 2

A short introduction to QCD

A very short introduction to QCD is given in this chapter, presenting only concepts that are necessary for understanding the following chapters.

2.1 QCD and colour

Quantum Chromodynamics (QCD) [1–4] is the current most successful theory describing the strong nuclear interactions in nature. The fundamental degrees of freedom in this theory are the quarks and gluons. The underlying gauge group of the theory is $SU(3)_c$ (colour group) [7, 8] and the Lagrangian describing the theory is

$$L_{QCD} = \sum_{f=u,d,..} \overline{q}_f (i\gamma^\mu D_\mu - m_f) q_f - \frac{1}{4} G^a_{\mu\nu} G^a_{\mu\nu}. \tag{2.1}$$

There are six different flavours of quarks labeled by the index $f = u, d, c, s, t, b$ and the m_f is the current quark mass for quark with flavour f. The q_f are the quarks fields, which are Dirac fermions (Dirac index is omitted) transforming under the fundamental representation of the $SU(3)_c$ gauge group [1]. The covariant derivative D^μ and the field strength tensor $G^a_{\mu\nu}$ are given by

$$\begin{aligned} D_\mu &= \partial_\mu - ig\frac{\lambda^a}{2} A^a_\mu \,, \\ G^\alpha_{\mu\nu} &= \partial_\mu A^a_\nu - \partial_\nu A^a_\mu + g f^{abc} A^b_\mu A^c_\nu \,, \end{aligned}$$

[1] Quarks come in three colours, red, green and blue.

where A^a_μ are the gauge fields (gluons) transforming in the adjoint representation of $SU(3)_c$ and λ^a are the Gell-Mann matrices, which obey the following commutation relations

$$[\frac{\lambda^a}{2}, \frac{\lambda^b}{2}] = if^{abc}\frac{\lambda^c}{2}.$$

The colour index a takes the values $a = 1, \cdots, 8$.

2.2 Beta function of QCD

Quantum field theory, when radiative corrections are considered, suffers from divergences e.g in the couplings or masses of the particles. In order to remove these infinities and to derive meaningful quantities, renormalisation techiniques are applied which require the introduction of a renormalisation scale μ. A very important quantity that arises from this procedure is the renormalised coupling constant g, whose dependence on μ is expressed by the beta function

$$\beta(g) = \frac{\partial g(\mu)}{\partial \log \mu}. \tag{2.2}$$

The beta function for the case of a non abelian $SU(N_c)$ gauge theory with N_c number of colours and n_f number of active flavours of quarks [2] in the fundamental representation is given by the following expression (at one-loop level)

$$\beta(g) = -\frac{g^3}{(4\pi)^2}(\frac{11}{3}N_c - \frac{2}{3}n_f). \tag{2.3}$$

In the case of QCD $N_c = 3$. If the beta function is solved in terms of the coupling constant, the expression becomes

$$g^2(\mu) = \frac{g^2(M)}{1 + \frac{g^2(M)}{(4\pi)^2}(\frac{11}{3}N_c - \frac{2}{3}n_f)\log(\frac{\mu^2}{M^2})} \tag{2.4}$$

[2]The number n_f of active flavours depends on the scale μ we are considering. Only the quarks with masses smaller than the scale μ affect the beta function.

and it can be rewritten in a way so that it depends on only one parameter

$$g^2(\mu) = \frac{(4\pi)^2}{(\frac{11}{3}N_c - \frac{2}{3}n_f)\log(\frac{\mu^2}{\Lambda^2_{QCD}})}. \tag{2.5}$$

At large energies μ the coupling tends to zero, which means that the quarks tend to behave as free particles in this regime. This phenomenon is called asymptotic freedom [1, 2] and is characteristic of all non abelian gauge theories with $n_f < \frac{11}{2}N_c$, at least in four dimensions. On the other hand, for small values of μ the coupling becomes very large and results in the colour confinement of quarks, where quarks form bound states. Λ_{QCD} is the scale at which the coupling diverges to infinity and its value is estimated to $\Lambda_{QCD} \sim 200$ MeV. Note that the size of the hadrons is of the order Λ^{-1}_{QCD} [15, 16].

Because QCD becomes asymptotically free at large energies, perturbation theory is a valid method for performing calculations in this regime. At small energies though the coupling becomes very large and perturbation theory can not be applied. Different tools are required for exploring the physics of the strong coupling. One such tool is introduced and applied in this thesis and it is called gauge/gravity duality. It is used to understand various strongly coupled field theories.

2.3 Wilsonian Approach

Before proceeding any further with QCD, let us introduce a different approach to renormalisation theory. As already mentioned, divergences appear in quantum field theories in some quantities like the masses and couplings. These divergence are a result of high energy momentum modes in the loop corrections. Apart from the infinities in those specific quantities, the high momentum modes do not really affect other computations in the theory and that is because generally the fields at different energy scales are independent degrees of freedom. A very geometrical and intuitive picture is the one given by Wilson [5], who instead of using the usual renormalisation techniques for removing the divergences in the theory, he described the physics at different energies through scale dependent quantities.

In the path integral formulation of quantum field theory, the degrees of freedom of the theory are variables of integration. In the following expression, the integration variables are the Fourier components of the fields $\phi(k)$

$$Z[J] = \int \mathcal{D}\phi e^{\int i[\mathcal{L}+J\phi]} = \prod_{k\leq\Lambda} \int \mathrm{d}\phi(k) e^{\int i[\mathcal{L}+J\phi]}, \tag{2.6}$$

where $\mathcal{L}$ is the bare Lagrangian, J is the source and Λ is the momentum scale at which the bare Lagrangian is define at. If we focus on phenomena which are related to some specific momentum scale $\Lambda^{'}$, where $\Lambda^{'} \leq \Lambda$, then, taking into account the fact that phenomena in different energy scales are decoupled, a new Lagrangian can be define which is valid for $k \leq \Lambda^{'}$. The new Lagrangian will result from the bare Lagrangian plus some correction which arise when all the modes with momentum $\Lambda^{'} \leq k \leq \Lambda$, in the path integral, are integrated out. This Lagrangian is called the effective Lagrangian and is defined (Euclidean signature) as

$$\begin{aligned} Z[J] &= \prod_{k\leq\Lambda^{'}} \int \mathrm{d}\phi(k) e^{-\int \mathrm{d}^4x\ \mathcal{L}_{eff}} \\ &= \prod_{k\leq\Lambda^{'}} \int \mathrm{d}\phi(k) e^{-\int \mathrm{d}^4x\ (\mathcal{L}+\text{sum of connected diagrams})}. \end{aligned} \tag{2.7}$$

The extra terms added to the Lagrangian compensate for the integration of modes with $\Lambda^{'} \leq k \leq \Lambda$. There are an infinite number of effective Lagrangians, for all the different $\Lambda^{'}$'s and they all form the renormalisation group flow [15].

2.4 QCD and global symmetries

In section 2.1 the QCD Lagrangian was introduced as well as the $SU(3)_c$ gauge symmetry. The global symmetries of the Lagrangian play an important role as well, especially at low energies, where the dynamics are determined by the symmetries of the QCD vacuum.

A sensible starting point for studying the low energy regime of QCD and its symmetries is to only consider the three lighter flavours of quarks, (u, d, s) and also to assume that those quarks are massless (chiral limit). This approximation is valid

because (u, d, s) are considerably lighter than c, t, b quarks and furthermore their masses are much smaller than 1GeV, the scale at which the lightest hadrons (which are not Goldstone bosons) are formed. For convenience (2.1) can be rewritten in terms of its chiral components[3], so that the symmetries that we wish to study become manifest. The chiral Lagrangian in the chiral limit is given by

$$L_{QCD} = \sum_{l=u,d,c} \overline{q}_{L,l}(i\gamma_\mu D^\mu)q_{L,l} + \overline{q}_{R,l}(i\gamma_\mu D^\mu)q_{R,l} - \frac{1}{4}G^a_{\mu\nu}G^a_{\mu\nu}. \tag{2.8}$$

By simple inspection, the Lagrangian[4] (2.8) has a global $SU(3)_L \times SU(3)_R$ flavour symmetry since the left and right handed components can be independently $SU(3)$ "rotated". The $SU(3)_L$ transformation is the following

$$q_L \to q'_L = \exp\left[-i\sum_{\alpha=1}^{8}\theta^L_\alpha \frac{\lambda_\alpha}{2}\right] q_L,$$

where θ^L_α are parameters of the $SU(3)$ group. The same applies for the right handed fields, for different parameters θ^R_α. By investigating further the symmetries of the lagrangian, it can be verified that the right and left handed fields can be rotated by the same phase

$$q_L \to q'_L = e^{-i\phi}q_L, \qquad q_R \to q'_R = e^{-i\phi}q_R, \tag{2.9}$$

without altering the lagrangian. This is the baryon $U(1)_B$ symmetry. Also, the lagrangian remains unchanged when the left handed fields are rotated by a phase and the right handed are rotated by minus the same phase

$$q_L \to q'_L = e^{-ia}q_L, \qquad q_R \to q'_R = e^{ia}q_R. \tag{2.10}$$

This symmetry is the axial $U(1)_A$ symmetry of the Lagrangian

To summarise, the QCD Lagrangian, at a classical level, is characterised by a global $SU(3)_L \times SU(3)_R \times U(1)_B \times U(1)_A$ symmetry. In the field theory level, only the

[3]The Dirac fields can be rewritten in terms of their chiral components. One way to do that is to use the right and left hand projection operators $P_L = 1 - \gamma_5$, $P_R = 1 + \gamma_5$, which when applied on the Dirac fields return back their chiral components $q_{L,l} = P_L q_l$.

[4]Notice that the covariant derivative is independent of flavour.

$SU(3)_L \times SU(3)_R \times U(1)_B$ is a symmetry of the theory. The $U(1)_A$ singlet vector axial current is not conserved and the symmetry is called anomalous[5].

In nature the quarks are not really massless and therefore mass terms should be added to (2.1)

$$L_{QCDm} = \sum_{l=u,d,s} \left(m_l \overline{q}_{L,l} q_{R,l} + m_l \overline{q}_{R,l} q_{L,l} \right). \tag{2.11}$$

These mass terms mix the right with the left handed fields and therefore explicitly break $SU(3)_L \times SU(3)_R$ symmetry. The $U(1)_B$ symmetry is not affected by the presence of mass terms and therefore is always conserved. If it is assumed that the masses m_l are not only finite but equal as well, then the symmetry of the Lagrangian is enhanced to $SU(3)_V \times U(1)_B$[6]. In the case where the masses are equal and small the chiral symmetry can be considered an approximate symmetry of the Lagrangian.

Of course, the assumption that the three lightest quarks have equal masses is not very good. A better approximation is to assume that the up and down quarks have equal masses and the strange quark has an infinite mass, which is more realistic. Then the chiral symmetry would be $SU(2)_L \times SU(2)_R$.

2.5 Spontaneous chiral symmetry breaking in QCD

One of the most celebrated examples of spontaneous symmetry breaking is the Higgs mechanism [9–11] that gives rise to the mass of the particles in the standard model of particle physics. In QCD, a different mechanism spontaneously breaks chiral symmetry which results in a dynamical generation of mass for the quarks. This dynamical generation of mass explains the large mass of the proton, when compared to the sum of the current masses of the two up and one down quarks that form the proton.

There are different possible ways to break a symmetry. One way is to explicitly

[5] In the large N_c (number of colours) limit the symmetry is restored. The axial vector current divergence is proportional to $g^2 \sim \frac{1}{N_c}$ and therefore in the large N_c limit it becomes zero [14].

[6] The $SU(3)_V$ is the group that $SU(3)$ "rotates" both right and left handed fields by the same angle, $\theta_\alpha^L = \theta_\alpha^R = \theta_\alpha^V$.

break it by adding a term in the lagrangian that doesn't respect its symmetries e.g mass term in QCD Lagrangian. A symmetry can also be broken spontaneously which means that although the Lagrangian describing the system is invariant under some symmetry, the ground state of the system does not respect that symmetry. That symmetry is said to be spontaneously broken [12, 13].

The implications of having a symmetry spontaneously broken are described by the the Nambu-Goldstone theorem which states that when a continuous global symmetry is spontaneously broken a number of massless scalar particles (Nambu-Goldstone bosons) arise. This number is equal to the number of the broken symmetry generators. Note that the massless scalars share the same quantum numbers with the broken generators. Usually the Lagrangians used to motivate spontaneous symmetry breaking have a potential that exhibits a degeneracy of the ground state. When exactly one possible ground state is chosen then the symmetry is spontaneously broken. In the case of QCD the spontaneous chiral symmetry breaking can not be seen from the Lagrangian but it is a result of the formation of a chiral condensate that fills the vacuum of QCD.

Why is it believed that chiral symmetry is spontaneously broken in QCD? If it is assumed that $SU(3)_L \times SU(3)_R$ is a symmetry of QCD, then this should be reflected in the hadron spectrum. The experimental expectations should be the that hadrons organise themselves into two degenerate octets, one for each $SU(3)$ group, with opposite parities. Experiment reveals that this is not the case. A vector hadron octet is present and therefore it seems that only the $SU(3)_V$ symmetry is present in the QCD vacuum [6]. Furthermore, a second pseudoscalar meson octet is present which is much lighter than the hadron vector octet. These observations can only be explained if the chiral symmetry is spontaneously broken in the QCD vacuum and therefore $SU(3)_L \times SU(3)_R$ is spontaneously broken to $SU(3)_V$. The eight light pseudoscalars observed are the Goldstone bosons due to the hidden $SU(3)_A$ symmetry. Although Goldstone bosons are expected to be massless, the observed Goldstone bosons have small mass due to the fact that chiral symmetry is explicitly broken in nature by the mass of the quarks. Therefore, chiral symmetry is only an approximate symmetry and that is why the Goldstone bosons are massive.

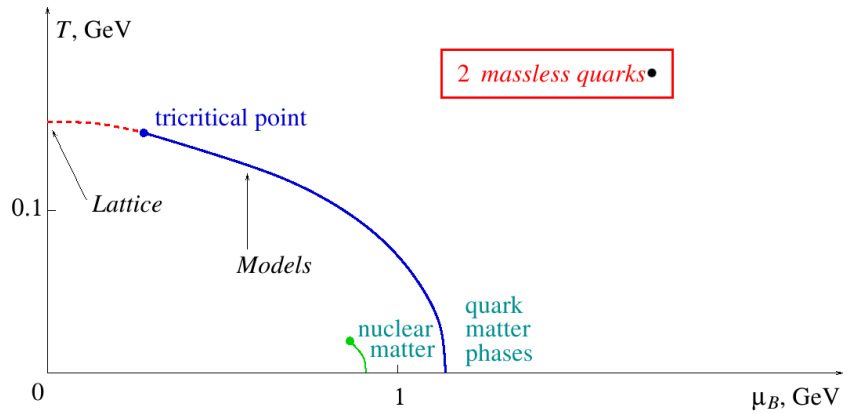

Figure 2.1: This is the standard picture of the QCD phase diagram for two massless flavours. The dashed line corresponds to a second order transition and the continuous lines to first order transitions.

The spontaneous chiral symmetry breaking is a result of the formation of a scalar chiral condensate in the QCD vacuum. Specifically, the chiral condensate $q\bar{q}$, which is not invariant under chiral transformations, has a non vanishing vacuum expectation value

$$< q\bar{q} > = < \bar{q}_R q_L + \bar{q}_L q_R > \neq 0, \tag{2.12}$$

but it is invariant under $SU(3)_V$. Therefore, in QCD the chiral symmetry is spontaneously broken to an $SU(3)_V$. The chiral condensate fills the vacuum of QCD and results in a dynamically generated mass for the quarks (constituent mass).

2.6 Phase Diagram of QCD

In the following chapters a detailed study of the phase diagrams of various strongly coupled field theories, which share some common features with QCD, is considered. Through this exploration of the various QCD-like theories we hope that we will gain some knowledge about the possible phase diagram of QCD. Here we attempt to summarise the current knowledge on the QCD phase diagram.

The phase diagram of QCD can be mapped as a function of temperature and finite chemical potential. Not many things are known about the phase diagram of QCD but a combination of various models, lattice QCD and heavy ion collision experiments suggest that the phase diagram could be like the one shown in figure

2.1. The exact structure of the phase diagram depends on various parameters, mainly the number of the quarks considered and their masses.

Nature lives in the vacuum of QCD where hadrons and pions are the excitations of the vacuum (confinement). Chiral symmetry is broken by the chiral condensate, as explained in section 2.5. For zero chemical potential and small temperature QCD is described by hadrons. As the temperature is increased a phase transition occurs and the system moves to a phase where the fundamental degrees of freedom are quarks and gluons (deconfinement) and where chiral symmetry is restored. The nature of the transition is speculated to be second order, when two massless flavours of quarks are considered, and the order parameter is the chiral condensate. If the fact that the quarks in nature are massive is taken into account then the second order chiral transition turns into a crossover[7], as a result of the explicit chiral symmetry breaking. The same chiral transition happens for zero temperature and finite chemical potential with the transition being first order. The first and second order transitions should meet at some point of the phase diagram which is called the tricritical point (or critical in the case of massive quarks). Furthermore, lattice QCD calculations indicate that chiral transition and deconfinement transition overlap.

A different phase transition happens in zero temperature and for some finite chemical potential. As the chemical potential is increasing the vacuum of QCD becomes populated with quarks. When the chemical potential reaches a specific value (μ), baryon density is created in a non continuous way and a first order nuclear matter transition occurs. The phase transition separates a phase in which baryons are present but in a delute state to a phase where baryons are condensed. This first order phase transition extends to the finite but small temperature region and ends at a critical point ($T = T_c \sim 10MeV$).

Finally let us note that there are more phases in QCD, like the flavour superconducting and flavour locking phases, which are not considered here. More details regarding the QCD phase diagrams can be found in various review

[7]Lattice simulations suggest that the crossover happens at $T_c \sim 140 - 190MeV$ [22–25].

papers [17–21]

Chapter 3

Introduction to String Theory and Gauge/Gravity Duality

3.1 String Theory and D-branes

3.1.1 Introduction to string theory

Quantum field theory is built on the idea that the various particles in nature can be modeled by mathematical point-like particles. String theory, on the other hand, extends this idea further by considering a one dimensional object, a string, as the fundamental object of the theory. What we experience as particles in nature are just the result of oscillations of these strings.

If strings are the fundamental objects describing string theory, a more extensive study of these objects is required. Let us start with a string embedded in a curved d-dimensional target spacetime $(x^0, ..., x^{d-1})$, described by a metric $g_{\mu\nu}$. The string worldsheet, the area that the string sweeps out as it moves in time, can be parametrised by two coordinates (τ, σ), where τ is a time coordinate and σ is a space coordinate. In order to study the kinematics of the string, as moving in the target spacetime, an action should be defined whose variational principle should

minimise the area of the string worldsheet[1]. The action is given by

$$S[x] = -T \int dA = -T \int d\tau d\sigma \sqrt{-\det(h_{ab})}, \tag{3.1}$$

where dA is the infinitesimal area element of the worldsheet, h_{ab} is the induced metric which describes the "pullback" of the background metric on the string worldsheet and is defined as

$$h_{ab} = g_{\mu\nu} \partial_a x^\mu(\tau, \sigma) \partial_b x^\nu(\tau, \sigma). \tag{3.2}$$

The functions $x^\mu(\tau, \sigma)$ describe the embedding of the string in the target spacetime and T is the string tension. The string tension has dimension of mass per unit length and is related to the string length l_s and the Regge slope parameter α' through

$$T = \frac{1}{2\pi\alpha'} = \frac{1}{2\pi l_s^2}. \tag{3.3}$$

The action (3.1) is called the Nambu-Goto action and it describes the relativistic string. The presence of the square root in the action makes its quantisation difficult. Polyakov suggested, as a solution to the square root problem, an alternative action that is equivalent to (3.1), at a classical level, and is given by

$$S[x] = -\frac{T}{2} \int d\tau d\sigma \sqrt{-\det(\gamma_{ab})} g_{\mu\nu} \gamma^{ab} \partial_a x^\mu \partial_b x^\nu. \tag{3.4}$$

The Polyakov action introduces a new auxiliary field, the symmetric tensor γ^{ab}, which has a physical interpretation as the worldsheet metric. It is natural that (3.4) should be supplemented with some constraints, if is to be equivalent to (3.1), coming from the equation of motion of the auxiliary tensor γ^{ab}. These constraints are $T_{ab} = 0$[2] and reflect the presence of two local symmetries of the worldsheet action, the reparametrisation invariance and the Weyl invariance

$$\text{Reparametrisation :} \qquad (\tau, \sigma) \to (\tau(\tau', \sigma'), \sigma(\tau', \sigma')), \tag{3.5}$$

$$\text{Weyl invariance :} \qquad \gamma_{ab} \to e^{2\rho(\tau,\sigma)} \gamma_{ab}, \tag{3.6}$$

[1] Greek letters $\mu, \nu, \cdots$ will be used for labeling target spacetime and Latin letters $a, b, \cdots$ will be used for labeling worldsheet coordinates.

[2] T_{ab} is the energy momentum-tensor of the $1+1$ dimensional worldsheet field theory.

where $\rho(\tau, \sigma)$ is an arbitrary function. The existence of these symmetries allow us to completely gauge fix the action in the case of a string. Convenient choices of gauge can simplify the problem e.g conformal gauge.

The next natural step to be taken, is finding the equation of motion of the string by varying the Polyakov action with respect to $x^\mu(\tau, \sigma)$. The variation of the action generates some boundary terms which can only be eliminated by imposing appropriate boundary conditions to the string endpoints. The boundary condition choice is not unique and can result in two type of strings, open and closed strings. One possible choice is

$$x^\mu(\tau, 0) = x^\mu(\tau, \pi) \quad \text{and} \quad \frac{dx^\mu}{d\sigma}(\tau, 0) = \frac{dx^\mu}{d\sigma}(\tau, \pi), \tag{3.7}$$

which describes periodic boundary conditions and it corresponds to a closed string[3]. Alternative choices of boundary conditions (b.c.), which still satisfy $\delta S = 0$, can be either

$$\frac{dx^\mu}{d\sigma}(\tau, \sigma)\bigg|_{\sigma=0,\pi} = 0 \quad \text{(Neumann b.c.)} \tag{3.8}$$

or

$$\frac{dx^\mu}{d\tau}(\tau, \sigma)\bigg|_{\sigma=0,\pi} = 0 \quad \text{(Dirichlet b.c.).} \tag{3.9}$$

The boundary conditions (3.8), (3.9) apply for the open string case. If a string obeys Neumann boundary conditions for all μ, then Poincare invariance is preserved. If at least one of the d directions of the string obeys Dirichlet boundary conditions, then the string endpoints do not oscillate in these directions and therefore the string endpoints are fixed. Note that Dirichlet boundary conditions break Poincare invariance. Finally, the solution to the equation of motion of $x^\mu(\tau, \sigma)$ can be found for both open and closed strings. These solutions include terms describing the center of mass position of the string x_0^μ, momentum of the string p_0^μ and oscillation of the string[4].

[3] We have assumed that the closed and open string space coordinate σ can acquire values in the interval $0 \leq \sigma \leq \pi$.

[4] The oscillation of the string is described by a sum of the different oscillation modes which are described by the coefficients $\alpha_\nu^\mu, \tilde{\alpha}_\nu^\mu$, where ν is an integer giving the oscillation mode and μ is the

Sector	**Boson/Fermion**	**Massless fields**
NS-NS	Boson	$g_{\mu\nu}, B_{\mu\nu}$,Φ
NS-R	Fermion	Ψ_{μ},λ
R-NS	Fermion	Ψ'_{μ},λ'
R-R	Boson	Ramond Ramond fields

Table 3.1: Closed string spectrum in IIB superstring theory [29]

Sector	**Boson/Fermion**	**Massless fields**
NS	Boson	$A_{\mu}(x)$
R	Fermion	Spinor

Table 3.2: Open string spectrum in superstring theory

The picture of the string given until now is purely classical. If we wish to describe a quantum field theory on the worldsheet, then the classical theory should be quantised. The bosonic string can be quantised by following the standard canonical quantisation techniques [5]. The outcome of this analysis reveals two very important features of the bosonic string. Firstly, the bosonic string requires the presence of at least twenty six dimensions and secondly the string spectrum, for closed and open strings, contains tachyonic modes. If string theory is going to be of any physical interest, it should be free from instabilities (tachyons). Furthermore, nature has many fermionic particles which somehow need to be included in string theory.

A solution to the bosonic string problems is given by superstring theory. It proves that when supersymmetry is introduced in the theory, fermions are included and instabilities are cured. The critical number of dimensions required for the theory to be free from anomalies is reduced to ten. This new theory is called superstring theory[6].

Superstring theory is a very extensive subject so we have chosen to restrict our discussion here to a brief presentation of the ten dimensional IIB superstring massless ($\alpha^{'} \to 0$) spectrum (see tables 3.1, 3.2) which is relevant to the following sections. The NS-NS sector of the closed string spectrum contains: the symmetric tensor $g_{\mu\nu}$ which describes the background metric, $B_{\mu\nu}$ which is an antisymmetric Kalb-Ramond tensor and Φ which is a scalar field called the dilaton and which is

spacetime index.

[5] In canonical quantisation $x_0^{\mu}, p_0^{\mu}, \alpha_{\nu}^{\mu}, \tilde{\alpha}_{\nu}^{\mu}$ should be promoted to operators.

[6] There are 5 different superstring theories but for our purposes we limit our interest to the type IIB superstring theory.

related to the string coupling through $e^{\Phi} = g_s$. The R-R sector contains three n-form fields $C^{(n)}$, specifically $C^{(0)}, C^{(2)}, C^{(4)}$. The fermionic sector (R-NS,NS-R) consists of Ψ_μ and $\Psi_\mu^{'}$, which are spin $\frac{3}{2}$ gravitino fields, λ and λ' which are spin $\frac{1}{2}$ dilatino fields. The open string spectrum contains a ten dimensional gauge field $A_\mu(x)$ in the NS sector and a Spin(8) spinor in the R sector. For more details regarding superstring theory see [26–29]

3.1.2 T duality

The T duality is a very unique symmetry, characteristic of bosonic string theory with no quantum field theory counterpart. If bosonic closed string theory has at least one compact dimension then some new quantum numbers arise, Kaluza Klein number K and sometimes the winding number W. If the Kaluza Klein number is interchanged with the winding number and simultaneously the radius of the compact dimensions R is interchanged with a new radius $R^{'} = \frac{\alpha^{'}}{R}$, then the theory remains unchanged. This symmetry is called T duality. This duality is of great interest, as we are going to discover in this section, because it postulates the existence of new objects in string theories, the D branes.

In more detail, imagine a closed string living in a nine dimensional flat Minkowski spacetime described by x^μ $(\mu = 0, 1, \cdots, 8)$ with the tenth dimension x^9 compactified on a circle of radius R. Naturally x^9 should be periodic, obeying $x^9 \sim x^9 + 2\pi R$. Since the points $x^9 = 0$ and $x^9 = 2\pi R$ should be identical, the translation operator acting on the x^9 direction should be single-valued at these two points and therefore $e^{-ip_9 x^9} = e^{-ip_9(x^9+2\pi R)}$ should hold, leading to the conclusion

$$p^9 = \frac{K}{R} \quad \text{and} \quad K \in \mathbb{Z}, \tag{3.10}$$

where K is called Kaluza-Klein excitation number. Relation (3.10) implies that momentum on the compact direction is quantised, as expected from quantum mechanics. In addition, the string has the possibility of being wrapped W times around the spacetime circle, something that a point particle can not do. That

implies

$$x^9(\tau, \sigma + \pi) = x^9(\tau, \sigma) + 2\pi W R \quad \text{and} \quad W \in \mathbb{Z}, \tag{3.11}$$

where W is called winding number.

Now let us have a look on how the compactification of the x^9 affects the mass spectrum of the string as seen by an nine dimensional point of view. The mass is expressed by the relation

$$m^2 = \frac{K^2}{R^2} + \frac{W^2 R^2}{\alpha'^2} + ... \tag{3.12}$$

The first term is proportional to K and is a result of compactification and the second term is proportional to W and is a strictly stringy effect, only a string can wind around a compact dimension. The ellipsis represents the usual mass terms arising from the oscillation of the string for $K = W = 0$.

If we take a closer look at (3.12), it is not difficult to notice that when the following interchanges

$$K \longleftrightarrow W \qquad \text{and} \qquad R \longleftrightarrow R' = \frac{\alpha'}{R} \tag{3.13}$$

happen simultaneously, then (3.12) remains invariant. Therefore, (3.13) is a symmetry of the closed string spectrum, called T-duality. In the limit where $R \to 0$, the K modes become infinitely heavy and decouple from the theory. The W modes for $K = 0$ form a continuum tower of modes. This picture contradicts the expectations from quantum field theory, where no continuum tower of modes is present. Although $R \to 0$ implies a "disappearing" dimension, the result reveals that the x^9 dimension is recovered.

What happens in the case of open string? Open strings can not wind around compact dimensions and therefore W is meaningless and also Kaluza-Klein excitation number K is a result of compactification and it should be present. The open string picture resembles that of $R \to 0$ from the quantum field theory point of view. Therefore, when $K \neq 0$ the modes are infinitely heavy and decouple but in the case of $K = 0$ no new continuum tower of states is revealed, therefore x^9 dimension is not recovered. When T-duality is applied to the open string, which obeys Neumann boundary condition in the compact string theory direction, the T-dual

picture is an open string obeying Dirichlet boundary condition in the compact x^9 direction and Neumann in the rest of the dimensions. The T dual picture should be interpreted as a string having its endpoints fixed in the x^9 direction but which is free to move in the other directions. Therefore, the T dual string have its endpoints confined in a hypersurface. Generally, T duality can be applied to a larger number m of compact dimensions. The T dual picture necessitates the presence of hypersurfaces of dimension $d+1-m$, called D branes [29].

Finally, in the T-dual picture the open string endpoints attached to the D brane obey the following relation

$$x^{9'}(\tau,\pi) - x^{9'}(\tau,0) = \frac{2\pi\alpha' K}{R} = 2\pi K R', \tag{3.14}$$

where the $x^{9'}$ indicates the T-dual x^9 direction. If we take a closer look at (3.14), we can conclude that under T-duality the Kaluza-Klein number K, of the initial string theory, becomes a kind of winding mode number for the dual open string. Furthermore, the T-dual theory is compactified on a circle with radius $R' = \frac{\alpha'}{R}$. Finally, T-duality is a symmetry for the open string, as well.

From all the above we can conclude that T-duality is a symmetry of bosonic string theory. Let us note that T duality applies to superstring theories as well but with the extra feature that the T dual theory of IIB superstring is IIA superstring and vice versa[7]. T duality is of great importance because it gives rise to some new objects in superstring theories, the D branes. These new objects are going to be explored in more detail in the following section.

3.1.3 D branes

Dp branes are $p+1$ dimensional hypersurfaces arising from T duality and on which open strings can end. They are fundamental objects in superstring theories and their existence opened the way to new applications of string theory, like AdS/CFT correspondence. The objective of this section is to define the physics of the Dp

[7]This is true when an odd number of dimensions are T-dualised. When T duality is applied for an even number of dimensions then IIB theory returns a IIB theory and the same applies for IIA.

branes through a definition of their worldvolume action and also to understand how D branes can give rise to non-abelian gauge theories.

D branes are dynamical objects in superstring theory that can fluctuate both in shape and position. This is obvious if we keep in mind that open strings are attached to D branes and therefore control both its shape and position. These open strings respond to the various background fields and therefore the D branes should respond to the background fields as well [28]. From this it should be clear that background fields define the dynamics of the D brane worldvolume and therefore the most general action describing the branes should depend on them.

Furthermore, the action describing the D branes should depend on the fields living in its worldvolume, which are scalars and gauge fields. These fields arise from the open string spectrum which contains a massless[8] ten dimensional gauge field. Because the open string endpoints are attached to the branes, the gauge field decomposes to components parallel and perpendicular to the D brane. As a result the ten dimensional gauge field give rise to an U(1) gauge field A_a $(a = 0, \cdots, p)$ and $9 - p$ scalars describing the fluctuation of the brane in the perpendicular direction to its worldvolume [29].

As a first attempt to describe the D brane worldvolume action let us consider only the scalar fields. The most obvious way to proceed, is to perform a geometrical extension of the Nambu-Goto action in the case of a D brane. A reasonable extension is

$$S \sim \int d^{p+1}\xi \sqrt{-\det\left(P\left[G_{ab}\right]\right)}, \tag{3.15}$$

where $P[G_{ab}]$ is the pullback of the background metric which is defined as

$$G_{ab} = g_{\mu\nu} \frac{\partial x^\mu}{\partial \xi^a} \frac{\partial x^\nu}{\partial \xi^b}. \tag{3.16}$$

Action (3.15) when varied minimises the D brane worldvolume. Of course (3.15) is not the end of the story. As already discussed, a gauge field lives on the brane as

[8] We only care about the massless modes of the strings because we will only consider the low energy limit of the D brane action. All the massive modes in the string spectrum decouple in this limit.

well. Also, background fields interact with the brane. Our purpose is to define a low energy effective action, where only the massless fields of the closed and open string spectrum contribute. This action should respect all of the symmetries of the D brane worldvolume and gauge invariance. The most general form of the action in the static gauge is[9]

$$S_{DBI} = -T_p \int d^{p+1}\xi e^{-\Phi} \sqrt{-\det(P[G_{ab} + B_{ab}] + 2\pi a' F_{ab})} \tag{3.17}$$

and is called the Dirac-Born-Infeld (DBI) action, where $P[B_{ab}]$ is the pullback of the background antisymmetric Kalb-Ramond tensor on the brane and F_{ab} is the field strength tensor of the gauge fields living on the brane and Φ is the dilaton field. T_p is D brane tension, which expresses how much the brane responds to changes and it has dimension of mass per worldvolume. The brane tension is defined as

$$T_p = \frac{1}{g_s (2\pi)^p (\alpha')^{\frac{p+1}{2}}}. \tag{3.18}$$

The Dirac-Born-Infeld action has accounted for the NS-NS massless closed string sector only. The closed string spectrum contains a R-R sector as well which is made of n-form gauge fields $C^{(n)}$, as explained in string theory section, which couple to the brane. In the same manner that a pointlike particle carries a charge which acts as a sources to the one-form gauge field, Dp branes carry a charge which act as a source to the $C^{(p+1)}$ fields living in the background. In type IIB superstring theory the R-R sector consists of n-form gauge fields $C^{(n)}$, where $n = 0, 2, 4$, that can couple electrically or magnetically to stable Dp branes with $p = -1, 1, 3, 5, 7$[10]. In type IIA, n takes the values $n = 1, 3$ and therefore stable branes are those with $p = 0, 2, 4, 6, 8$[11] [26]. The contribution of the R-R sector to the dynamics of the D

[9] The D brane worldvolume is characterised by reparametrisation invariance. It is possible to use this symmetry to choose a convenient gauge that simplifies our calculations. If x^μ, $\mu = 0, \cdots, 9$ are the target spacetime coordinates and ξ^a, $a = 0, \cdots, p$ are the D brane worldvolume coordinates then the static gauge corresponds to $x^\mu = \xi^a$ for $\mu = a = 0, \cdots, p$.

[10] A $C^{(n)}$ field can couple electrically to $D_{(n-1)}$ and magnetically to $D_{(7-n)}$ branes.

[11] Generally, it is possible to have branes with odd values of p in IIA and even values of p in IIB superstring theory, but in that case the branes do not carry conserved charge and therefore are unstable. Those branes are called non-BPS states.

brane worldvolume is expressed by the Chern-Simon action

$$S_{CS} = -T_p \int d^{p+1}\xi \ \left[C \ e^{B_{ab}+(2\pi\alpha^{'})F_{ab}} \right]_{p+1}, \tag{3.19}$$

where C is the sum of the $C^{(n)}$ fields that couple magnetically or electrically to the brane considered. The Chern-Simon action plays a crucial role in chapter 7, where holographic baryons are defined.

The final low energy effective action is given by the sum $S_{DBI} + S_{CS}$. This is a purely bosonic action[12]. Furthermore, the action defined here applies to the abelian case only. For the non-abelian action see [28].

Now let us move towards a different direction and discuss, a perhaps surprising but at the same time very powerful feature of D branes, the appearance of a non-abelian $U(N_c)$ gauge theory from a group of N_c coincident D branes. Let us start from the beginning. In the presence of a single brane, open strings can start and end on the same brane. In this case, there is nothing that can stop the strings from shrinking to zero length and give rise to massless $U(1)$ gauge fields. If a second parallel brane is added, separated by a distance r from the first one, then there are some additional choices from where the open strings can start and end[13]. Apart from the possibility of having an open string starting and ending on the same brane, strings can start from the first brane and end on the second one and vice versa. To distinguish the different gauge fields arising, new indices are assigned to each string endpoint which are called Chan-Paton factors. The value of the index is defined by the brane on which the string endpoint is attached to. Therefore the gauge fields, coming from the open string spectrum, could be written as $(A_\mu)_{ij}$ ($i, j = 1, 2$), where the i index indicates the brane at which the string starts from and j the brane it ends. An open string stretching between different branes are always massive (the mass is given by $m = Tr$) and therefore an $U(1) \times U(1)$ gauge theory arises from these two branes. If we bring the two branes on top of each other, then all four gauge fields become massless. As a result the gauge symmetry is

[12]There is a contribution to the DBI action from the fermionic fields as well but since is not considered in the next chapters we will not write it down explicitly. For more details see [41].

[13]Open strings in IIB Superstring are oriented strings, meaning that the endpoints of the string are distinguished.

enhanced to a $U(2)$ gauge group. If we extend this to the case of N_c coincident D branes then a $U(N_c)$ gauge theory arises. Notice that the degrees of freedom available, N_c^2 gauge fields, indicate that the gauge fields transform in the adjoint representation of the gauge group. The fact that from a group of two coincident D branes give rise to a $U(2)$ gauge theory which can be broken to a $U(1) \times U(1)$ symmetry when the branes are separated, is an example of a Higgs mechanism in string theory. The same applies for a larger number of branes.

3.2 Large N_c gauge theories

For many years a relation between gauge theories and string theory was speculated. That is not very surprising since string theory itself was invented as a candidate theory of strong interaction. A possible description of a gauge theory through some other equivalent (dual) theory, in this case the dual theory is string theory, could be of great importance. It is well known that not many tools are available for tackling strong coupling physics, as perturbation theory fails in this regime and only numerical methods provide an alternative tool. It is hoped that a possible duality can open the way for exploring the strong coupling regime of any quantum field theory. This section is based on [32, 37].

The first strong evidence connecting gauge theories and string theories was provided by t'Hooft [31]. He studied the case of an $SU(N_c)$ gauge theory and suggested that the number of colours N_c can provide an expansion parameter that allows a perturbative expansion in $\frac{1}{N_c}$, in the large N_c limit. This large N_c limit should be taken with care so that it does not affect the Λ_{QCD} scale of the theory. For this reason a new parameter $\lambda = g_{YM}^2 N_c$ (t'Hooft coupling) is defined that is kept fixed.

In more detail, let us assume that there is a general theory with fields Φ_i^α in the adjoint of $SU(N_c)$, where α is the adjoint index and i is some label for the field. We can write down a schematic Lagrangian of the form

$$\mathcal{L} \sim \mathrm{Tr}[d\Phi_i d\Phi_i] + g_{YM}\, c^{ijk}\, \mathrm{Tr}[\Phi_i \Phi_j \Phi_k] + g_{YM}^2\, d^{ijkl}\, \mathrm{Tr}[\Phi_i \Phi_j \Phi_k \Phi_l],$$

where g_{YM} is the coupling constant of the theory. If the fields are redefined as $\Phi_i^{'} = g_{YM}\Phi_i$ the new Lagrangian takes the form

$$\mathcal{L}^{'} \sim \frac{1}{g_{YM}^2}\left(\mathrm{Tr}[d\Phi_i^{'}d\Phi_i^{'}] + c^{ijk}\,\mathrm{Tr}[\Phi_i^{'}\Phi_j^{'}\Phi_k^{'}] + d^{ijkl}\,\mathrm{Tr}[\Phi_i^{'}\Phi_j^{'}\Phi_k^{'}\Phi_l^{'}]\right). \tag{3.20}$$

This rescaling has brought an overall factor $\frac{1}{g_{YM}^2}$ in front of all the terms of $\mathcal{L}^{'}$, which factor can be written in terms of the t'Hooft coupling λ as $\frac{1}{g_{YM}^2} = \frac{N_c}{\lambda}$. If we wish to derive the Feynman rules of the theory from the Lagrangian (3.20), it is convenient to draw the Feynman diagrams in double line notation. To make the double line notation possible the fields in the adjoint representation should be written as Φ_i^j, where the i, j are now the fundamental and antifundamental representation indices respectively. In this notation the Feynman diagrams are arranged by their topology, each Feynman diagram corresponds to a compact, closed, oriented two dimensional surface. The contribution of each Feynman diagram to the vacuum-vacuum amplitude is given by

$$N^{V-P+L}\lambda^{P-V} = N_c^{2-2h}\lambda^{P-V}, \tag{3.21}$$

where V, P, L are the numbers of vertices, propagators and loops respectively and h is the genus of the two dimensional surfaces. The total contribution to the vacuum to vacuum amplitude is given as

$$\log Z = \sum_{h=0}^{\infty} N_c^{2-2h} f_h(\lambda), \tag{3.22}$$

where $f_h(\lambda)$ is a polynomial of λ.

Finally, in the large N_c limit it becomes clear that the planar diagrams ($h = 0$) dominate the expansion and the contribution of the rest of the diagrams is suppressed by powers of $\frac{1}{N_c^2}$.

The most striking characteristic of this large N_c expansion is the fact that it resembles the perturbative expansion of closed string theory

$$\mathcal{A} = \sum_{h=0}^{\infty} g_s^{2h-2} F_h(\alpha^{'}), \tag{3.23}$$

where $F_h(\alpha^{'})$ is the contribution of the $2d$ surfaces with genus h, if N_c is substituted by $\frac{1}{g_s}$. This resemblance is more evident in the large N_c limit and supports the statement that a string theory and a gauge theory can be related. Which precise string theory is related to the $SU(N_c)$ gauge theory is not clear from t'Hooft's idea. In the next section the AdS/CFT correspondence expands and makes more specific the idea of the duality between a gauge theory and a string theory and at the same time provides further evidence for its existence and makes quantitative calculations possible.

3.3 Introduction to AdS/CFT correspondence

3.3.1 AdS/CFT correspondence

Gauge/gravity duality is a hypothesis stating that certain string theories can be equivalently described by certain field theories. The first to suggest this conjecture was Maldacena in 1998. In his paper [46], he made the conjecture that a four dimensional $SU(N_c)$ $\mathcal{N} = 4$ Super Yang Mills (SYM) conformal field theory is equivalent to ten dimensional IIB Superstring theory on $AdS_5 \times S_5$. Maldacena's conjecture is an example of a gauge/gravity duality that is called the AdS/CFT [14] correspondence. The AdS/CFT conjecture originated from the dual interpretation of D branes, as a gauge theory and as a gravity theory. In this section we are going to focus on the AdS/CFT correspondence and we are going to present the various arguments supporting this hypothesis.

Consider a stack of N_c parallel D3 branes, placed on top of each other. Branes are massive objects which couple to gravity with a strength given by the string coupling g_s. Their total effect on the curvature of spacetime is measured by $g_s N_c$ [33].

Let us first consider the limit $g_s N_c << 1$ where branes live in a flat ten dimensional background. There are two types of string excitations in this case, open and closed strings. The open strings are excitations of the D3 branes and closed strings are

[14] AdS stands for Anti de Sitter and CFT for conformal field theory.

excitations of the bulk. In the low energy limit [15], the fields living on the branes decouple from the fields living in the bulk and also only the massless degrees of freedom contribute to the Lagrangian of the system. In this limit, the open string excitations, described by an $\mathcal{N} = 4$ SYM theory with an $SU(N_c)$ gauge group, are decoupled from the closed string excitations, described by ten dimensional IIB Supergravity.

In more detail, the complete effective action[16] describing the massless modes is given by

$$S = S_{bulk} + S_{brane} + S_{int}. \tag{3.24}$$

There are three distinct contributions to the effective action coming from the massless modes in the bulk (S_{bulk}), the brane (S_{brane}) and the interaction between them (S_{int}). The S_{bulk} is the ten dimensional IIB supergravity action plus some higher derivative terms and S_{brane} contains the four dimensional $SU(N_c)$ $\mathcal{N} = 4$ Super Yang Mills plus some higher derivative corrections. In the low energy limit ($\alpha^{'} \to 0$), the higher derivative terms in S_{brane} and S_{bulk} vanish because they are proportional to the square root of the Newton coupling $\sqrt{G_N} \sim g_s a^{'2}$. Furthermore, all the terms in S_{int} are proportional to $\sqrt{G_N}$ and therefore $S_{int} \to 0$ when $\alpha^{'} \to 0$, which results in the decoupling between the ten dimensional IIB supergravity in the bulk from the $3 + 1$ dimensional gauge theory living on the branes.

If we choose to consider the limit where $g_s N_c >> 1$, then gravity is not negligible anymore and D3 branes arise as a supergravity solution [34] given by

$$ds^2 = f^{-\frac{1}{2}}(-dt^2 + dx_1^2 + dx_2^2 + dx_3^2) + f^{\frac{1}{2}}(dr^2 + r^2 d\Omega_5^2), \tag{3.25}$$

$$F_5 = (1 + *)dt \wedge dx_1 \wedge dx_2 \wedge dx_3 \wedge df^{-1}, \tag{3.26}$$

$$f = 1 + \frac{R^4}{r^4}, \qquad R^4 = 4\pi g_s \alpha^{'2} N_c, \tag{3.27}$$

where F_5 is the field strength of the $C_{(4)}$ field sourced by the D3 branes, x_i $(i = 1, 2, 3)$ are the space coordinates along the worldvolume of the D3 branes and

[15] Low energy compared to the inverse string length l_s.

[16] It is an effective action in the Wilsonian sense where all massive degrees of freedom are integrated out.

$d\Omega_5^2$ is the metric of a unit radius five sphere. In the supergravity description there are only closed string excitations. In the low energy limit the modes of the closed strings that survive are, either the massless modes propagating in the bulk or closed strings that are very close to $r = 0$ (horizon). These two type of excitations decouple from each other in the low energy limit. Therefore, the low energy theory consists of free bulk supergravity in the asymptotic flat Minkowski spacetime and string theory on the near horizon region of the geometry. The near horizon metric is

$$ds^2 = \frac{r^2}{R^2}(-dt^2 + dx_1^2 + dx_2^2 + dx_3^2) + \frac{R^2}{r^2}dr^2 + R^2 d\Omega_5^2 \tag{3.28}$$

and it describes an $AdS_5 \times S_5$ spacetime [32, 37]. The parameter R corresponds to the radius of both the AdS_5 spacetime and the S^5 sphere.

By comparing the two descriptions of D branes for the two different $g_s N_c$ limits we can observe that each limit consists of two low energy decoupled sectors. Since both limits have a common sector, which is free supergravity in ten dimensional Minkowski spacetime, it is conjectured that the two sectors left are equivalent descriptions of the same physical phenomena. Therefore, the most general statement for the AdS/CFT correspondence is

$3+1$ dimensional $\mathcal{N} = 4$ SYM theory with an $\mathbf{SU(N_c)}$ gauge group

$$\Updownarrow$$

ten dimensional IIB string theory on $\mathbf{AdS_5 \times S_5}$.

This is the first time that a connection between string theory and gauge theory was found. The AdS/CFT correspondence as presented here does not provide a quantitative connection between the two descriptions. A more quantitative version of the correspondence is going to be presented later in section 3.3.6.

3.3.2 $\mathcal{N} = 4$ SYM theory

It has been claimed in the previous section that a stack of parallel coincident D3 branes in the low energy limit gives rise to a four dimensional $SU(N_c)$ $\mathcal{N} = 4$ Super

Yang Mills (SYM) theory. Although it has been explained in section 3.1.3 why is the gauge group of the conformal field theory an $SU(N_c)$ group and not some other group, it has not been discussed yet the field content of the theory.

The $SU(N_c)$ $\mathcal{N}=4$ Super Yang Mills theory is a conformal field theory whose beta function is zero up to all orders in perturbation theory. The fact that the theory is highly supersymmetric restricts its content to a unique supermultiplet. The field content is as follows. There is a gauge boson A_μ transforming as a singlet of $SU(4)$, six real scalars ϕ^I $(I=1,\cdots,6)$ transforming in the $\mathbf{6}$ of $SU(4)$ and two 4-component fermions transforming in the $\mathbf{4}$ and $\bar{\mathbf{4}}$ of $SU(4)$. The theory has a global $SU(4)$ (isomorphic to $SO(6)$) symmetry which is an R- symmetry[17] [36, 39].

Now that the field content of the conformal gauge theory is known, it is obvious that the fields of $SU(N_c)$ $\mathcal{N}=4$ SYM are exactly the same as the fields living on the stack of N_c coincident D3 branes, as described in section 3.1.3.

3.3.3 Symmetry and parameter matching

If the two sides of the correspondence are to be considered as different descriptions of the same physical phenomena, it is necessary that firstly, the parameters of the two theories are related and secondly, both theories share the same symmetries.

The gauge theory has two dimensionless parameters, the SYM coupling constant g_{YM} and N_c. The string theory has a dimensionless parameter g_s and two dimensionful parameters, l_s and R, whose ratio gives a dimensionless parameter. The matching between the dimensionless parameters is the following. In the gravity side the g_s can be matched to g_{YM} through

$$g_{YM}^2 = 4\pi g_s \tag{3.29}$$

and the N_c is interpreted as the total integrated flux of the F_5 field strength over

[17] An R-symmetry is a symmetry whose operators do not commute with the supercharges. In this particular case because of the R symmetry each different component of the supermultiplet has a different $SO(6)$ quantum number.

the S_5 sphere of radius R. The second relation connecting the various parameters is

$$\frac{R^4}{l_s^4} = (4\pi g_s N_c). \tag{3.30}$$

Regarding the symmetries of the gauge theory and the string theory, the conformal field theory has a $Conf(1,3)$ symmetry which matches with the $SO(2,4)$ isometry of the AdS_5 spacetime and the $SU(4)_R$ R-symmetry of the gauge theory can be matched to the $SO(6)$ isometry of the S_5 sphere. Furthermore, supersymmetries are matched in both sides of the correspondence. The conformal field theory has in total 32 supercharges, the same number as the AdS_5 spacetime. All these symmetries can be described by the superconformal group $SU(2,2|4)$. Note that gauge symmetries in the field theory side should not be matched by some symmetry in the gravity side because gauge symmetry is a result of the use of redundant variables (gauge fields).

3.3.4 Validity and the three versions of the correspondence

In section (3.3.1) a conjecture has been made that IIB string theory on $AdS_5 \times S_5$ is equivalent to a $3+1$ dimensional $\mathcal{N}=4$ SYM theory with an $SU(N_c)$ gauge group. Although this statement is very general (it applies for all values of N_c and g_s) and of great theoretical power, it poses some serious computational difficulties which can not be overcome with our current knowledge. Specifically, string theory on curved spacetimes with finite R-R flux is not well understood. Furthermore, gauge theories are tractable only in the weak coupling limit, when perturbation theory can be applied. Luckily, specific limits can be taken that return simpler versions of the correspondence. One such limit is the t'Hooft limit at which $\lambda = g_s N_c$ is taken to be finite and fixed along with $N_c \to \infty$ [31]. The advantage of this limit is that the string coupling $g_s = \frac{\lambda}{N_c}$ is small and therefore string perturbation theory can be used as a tool for performing certain calculations. Moreover, the SYM theory is simplified in this limit in the sense that only the planar diagrams contribute to the theory, see section 3.2. Even though the t'Hooft limit simplifies the correspondence considerably, that is not always enough because

neither perturbative string theory or the simplified gauge theory are easy to solve. Luckily, if an extra limit is taken, the correspondence becomes tractable. Specifically, if λ is fixed to a large value, string theory can be approximated by classical IIB supergravity in $AdS_5 \times S_5$ and therefore computations in this side of the correspondence are possible. Also, in the large λ limit the field theory lives in the strong coupling regime where computational tools are limited. Exactly at this point is where the power of the correspondence is made apparent. The correspondence can be used as a tool for accessing the, otherwise difficult to deal with, strongly coupled regime of the field theory through supergravity calculations. This weaker form of the correspondence (t'Hooft limit and large λ) is the one used in the following chapters as a tool for studying strongly coupled gauge theories.

3.3.5 Holographic Energy scale

The gravity side of the correspondence has five non-compact dimensions[18] as opposed to the four dimensions of the gauge theory. The fact that a five dimensional gravitational theory encodes the same amount of information as a theory in four dimensions poses a very interesting question about the nature of this extra dimension. An easy way of probing the fifth dimension is by using the dilation symmetry of the theory. Since dilation is a symmetry of both theories, it should leave them unchanged. Consider a scalar field in the gauge theory whose action is given by

$$S = \int d^4x (\partial\phi)^2. \tag{3.31}$$

If the transformation $x \to e^{\alpha} x$ is applied, then the only way for the action to remain unchanged is if ϕ transforms as $\phi \to e^{-\alpha}\phi$. Therefore, the scalar field ϕ has energy dimension and the x has inverse energy dimension. If the same transformation is applied in the gravity side of the correspondence and by requiring the metric (3.28)

[18]The fields living on $AdS_5 \times S_5$ are ten dimensional but because S_5 is a compact space a Kaluza-Klein reduction of the fields to five dimensions is possible. Since we only consider the low energy limit of the theory, where only the massless modes contribute from all the modes of the Kaluza Klein tower, we keep only the lower excitation terms.

to remain invariant, the fifth dimension r of the metric should transform as

$$r \to e^{-\alpha} r. \tag{3.32}$$

Therefore, the extra dimension in the gravity side transforms in the same manner as the scalar field in the gauge theory and therefore has energy dimension. It is natural to interpret this extra dimension r as the Renormalisation group scale of the gauge theory [39].

With this holographic identification, a natural question that arises is where is the dual field theory located? The most fundamental field theory is considered the one without any degrees of freedom integrated out (in the Wilsonian sense) and therefore is defined in an infinite energy scale. According to the holographic description of the correspondence, in this case the dual field theory should live at the boundary $r \to \infty$ of the AdS_5 spacetime, since r is identified with the energy scale of the theory. If some UV degrees of freedom are integrated out in the field theory (moving in lower energy scale), that will correspond in the gravity side as moving towards the horizon $r = 0$ of the AdS_5 spacetime [26, 40].

3.3.6 Operator matching

According to the gauge/gravity duality, string theory and a gauge theory can describe the same physical system. It is then logical that both descriptions should respond to perturbations in a similar way [38]. More precisely, studying the perturbations in each of the two theories could be very useful in creating a dictionary that links the two different descriptions [47, 48], based on the responses to the perturbations.

Let us study a known example that can provide some insight on how to relate the two theories. The SYM coupling g_{YM} is related to the string coupling through (3.29) and also the string coupling g_s is given by the expectation value of the dilaton field at the AdS_5 boundary ($r \to \infty$). If a perturbation (sometimes called deformation) is applied to the gauge theory by changing the SYM coupling

constant, then the expectation value of the dilaton field at the boundary should change as well so that the relation (3.29) will still hold. This example can be generalised by considering a general deformation of the gauge theory of the form

$$S \to S + \int \mathrm{d}^4x \; \phi_0(x)\mathcal{O}(x), \tag{3.33}$$

where $\mathcal{O}(x)$ is a local, gauge invariant operator and $\phi_0(x)$ is the source of the operator. The g_{YM} in our example is a source to some operator. Therefore, in the general case there should be a field in the gravity side whose asymptotic value matches with the source $\phi_0(x)$, as the dilaton in the above example, for each operator in the field theory [37]. This one to one matching between the fields in the bulk and the field theory operators is called field/operator matching. In [47, 48] the field/operator matching was stated in a path integral language as

$$\mathcal{Z}_{string}\Big[\phi(\vec{x},r)\big|_{r=\infty} = \phi_0(x)\Big] = \Big\langle e^{\int d^4x \; \phi_0(x)\mathcal{O}(x)} \Big\rangle_{FT}, \tag{3.34}$$

where $\mathcal{Z}_{string}$ is the full partition function in string theory and the r.h.s is the generating functional in the field theory. This is the most general operator/field matching recipe arising from the gauge/gravity duality. It is possible to approximate the string theory partition function with the supergravity partition function, when using the weak form of the correspondence (see 3.3.4), and therefore (3.34) becomes

$$e^{-I_{SUGRA}} \sim \Big\langle e^{\int d^4x \; \phi_0(x)\mathcal{O}(x)} \Big\rangle_{FT}, \tag{3.35}$$

where I_{SUGRA} is the on-shell supergravity action[19].

The next obvious question is how to determine the dual field for a given field theory operator? This is not always possible but a guide for the identification should be provided by the quantum numbers and symmetries. Specifically, the field and operator should share the same quantum numbers under the global symmetries of the theory [37].

[19]It is possible to have more than one on-shell supergravity actions, if there are more than one solutions to the equation of motion of the bulk field of interest. In this case, it is necessary to decide which solution is the real vacuum of the theory by comparing their free energies [32].

To explore further the operator/field matching it is very instructive to consider the case of a five dimensional massive scalar field $\Phi(\vec{x}, r)$ living in $AdS_{d+1} \times S_5$. This field is dual to some operator $\mathcal{O}(x)$, which lives on the d dimensional Minkowski boundary of $AdS_{d+1} \times S_5$, where the gauge theory lives. The bulk action is the following

$$S = -\frac{1}{2} \int \mathrm{d}r \mathrm{d}^d x \, \sqrt{-g} \left(g^{MN} \partial_M \Phi \partial_N \Phi + m^2 \Phi^2 \right), \tag{3.36}$$

where $M, N = 0, \cdots, d+1$. It is convenient to Fourier decompose the field Φ in the Minkowski directions x^μ and then calculate its equation of motion which is the following

$$r^{1-d} \partial_r (r^{d+1} \partial_r \Phi) - (k^2 R^2 r^{-2} + m^2 R^2) \Phi = 0, \tag{3.37}$$

where $k^\mu = (E, \vec{p})$ and therefore $k^2 = -E^2 + \vec{p}^2$. The (3.37) describes the scalar field Φ in the bulk. Since a connection between the field Φ in the bulk and the operator on the boundary is investigated, the study is limited to the $r \to \infty$ case. The solution to the asymptotic equation of (3.37) is[20]

$$\Phi(\vec{x}, r) \sim A(x) r^{\Delta - d} + B(x) r^{-\Delta}, \tag{3.38}$$

where

$$\Delta = \frac{d}{2} + \nu \quad \text{and} \quad \nu = \sqrt{m^2 R^2 + \frac{d^2}{4}}. \tag{3.39}$$

The next step is the interpretation of the asymptotic solution. There are two linear contributions of which the first term $\sim A(x)$ is non-normalisable and the second term $\sim B(x)$ is normalisable[21]. The non-normalisable term is dominant at the boundary and therefore it is natural to match the non-normalisable asymptotic value of the field to the source of the operator $\mathcal{O}(x)$ at the boundary. The solution is singular at the boundary and needs to be regularised. The exact matching is

$$\phi_0(x) = \lim_{r \to \infty} r^{d-\Delta} \Phi(\vec{x}, r). \tag{3.40}$$

[20] The solution is Fourier transformed back to position coordinate space.

[21] It is possible that both terms are normalisable when the mass is in the range $-\frac{d^2}{4} \leq m^2 R^2 \leq -\frac{d^2}{4} + 1$ but this case is not going to be considered here.

This last expression implies that the source acquires a mass dimension $d - \Delta$ and therefore the operator $\mathcal{O}(x)$ has mass dimension Δ.

The normalisable terms should be identified with the states of the boundary theory and more specifically the coefficient $B(x)$ should be identified with the expectation value of the operator $\mathcal{O}(x)$ [37].

Finally, let us make some observations regarding (3.39). This relation indicates a correspondence between the mass dimension of the gauge theory operator and the mass of the field in the bulk. For example, in the case of a massless scalar field the mass dimension of the corresponding operator is d. The relation between mass and dimension can be generalised for any p-form field in the bulk and the expression that relates the mass of the bulk field with the dimension of the field theory operator is

$$m^2R^2 = (\Delta - p)(\Delta + p - d). \tag{3.41}$$

Moreover, the definition of ν imposes a limit on the values of mass as a result of the requirement that the square root should be real. The specific limit is

$$m^2R^2 \geq -\frac{d^2}{4}. \tag{3.42}$$

The conclusion from the above relation is that the mass of the scalar field in the bulk can have negative values as long as it doesn't become too negative. Generally, all the fields in the bulk have a minimum allowed value for the mass which is called Breitenlohner-Freedman(BF) bound [49, 50] [22].

3.4 Generalisations of AdS/CFT

The discussion of the AdS/CFT correspondence in the previous sections was restricted to a specific example of the duality, the case of $\mathcal{N} = 4$ $SU(N)$ SYM theory being dual to a ten dimensional IIB superstring (supergravity) theory on $AdS_5 \times S_5$. The gauge theory considered in this case has no connection with nature

[22] Equation (3.42) holds for the case of a scalar field. For gauge fields, tensor fields e.t.c the BF bound is different.

and therefore is not directly useful for physical applications, but it can serve as a starting point for the development of dualities between other more realistic field theories and their gravity duals. The example discussed can be "deformed" in many different ways like adding temperature, adding fundamental matter, non-trivial dilaton e.t.c. so that the gauge theory will exhibit some interesting characteristics like confinement, running coupling e.t.c. which will bring the theory closer to QCD. The purpose of the present section is to present some ways that these deformation can be achieved. More details will be provided in the following chapters when necessary.

3.4.1 Adding flavour

The example of the $\mathcal{N} = 4$ SYM theory with $SU(N)$ gauge group, discussed in the previous sections, includes only fields transforming in the adjoint representation of the gauge group. In real QCD, quarks transform in the fundamental representation of $SU(3)$ and gauge fields in the adjoint representation of the same group. Therefore, there is a need for extending the correspondence in a way that fundamental degrees of freedom can be accommodated as well. One possible way to do that is by introducing a small number of N_f Dp probe branes which was originally suggested in [51]. In the next chapters we focus our interest in specific cases of D7 and D5 branes. Understanding how to introduce these branes and how the AdS/CFT correspondence is modified by them is the main purpose of this subsection.

How does the introduction of a different type of Dp brane, where $p > 3$ and odd, introduce fundamental matter in the theory? When a new type of brane is introduced, additional types of open strings are present, those stretching between D3-Dp and Dp-Dp branes. Open strings having both ends attached to D3 branes produce fields transforming in the adjoint representation of the $U(N_c)$ gauge group. When only one end is ending on the D3 brane, naturally such a string describes matter in the fundamental representation of the same gauge group.

Let us explain how the correspondence works in the case of a D7 brane, following a

	x_0	x_1	x_2	x_3	x_4	x_5	x_6	x_7	x_8	x_9
D3	X	X	X	X						
D7	X	X	X	X	X	X	X	X		

Table 3.3: The background D3 and the probe D7 branes embedded in a ten dimensional Minkowski background.

similar logic to 3.3.1 . In the $g_s N_c << 1$ case, a stack of N_c coincident D3 branes is placed in a flat ten dimensional spacetime and N_f D7 branes are added in a way summarised in the above table. The D3 branes [23] share all of their directions $x_0 - x_3$ with the D7 branes. In addition, the D7 branes extend in another four directions $x_4 - x_7$. The x_8 and x_9 directions are perpendicular to both types of branes. In this setup, there is an apparent $SO(4) \times SO(2)$ isometry characterising the directions perpendicular to the D3 branes. SO(4) rotates the $x_4 - x_7$ directions and SO(2) rotates the $x_8 - x_9$ directions. The $SO(2)$ symmetry and its breaking are going to be of great importance in the next chapters for realising what is called spontaneous chiral symmetry breaking in D3/D7 brane system. Extended discussion is available in the next chapters. Let us also point out, before proceeding further, that this specific choice of embedding the D7 branes into the $AdS_5 \times S_5$ brane, sharing the same directions as the D3 branes and wrapping an S_3 sphere, preserves a quarter of the total amount of supersymmetry in type IIB string theory [39, 51].

There are two type of excitations in the D3/D7 system, open and closed strings. Specifically, there are three types of open strings, the D3-D3, D7-D7 and D3-D7 strings. The first type was discussed in detail in section 3.3.1 and in the low energy limit corresponds to an $\mathcal{N} = 4$ SYM theory with an $SU(N_c)$ gauge group. The D7-D7 strings decouple in the low energy limit because the eight dimensional t'Hooft coupling $\lambda_{D7} = \lambda_{D3}(2\pi l_s^2)^4 \frac{N_f}{N_c}$, controlling the interactions on the D7 branes, becomes zero in low energies. This decoupled D7-D7 sector gives rise to a global $U(N_f)$ flavour symmetry which is the flavour symmetry expected in the four dimensional gauge theory when N_f equal mass quarks are present [37]. The D3-D7 strings interact with the D3-D3 strings through the four dimensional t'Hooft

[23] In some occasions the D3 branes are called colour branes and the D7(or D5) branes flavour branes.

coupling which has a finite value in the low energy limit, but do not interact with the D7-D7 strings. Moreover, the closed strings, which are the excitations of the background, decouple from the brane dynamics in the low energy limit, as explained in section 3.3.1. To summarise, the $g_sN_c << 1$ description includes two decoupled sectors. The first sector, which is free, consists of the closed strings in the bulk and the D7-D7 open strings on the D7 branes. The second sector, which is interacting, consists of the D3-D3 and D3-D7 open strings.

In the $g_sN_c >> 1$ limit where gravity becomes important, the stack of N_c coincident D3 branes curves spacetime and results in a near horizon $AdS_5 \times S_5$ geometry. The D7 branes can be considered as probes in the limit $N_f << N_c$, which means that they do not backreact on the geometry [24]. In the $g_sN_c >> 1$ limit there are two different type of excitations, closed strings and D7-D7 open strings, which exist both in the asymptotic region of the spacetime and in the throat of $AdS_5 \times S_5$. In the low energy limit the degrees of freedom in the asymptotic region become free and they decouple from the degrees of freedom in the throat, which remain interacting. Therefore two decoupled sectors are present, a free and an interacting.

Following the same logic that led to the original AdS/CFT correspondence, it is conjectured that the free sector of each description can be matched with the free sector of the other description and the same applies for the interacting sectors. Therefore, the strong version of the duality in the presence of Dp branes is stated as

$\mathcal{N} = 4$ SYM with SU($\mathbf{N_c}$) gauge group coupled to $\mathbf{N_f}$ $\mathcal{N} = 2$ hypermultiplets

$$\Updownarrow$$

IIB closed strings in $\mathbf{AdS_5 \times S_5}$ coupled to open strings on the worldvolume of $\mathbf{N_f}$ Dp probes

In the gauge theory side, $\mathcal{N} = 4$ SYM is a conformal theory. The addition of fundamental matter is equivalent to the addition of N_f $\mathcal{N} = 2$ hypermultiplets in

[24] In lattice QCD this approximation is called quenched approximation. Practically, in the study of the gauge dynamics the quark loops are neglected.

the gauge theory. The final theory is an $SU(N_c)$ $\mathcal{N}=2$ SYM and the expression for its beta function is $\beta \propto \lambda^2 \frac{N_f}{N_c}$. In the t'Hooft limit (fixed and finite λ, $N \to \infty$) and for N_f fixed, $\beta \to 0$ and the new gauge theory is conformal. In these limits and for large λ the above duality simplifies and string theory can be described by supergravity in the low energy limit. More accurately, the closed strings in $AdS_5 \times S_5$ can be approximated by supergravity in $AdS_5 \times S_5$. The Dp branes are considered as probe branes when $N_f << N_c$ and therefore a supergravity solution is not necessary for these branes in the quenched approximation.

Let us know proceed by explaining how the AdS/CFT dictionary works in the case of Dp branes, a step necessary for understanding the following chapters. For simplicity, let us focus on the specific example of a D7 probe brane embedded in an $AdS_5 \times S_5$ geometry. First of all, it is more convenient to parametrise the directions perpendicular to the D3 branes in a different way such that the $SO(4) \times SO(2)$ symmetry becomes manifest, so we rewrite the metric (3.28) as follows

$$ds^2 = \frac{r^2}{R^2}(-dt^2 + dx_1^2 + dx_2^2 + dx_3^2) + \frac{R^2}{r^2}(d\rho^2 + \rho^2 d\Omega_3^2 + dL^2 + L^2 d\phi^2), \qquad (3.43)$$

where $\rho^2 = x_4^2 + \cdots + x_7^2$ and $r^2 = \rho^2 + L^2$. To describe the embedding of the D7 brane in $AdS_5 \times S_5$ one must specify the two directions perpendicular to the D7 brane, L and ϕ. Due to the $SO(2)$ rotational symmetry between these two coordinates, it is sufficient to study $L = L(\rho)$ and fix $\phi = 0$.

The low energy dynamics of the D7 brane are governed by the DBI action plus the Chern-Simons action, as explained in section 3.1.3 but repeated here for convenience

$$S_{D7} = -\mu_7 \int \mathrm{d}^8\xi \sqrt{-\det(P[G_{ab}] + 2\pi\alpha' F_{ab})} + \frac{(2\pi\alpha')^2}{2}\mu_7 \int \mathrm{d}^8\xi P[C^{(4)}] \wedge F \wedge F. \qquad (3.44)$$

The next step is to find the equation of motion for the embedding which is

$$\frac{\mathrm{d}}{\mathrm{d}\rho}\left[\frac{\rho^3 L'(\rho)}{\sqrt{1 + L'(\rho)^2}}\right] = 0. \qquad (3.45)$$

The embedding $L(\rho)$ is a scalar field in the bulk and according to the AdS/CFT

dictionary it should correspond to a gauge invariant operator in the gauge theory, which lives on the boundary of the AdS_5 spacetime. To form a connection with the gauge theory we find the asymptotic solution $\rho \to \infty$ to (3.45) which has the following form

$$L(\rho) = m + \frac{c}{\rho^2} + \cdots , \tag{3.46}$$

where m is proportional to the bare quark mass in the gauge theory and c is the vev of an operator which clearly has dimensions of mass 3 (ρ carries an energy dimension) and shares the same symmetries with mass m. Therefore, c should correspond to a quark bilinear vev $< \overline{q}q >$ in the gauge theory. Notice that according to this prescription, separating the D7 branes from the D3 branes in the L (or ϕ) direction is equivalent to giving a mass to the fundamental hypermultiplets. Also a finite mass explicitly breaks the $SO(2)$ symmetry of the theory and consequently the chiral symmetry is explicitly broken.

There are various other ways that flavour can be added to the theory. A choice of a different type of brane is possible, one such example is adding a D5 brane in the system instead of a D7 brane. A different model for adding flavour to the AdS/CFT is the Sakai-Sagimoto model [42, 43].

3.4.2 Finite temperature

In all the cases considered until now, zero temperature was assumed. If more realistic theories are to be achieved, finite temperature should be considered. The extension of the gauge/gravity duality to the finite temperature case was initially studied in [44].

The gravitational dual of the zero temperature $\mathcal{N} = 4$ SYM theory is supergravity on $AdS_5 \times S_5$. If the finite temperature case is to be considered, $AdS_5 \times S_5$ spacetime should be substituted by a Schwarzschild black hole geometry

$$\begin{aligned} ds^2 &= \frac{r^2}{R^2}(-f(r)dt^2 + dx_1^2 + dx_2^2 + dx_3^2) + \frac{R^2}{f(r)r^2}(dr^2 + r^2 d\Omega_5^2), \\ f(r) &= 1 - \frac{r_H^4}{r^4}\,, \end{aligned} \tag{3.47}$$

which satisfies the same supergravity equation of motion as the $AdS_5 \times S_5$ geometry, subject to the same boundary conditions.

The natural framework to work in a finite temperature field theory is to consider periodic imaginary time with period $\beta = \frac{1}{T}$, where T is the temperature of the theory. It is also natural to implement this recipe to the gravity side of the correspondence. The first step is to write the metric in the Euclidean signature (Wick rotate). This Euclidean metric should not be continued for $r \leq r_H$, otherwise the Euclidean character is spoiled. Also the metric should end smoothly on the horizon. These two requirements are fulfilled if the time is periodic with period

$$\beta = \frac{1}{T} = \frac{\pi R^2}{r_H}. \tag{3.48}$$

Note that, the temperature of the black hole (Hawking temperature) is the same as the temperature in the field theory.

The advantage of working in the Euclidean signature is that allows the exploration of various thermodynamic quantities using the gauge/gravity duality. All the thermodynamic properties of the black hole e.g. entropy are related with those in the field theory[25]. A very important quantity, for understanding the next chapters, is the free energy F. The free energy F is defined using the statistical mechanics partition function

$$Z_{CFT} = \sum e^{-\beta F}. \tag{3.49}$$

The corresponding generating functional in the gravity theory is given by [26]

$$Z_{gravity} = e^{-S}, \tag{3.50}$$

where S is the on-shell Euclidean action. Since the last two expressions should be equal according to (3.35) we can conclude that [45]

$$S = \frac{F}{T}. \tag{3.51}$$

[25] The field theory in the Euclidean signature is described by statistical mechanics.

[26] Assuming of course large N_c and large t'Hooft coupling λ, so that the supergravity approximation is valid.

Keep in mind that the free energy is an infinite quantity which should be regularised. Also, note that when more than one solutions satisfy the supergravity equations of motion, satisfying the same boundary conditions at infinity, the solution with the lowest free energy is the real vacuum of the theory. In the case of finite temperature $\mathcal{N} = 4$ SYM for the infinite volume limit ($\mathbb{R}^3 \times S^1$ boundary topology), which is the case considered in this thesis, the AdS-Schwarzschild black hole is the preferred solution for all non zero temperatures.

A very important implication of finite temperature is the fact that supersymmetry is broken explicitly due to the fact that fermions obey antiperiodic boundary conditions in the Euclidean time direction [39]. Moreover, temperature introduces a scale in the theory and therefore conformal invariance is broken.

3.5 Wilson loops and confinement in gauge gravity duality

Wilson loops are gauge invariant non local operators in gauge theories which are generally defined as

$$W(C) = Tr\Big[\mathcal{P}e^{ig\oint_P dx^\mu A^\alpha_\mu(x)t^\alpha}\Big], \tag{3.52}$$

where $\mathcal{P}$ is the path ordering[27], t^α are the generators of the gauge group in some representation and g is the gauge coupling constant [15].

The expectation value of a Wilson loop contains information about the non perturbative physics and is very useful for studying various phenomena in strongly coupled gauge theories like confinement, quark screening etc. In QCD a Wilson loop is related to a string stretching between a quark and an antiquark [32] and therefore is an appropriate operator for studying confinement.

A Wilson loop in holography was originally studied in [121, 122] and it was suggested that the dual picture of a Wilson loop in the gravity side of the correspondence is described by an open string attached to a Dp probe brane placed

[27] Path ordering is necessary in the non-Abelian case and the trace is for giving a gauge invariant non abelian operator.

at some radial position in some gravity background. The endpoints of the string correspond to the quark and antiquark. If the path C of the Wilson loop is thought as the path transversed by the quark, then the boundary of the open string worldsheet should coincide with this path C [37]. The AdS/CFT dictionary for the case of a Wilson loop according to (3.35) is

$$< W(C) > = \ Z_{string}[\partial\Sigma = C] \sim e^{iS(C)}, \tag{3.53}$$

where the approximation made is valid only for large N_c and large t'Hooft λ coupling. $S(C)$ is the on-shell Nambu-Goto action (3.1) for the string worldsheet satisfying the boundary conditions $\partial\Sigma = C$.

As mentioned before, Wilson loops provide a way for studying confinement. This is possible by investigating what happens to the potential between an infinitely heavy quark and antiquark. The quarks probe the dynamics of the gauge theory and are chosen to be infinitely heavy so that they do not affect the gauge dynamics in any way. The gauge dynamics are the geometry itself, in the context of the duality. To achieve this infinitely heavy quarks, the probe Dp brane is placed at the boundary of the gravitational background, so that the strings stretching between the stack of D3 branes and the boundary are infinitely massive. For calculating the potential the path should be chosen to be a rectangular loop with sides L, the distance between the quark and the antiquark, and time $\mathcal{T}$. When $\mathcal{T} >> L$, the Wilson loop in the field theory is expected to be

$$< W(C) > \sim e^{-\mathcal{T}(2M+V(L))}, \tag{3.54}$$

where M is the mass of the quark/antiquark. Therefore, by working in the gravity side of the correspondence the calculation of the $S(C)$ is possible, after regularising the action, and the calculation of the quark potential $V(L)$ is straightforward.

The next step is the interpretation of the $V(L)$. The $V(L)$ can have many different forms which reflect some properties of the background geometry. One case is $V(L)$ to be constant, in some range of values of L, which means zero energy is required

for the quarks to be separated. What has happened in this case is that the quarks are completely screened by the gluon plasma between them. Another possible scenario is that $V(L)$ has the form $V(L) \sim \frac{1}{L}$, which resembles the Coulomb potential and is characteristic of conformally invariant backgrounds. Finally, it is possible that $V(L)$ has the form $V(L) \sim L$ which means that the potential between the quark and antiquark is growing linearly as the distance between them is increasing. This is a sign that the quark and antiquark are confined.

There are many Wilson loop calculations in the context of holography. An interesting example is the calculation of the Wilson loop for a Schwarzschild black hole background, given in [133]. In [133] the case of $\mathcal{N} = 4$ SYM in finite temperature, with the field theory living in a non-compact $\mathbb{R}^3 \times S^1$ boundary, is considered. The Wilson loop calculation indicates that the theory is in a deconfined phase, for all values of temperature.

Chapter 4

Holographic Description of the Phase Diagram of a Chiral Symmetry Breaking Gauge Theory

4.1 Introduction

The phase diagram in the temperature chemical potential (or density) plane is a matter of great interest in both QCD and more widely in gauge theory [18–20]. In QCD there is believed to be a transition from a confining phase with chiral symmetry breaking at low temperature and density to a phase with deconfinement and no chiral symmetry breaking at high temperature. In the standard theoretical picture for QCD with massless quarks, the transition is first order for low temperature but growing density, whilst second order at low density and growing temperature. The second order transition becomes a cross over at finite quark mass. There is a (tri-)critical point where the first order transition mutates into the (second order) cross over transition. In fact though there could still be room in QCD for a more exotic phase diagram [20] as we will discuss in the context of our

results in our final section.

In this chapter we will present a precise holographic [46–48] determination of the phase diagram in the temperature chemical potential plane for a gauge theory that displays many of the features of the QCD diagram, although the precise details differ. A pictorial comparison of our theory to QCD can be made by comparing Fig 4.5 to Fig 4.10.

The theory we will consider is the large N $\mathcal{N}$=4 gauge theory with quenched $\mathcal{N}$=2 quark matter [51–54] which has been widely studied [39]. An immediate difference between the $\mathcal{N}$=4 glue theory and QCD is that the thermal phase transition to a deconfined phase occurs for infinitesimal temperature since the massless theory is conformal [47]. Essentially the entire temperature chemical potential phase diagram of our theory is therefore characterized by strongly coupled deconfined glue.

The quark physics is more subtle though - the phase diagram in the temperature chemical potential (density) plane for the $\mathcal{N} = 2$ quark matter has been studied in [55–60]. When the quark mass is zero the theory is conformal and the origin of the phase diagram is a special point with confined matter. Immediately away from that point, in either temperature or chemical potential, a first order transition moves the theory to a deconfined theory (the mesons melt [61–64]).

When a quark mass is present in the $\mathcal{N}$=2 theory the meson melting transition occurs away from the origin. This transition has been reported as first order with a second order transition point where the first order transition line touches the $T = 0$ chemical potential axis [58, 59] (in the grand canonical ensemble). Interestingly there is a phase transition line in the temperature versus density plane (in the canonical ensemble) in which the quark condensate jumps [55, 56]. This area of the phase diagram is intrinsically unstable though and not realizable by imposing any chemical potential [59].

The crucial ingredient we will add to the theory is chiral symmetry breaking which will also bring the theory closer in spirit to QCD. As shown in [65–67, 69–72] the $\mathcal{N} = 2$ theory in the presence of a magnetic field displays chiral symmetry breaking through the generation of a quark anti-quark condensate. At zero density the finite

temperature behaviour has been studied [65–67, 69] and there is a first order transition from a chiral symmetry broken phase at low temperature to a chiral symmetry restored phase at high temperature. In this chapter we will include chemical potential as well to map out the full phase diagram in the temperature chemical potential plane. We will find a chiral symmetry restoration phase transition, which is first order for low density and second order for low temperature - there is a tri-critical point where these transitions meet. This physics is in addition to a meson melting transition which is first order at large temperature but apparently second order at low temperature. This latter region of transition is interesting because it is associated with a discontinuous jump from an embedding off the black hole to one that ends on it and it looks naively first order. However, when we plot any available order parameter in the boundary theory it appears second order.

We will also track the movement of these transition lines and critical points as the quark mass rises relative to the magnetic field. The infinite mass limit corresponds to the pure $\mathcal{N}$=2 theory without magnetic field [57, 59]. The second order chiral symmetry restoration transition becomes a cross over the moment a mass is introduced. The first order transition structure though remains, even to the infinite mass limit, with two critical points: one is the end point of the first order transition and the other is the the end point of the second order meson melting transition. This structure was not reported in the results in [57, 59][1] but this is not surprising since the structure, in that limit, is on a very fine scale. We have only found it by following the evolution of the larger structure present at low quark mass with a magnetic field. In addition we present evidence to suggest the parameter space with a second order meson melting transition extends away from just the $T = 0$ axis, again, even in the infinite mass limit. We have confirmed these results in the strict $B = 0$ limit also.

The theory we study may appear to be a rather vague relative of QCD with

[1]The existence of two critical points is related with the existence of the black hole to black hole transition. It is actually just visible in Fig 2c of [57] but the authors had not probed it in detail previously. After discussion of our results with the authors of [57], they have refined their computations and confirmed our results.

magnetic field induced chiral symmetry breaking. On the other hand it is a theory of strongly coupled glue with the magnetic field inducing conformal symmetry breaking in the same fashion as $\Lambda_{\rm QCD}$ in QCD. In fact the magnetic field case in the basic $\mathcal{N}$=4 dual is the cleanest known example of chiral symmetry breaking in a holographic environment. Other deformations of the $\mathcal{N}$=4 gauge theory typically lead to an ill-understood IR singular hard wall - see for example [73, 74]. The magnetic field case provides a smooth IR wall where we have more control but the results are likely to be the same in those more complex cases. We can hope to learn some lessons for a wider class of gauge theories.

4.2 The holographic description

The $\mathcal{N}$=4 gauge theory at finite temperature has a holographic description in terms of an AdS_5 black hole geometry (with N D3 branes at its core) [46–48]. The geometry is

$$ds^2 = \frac{r^2}{R^2}(-f dt^2 + d\vec{x}^2) + \frac{R^2}{r^2 f} dr^2 + R^2 d\Omega_5^2, \tag{4.1}$$

$$f := 1 - \frac{r_H^4}{r^4}, \qquad r_H := \pi R^2 T, \tag{4.2}$$

where $R^4 = 4\pi g_s N \alpha'^2$ and r_H is the position of the black hole horizon which is related to the temperature T.

We will find it useful to make the coordinate transformation

$$\frac{dr^2}{r^2 f} \equiv \frac{dw^2}{w^2} \implies w := \sqrt{r^2 + \sqrt{r^4 - r_H^4}}, \tag{4.3}$$

with $w_H = r_H$. This change makes the presence of a flat 6-plane perpendicular to the horizon manifest. We will then write the coordinates in that plane as ρ and L according to

$$w = \sqrt{\rho^2 + L^2}, \quad \rho := w \sin\theta, \quad L := w \cos\theta, \tag{4.4}$$

The metric is then

$$ds^2 = \frac{w^2}{R^2}(-g_t dt^2 + g_x d\vec{x}^2) + \frac{R^2}{w^2}(d\rho^2 + \rho^2 d\Omega_3^2 + dL^2 + L^2 d\Omega_1^2), \tag{4.5}$$

where

$$g_t := \frac{(w^4 - w_H^4)^2}{2w^4(w^4 + w_H^4)}, \qquad g_x := \frac{w^4 + w_H^4}{2w^4}. \tag{4.6}$$

4.2.1 Quarks/D7 brane probes

Quenched ($N_f \ll N$) $\mathcal{N}$=2 quark superfields can be included in the $\mathcal{N}$=4 gauge theory through probe D7 branes in the geometry [51–54]. The D3-D7 strings are the quarks. D7-D7 strings holographically describe mesonic operators and their sources. The D7 probe can be described by its DBI action

$$S_{DBI} = -T_{D7} \int d^8\xi \sqrt{-\det(P[G]_{ab} + 2\pi\alpha' F_{ab})}, \tag{4.7}$$

where $P[G]_{ab}$ is the pullback of the metric and F_{ab} is the gauge field living on the D7 world volume. We will use F_{ab} to introduce a constant magnetic field (eg $F_{12} = -F_{21} = B$) [65–67] and a chemical potential associated with baryon number $A_t(\rho) \neq 0$ [56, 75, 76].

We embed the D7 brane in the ρ and Ω_3 directions of the metric but to allow all possible embeddings must include a profile $L(\rho)$ at constant Ω_1. The full DBI action we will consider is then

$$S = \int d\xi^8 \mathcal{L}(\rho) = \left(\int_{S^3} \epsilon_3 \int dt d\vec{x}\right) \int d\rho\ \mathcal{L}(\rho), \tag{4.8}$$

where ϵ_3 is a volume element on the 3-sphere and

$$\begin{aligned} \mathcal{L} \ := \ & -N_f T_{D7} \frac{\rho^3}{4} \left(1 - \frac{w_H^4}{w^4}\right) \sqrt{\left(\left(1 + \frac{w_H^4}{w^4}\right)^2 + \frac{4R^4}{w^4} B^2\right)} \\ & \times \sqrt{\left(1 + (\partial_\rho L)^2 - \frac{2w^4(w^4 + w_H^4)}{(w^4 - w_H^4)^2} (2\pi\alpha' \partial_\rho A_t)^2\right)}. \end{aligned} \tag{4.9}$$

Since the action is independent of A_t, there is a conserved quantity d $\left(:= \frac{\delta S}{\delta F_{\rho t}}\right)$ and we can use the Legendre transformed action

$$\widetilde{S} = S - \int d\xi^8 F_{\rho t} \frac{\delta S}{\delta F_{\rho t}} = \left(\int_{S^3} \epsilon_3 \int dt d\vec{x}\right) \int d\rho \; \widetilde{\mathfrak{L}}(\rho), \tag{4.10}$$

where

$$\widetilde{\mathfrak{L}} := -N_f T_{D7} \frac{(w^4 - w_H^4)}{4w^4} \sqrt{K(1 + (\partial_\rho L)^2)}, \tag{4.11}$$

$$K := \left(\frac{w^4 + w_H^4}{w^4}\right)^2 \rho^6 + \frac{4R^4 B^2}{w^4} \rho^6 + \frac{8w^4}{(w^4 + w_H^4)} \frac{d^2}{(N_f T_{D7} 2\pi\alpha')^2} \; . \tag{4.12}$$

To simplify the analysis we note that we can use the magnetic field value as the intrinsic scale of conformal symmetry breaking in the theory - that is we can rescale all quantities in (4.11) by B to give

$$\widetilde{\mathfrak{L}} = -N_f T_{D7} (R\sqrt{B})^4 \; \frac{\widetilde{w}^4 - \widetilde{w}_H^4}{\widetilde{w}^4} \sqrt{\widetilde{K}(1 + \widetilde{L}'^2)}, \tag{4.13}$$

$$\widetilde{K} = \left(\frac{\widetilde{w}^4 + \widetilde{w}_H^4}{\widetilde{w}^4}\right)^2 \widetilde{\rho}^6 + \frac{1}{\widetilde{w}^4} \widetilde{\rho}^6 + \frac{\widetilde{w}^4}{(\widetilde{w}^4 + \widetilde{w}_H^4)} \widetilde{d}^2, \tag{4.14}$$

where the dimensionless variables are defined as

$$(\widetilde{w}, \widetilde{L}, \widetilde{\rho}, \widetilde{d}) := \left(\frac{w}{R\sqrt{2B}}, \frac{L}{R\sqrt{2B}}, \frac{\rho}{R\sqrt{2B}}, \frac{d}{(R\sqrt{B})^3 N_f T_{D7} 2\pi\alpha'}\right)$$

In all cases the embeddings become flat at large ρ taking the form

$$\widetilde{L}(\widetilde{\rho}) \sim \widetilde{m} + \frac{\widetilde{c}}{\widetilde{\rho}^2}, \; \widetilde{m} = \frac{2\pi\alpha' m_q}{R\sqrt{2B}}, \; \widetilde{c} = \langle \bar{q} q \rangle \frac{(2\pi\alpha')^3}{(R\sqrt{2B})^3}. \tag{4.15}$$

In the absence of temperature, magnetic field and density the regular embeddings are simply $L(\widetilde{\rho}) = \widetilde{m}$, which is the minimum length of a D3-D7 string, allowing us to identify it with the quark mass as shown. $\tilde{c}$ should then be identified with the quark condensate with the relation shown.

We will classify the D7 brane embeddings by their small $\widetilde{\rho}$ behavior. If the D7

brane touches the black hole horizon, we call it a black hole embedding, otherwise, we call it a Minkowski embedding. We have used Mathematica to solve the equations of motion for the D7 embeddings resulting from (4.13). Typically in what follows, we numerically shoot out from the black hole horizon (for black hole embeddings) or the $\widetilde{\rho} = 0$ axis (for Minkowski embeddings) with Neumann boundary condition for a given $\widetilde{d}$. Then by fitting the embedding function with (4.15) at large $\widetilde{\rho}$ we can read off $\widetilde{m}$ and $\widetilde{c}$.

4.2.2 Thermodynamic potentials

The Hamilton's equations from (4.10) are $\partial_\rho d = \frac{\delta \widetilde{S}}{\delta A_t}$ and $\partial_\rho A_t = -\frac{\delta \widetilde{S}}{\delta d}$. The first simply means that d is the conserved quantity. The second reads as

$$\partial_{\widetilde{\rho}} \widetilde{A}_t = \widetilde{d}\, \frac{\widetilde{w}^4 - \widetilde{w}_H^4}{\widetilde{w}^4 + \widetilde{w}_H^4} \sqrt{\frac{1 + (\widetilde{L}')^2}{\widetilde{K}}}, \tag{4.16}$$

where $\widetilde{A}_t := \frac{\sqrt{2} 2\pi\alpha' A_t}{R\sqrt{2B}}$.

There is a trivial solution of (4.16) with $\widetilde{d} = 0$ and constant $\widetilde{A}_t$ [59]. The embeddings are then the same as those at zero chemical potential. For a finite $\widetilde{d}$, $\tilde{A}'_t$ is singular at $\widetilde{\rho} = 0$ and requires a source. In other words the electric displacement must end on a charge source. The source is the end point of strings stretching between the D7 brane and the black hole horizon. The string tension pulls the D7 branes to the horizon resulting in black hole embeddings [56]. For such an embedding the chemical potential($\widetilde{\mu}$) is defined as [56, 75, 76]

$$\begin{aligned} \widetilde{\mu} &:= \lim_{\widetilde{\rho}\to\infty} \widetilde{A}_t(\widetilde{\rho}) \\ &= \int_{\widetilde{\rho}_H}^{\infty} d\widetilde{\rho}\; \widetilde{d}\, \frac{\widetilde{w}^4 - \widetilde{w}_H^4}{\widetilde{w}^4 + \widetilde{w}_H^4} \sqrt{\frac{1 + (\widetilde{L}')^2}{\widetilde{K}}}, \end{aligned} \tag{4.17}$$

where we fixed $\widetilde{A}_t(\widetilde{\rho}_H) = 0$ for a well defined A_t at the black hole horizon.

The Euclideanized on shell bulk action can be interpreted as the thermodynamic potential of the boundary field theory. The Grand potential ($\widetilde{\Omega}$) is associated with the action (4.9) while the Helmholtz free energy ($\widetilde{F}$) is associated with the Legendre

transformed action (4.10):

$$\begin{aligned}\widetilde{F}(\widetilde{w}_H,\widetilde{d}) &:= \frac{-\widetilde{S}}{N_f T_{D7}(R\sqrt{B})^4 \mathrm{Vol}} \\ &= \int_{\widetilde{\rho}_H}^{\infty} d\widetilde{\rho}\ \frac{\widetilde{w}^4-\widetilde{w}_H^4}{\widetilde{w}^4}\sqrt{\widetilde{K}(1+(\widetilde{L}')^2)}, \end{aligned} \tag{4.18}$$

$$\begin{aligned}\widetilde{\Omega}(\widetilde{w}_H,\widetilde{\mu}) &:= \frac{-S}{N_f T_{D7}(R\sqrt{B})^4 \mathrm{Vol}} \\ &= \int_{\widetilde{\rho}_H}^{\infty} d\widetilde{\rho}\ \frac{\widetilde{w}^4-\widetilde{w}_H^4}{\widetilde{w}^4}\sqrt{\frac{(1+(\widetilde{L}')^2)}{\widetilde{K}}}\times \\ &\qquad \left(\left(\frac{\widetilde{w}^4+\widetilde{w}_H^4}{\widetilde{w}^4}\right)^2\widetilde{\rho}^6+\frac{1}{\widetilde{w}^4}\widetilde{\rho}^6\right), \end{aligned} \tag{4.19}$$

where Vol denote the trivial 7-dimensional volume integral except $\widetilde{\rho}$ space, so the thermodynamic potentials defined above are densities, strictly speaking. Since $\widetilde{K}\sim\widetilde{\rho}^6$, both integrals diverge as $\widetilde{\rho}^3$ at infinity and need to be renormalized. Thermodynamic potentials, (4.17),(4.18) and (4.19) are reduced to $B=0$ case if we simplify omit all $\frac{\widetilde{\rho}^6}{\widetilde{w}^4}$ and then tildes. See for example (4.20).

4.3 Chiral Symmetry Breaking and the Thermal Phase Transition

We begin by reviewing the results of [65–67, 69] on magnetic field induced chiral symmetry breaking and the thermal phase transition to a phase in which the condensate vanishes. While they show the embeddings for fixed T and different values of B, we will show the embeddings for fixed B and different values of T. By fixing B we are using it as the intrinsic scale of symmetry breaking in the same fashion as Λ_{QCD} plays that role in QCD.

Let us digress here to explain how to understand the figures we will present in this chapter. For example, in Fig 4.1 we have three columns. The left is the D7 brane embedding configuration. The middle shows a plot of the allowed values of the condensate $\widetilde{c}$ as a function of the quark mass $\widetilde{m}$ - these are thermodynamical

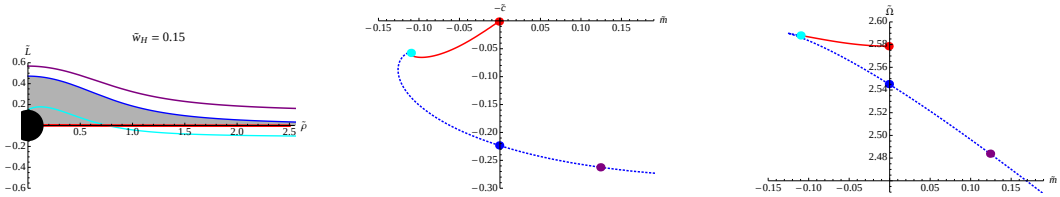

(a) Low temperature - $\widetilde{w}_H = 0.15$. Here we see chiral symmetry breaking with the blue embedding thermodynamically preferred over the red at $\widetilde{m} = 0$.

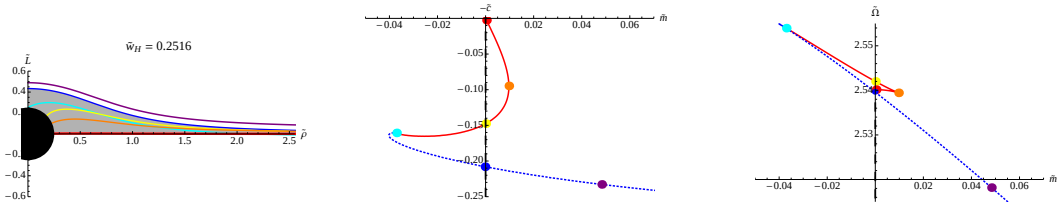

(b) Transition temperature - $\widetilde{w}_H = 0.2516$. This shows the point where the first order chiral symmetry phase transition occurs from the blue to the red embedding. The transition can be identified by considering Maxwell's construction(Middle) or the lowest free energy(Right).

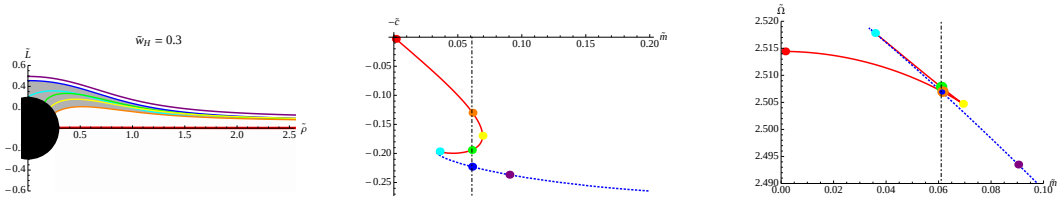

(c) Above the transition - $\widetilde{w}_H = 0.3$. This is the chiral restored phase with the $\widetilde{m} = 0$ curve lying along the $\widetilde{\rho}$ axis (red).

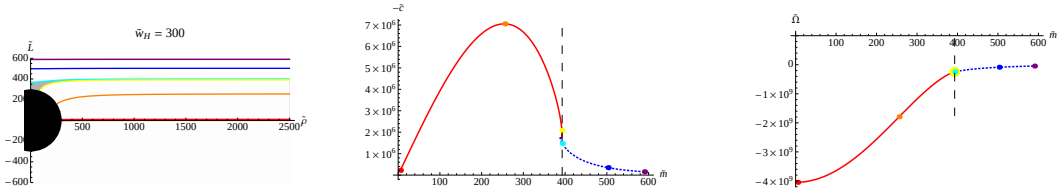

(d) High temperature - $\widetilde{w}_H = 300$. Here the magnetic field is negligible and the embeddings show the usual finite temperature meson melting transition.

Figure 4.1: The D7 brane embeddings(Left), their corresponding $\widetilde{m} - \widetilde{c}$ diagrams(Middle), and the Free energies(Right) in the presence of a magnetic field at finite temperature. (Parameters are scaled or $B = 1/2R^2$ in terms of parameters without tilde.)

conjugate variables. The right is the corresponding thermodynamic potential. Each row is for a fixed parameter we are varying - here it's temperature. The left and middle plots are plotted by solving the equation of motion (4.13) with the black hole boundary condition that the embedding is orthogonal to the horizon.

The right hand plot is calculated using (4.18) or (4.19). Both are the same at zero density. We subtract $\lim_{\widetilde{\rho}\to\infty} \frac{1}{4}\widetilde{\rho}^4$ to remove the common infinite component.

Every *point* in the middle and right plots corresponds to one embedding *curve* in the left plot. These points are color coded with the colors common across each of

the three plots. The order of colors follows the rainbow from the bottom embedding as a mnemonic.

In the middle plot we can find any transition point by a Maxwell construction (an equal area law), which is also confirmed by the minimum of the grand potential on the right. The vertical dashed line in the middle and right hand plots corresponds to the transition point.

In the left plots the gray region contains embeddings that are excluded since they are unstable, as shown in the middle and on the right.

The results for the case of a constant magnetic field and varying temperature are displayed in Fig 4.1a-d. The Fig 4.1a (Left) shows the D7 embeddings when $T \ll B$ and the black hole is small. The embeddings are driven away from the origin of the $\widetilde{L} - \widetilde{\rho}$ plane - this behaviour is a result of the inverse powers of $\widetilde{w}$, when $\widetilde{w}_H \ll 1$, in the Lagrangian (4.13) which lead the action to grow if the D7 approaches the origin (note that the factor of $\widetilde{\rho}^3$ multiplying the action means the action will never actually diverge). There are also embeddings that end on the black hole (shown in red) but they are thermodynamically disfavoured as shown in Fig 4.1a (Right).

At large $\widetilde{\rho}$ the stable embedding with $\widetilde{m} = 0$ has a non-zero derivative so $\widetilde{c}$ is non-zero and there is a chiral condensate *i.e.* chiral symmetry breaking. The U(1) symmetry in the Ω_1 direction is clearly broken by any particular embedding too. We can numerically read off the values of $\widetilde{m}$ and $\widetilde{c}$ from the embeddings and their values are shown in Fig 4.1a (Middle), where the dotted blue curves are for Minkowski embeddings, whilst the red curves are for black hole embeddings.

If the temperature is allowed to rise sufficiently then the black hole horizon grows to mask the area of the plane in which the inverse $\widetilde{w}$ terms in the Lagrangian are large. At a critical value of T the benefit to the $\widetilde{m} = 0$ embedding of curving off the axis becomes disfavoured and it instead lies along the $\tilde{\rho}$ axis - chiral symmetry breaking switches off. This first order transition occurs at $\tilde{w}_H = 0.2516$ as shown in Fig 4.1b by Maxwell's construction (Middle) and by lower grand potential (Right). Our value for the critical temperature agrees with the value $\widetilde{B} = 16$ in [69] since our $\widetilde{w}$ is the same as $\sqrt{\frac{1}{\widetilde{B}}}$ in [69].

We show an example of the embeddings above the critical temperature, their grand potential and the evolution of the curves in the $\widetilde{m} - \widetilde{c}$ plane in Fig 4.1c.

The Fig 4.1d shows a case when $T \gg B$ when the area of the plane in which B is important is totally masked by the black hole and the results match those of the usual finite T version of the $\mathcal{N}$=2 theory. For $\widetilde{m} > \tilde{w}_H$ the embeddings are Minkowski like whilst for small $\widetilde{m}$ they fall into the black hole. There is a first order phase transition between these two phases which is the meson melting phase transition discussed in detail in [77–81]. Minkowski embeddings have a stable mesonic spectrum [54] whilst in the case of black hole embeddings the black holes' quasi-normal modes induce an imaginary component to the meson masses [61, 62]. We can see that the previously reported "meson melting" transition at large quark mass becomes also the chiral symmetry restoring transition at zero quark mass.

4.4 Finite density or chemical potential at zero temperature

We can now turn to the inclusion of finite density or chemical potential in the theory with magnetic field. In this section we consider the zero temperature ($\tilde{w}_H = 0$) theory only, and will continue to finite temperature in the next section.

A finite density (chemical potential) at zero temperature has been studied in the $\mathcal{N}$=2 theory without a magnetic field in [58], where analytic solutions for both a black hole like embedding and a Minkowski embedding have been found. When a magnetic field is turned on, analytic solutions are not available any more, but we have found numerical solutions that continuously deform from the known analytic solutions at zero magnetic field.

Minkowski embedding solutions correspond to zero density and finite chemical potential. The black hole like embedding is the embedding deformed by the density - a spike forms from the D7 down to the origin of the $\widetilde{L} - \widetilde{\rho}$ plane (Fig 4.2d (Left)) which has been interpreted as an even distribution of strings (*i.e.* quarks) forming in the vacuum of the gauge theory.

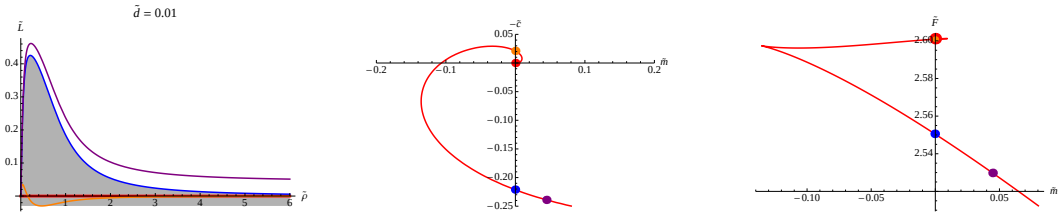

(a) Low density - $\widetilde{d} = 0.01$. Here we see chiral symmetry breaking (the blue embedding is preferred over the red embedding) and a spiral structure in the $\widetilde{m}$ vs $\widetilde{c}$ plane.

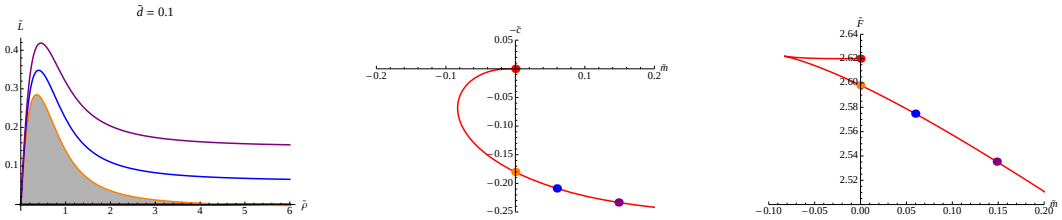

(b) Increasing density below the transition - $\widetilde{d} = 0.1$. There is still chiral symmetry breaking here with the orange embedding preferred to the red. Note the spiral structure in the $\widetilde{m} - \widetilde{c}$ plane has disappeared.

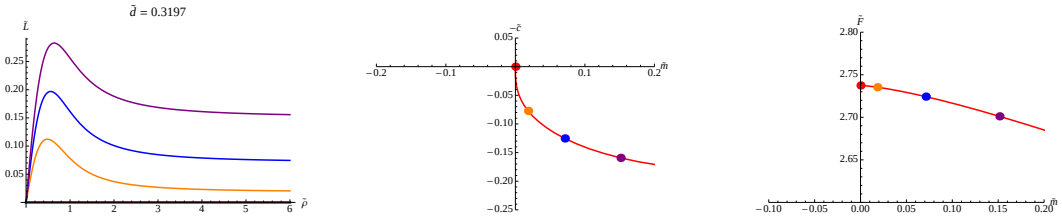

(c) Transition point - $\widetilde{d} = 0.3197$. This shows the point where the second order chiral symmetry phase transition occurs.

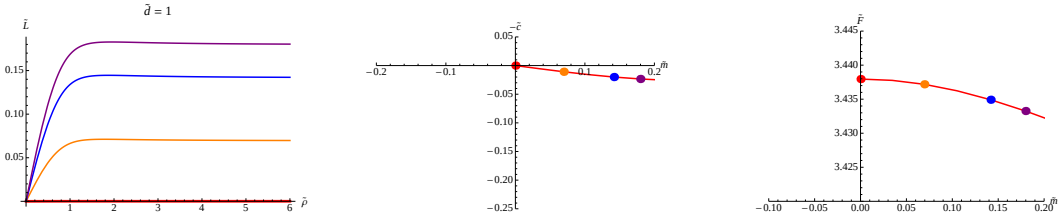

(d) High density $\widetilde{d} = 1$. This is the chiral restored phase with the $\widetilde{m} = 0$ curve lying along the $\widetilde{\rho}$ axis. For larger $\widetilde{m}$ the usual spike like embedding can be seen.

Figure 4.2: The D7 brane embeddings(Left), their corresponding $\widetilde{m} - \widetilde{c}$ diagrams(Middle), and the Free energies(Right) in the presence of a magnetic field at finite density. (Parameters are scaled or $B = 1/2R^2$ in terms of parameters without tilde.)

First of all it will be interesting to see how the repulsion from the origin induced by a magnetic field and the attraction to the origin by the density compete. Thus we start with the canonical ensemble (that is solutions with non-zero $\widetilde{d}$) and consider black hole like embeddings exclusively. The plot in Fig 4.2a (Left) shows the embeddings for a small value of density. The solutions show the chiral symmetry breaking behaviour induced by the magnetic field but then spike to the origin by the density at small $\widetilde{\rho}$. For $\widetilde{m} = 0$ one should compare the blue and red embeddings

- the blue one is thermodynamically preferred as shown in Fig 4.2a (Right). The theory shows similar behavior to that seen at zero density: there is a spiral structure in the $\widetilde{m}$ vs $\widetilde{c}$ plane (Fig 4.2a (Middle)) [65–67]. That will disappear as the density increases.

As the density increases the value of the condensate for the $\widetilde{m} = 0$ embeddings falls - we show a sequence of plots for growing $\tilde{d}$ in Fig 4.2b-d (Middle). There is a critical value of $\widetilde{d} = 0.3197$ where $\widetilde{c}$ becomes zero for the massless embeddings - above this value of $\widetilde{d}$, D7 embedding is flat and lies along the $\tilde{\rho}$ axis (4.2c-d (Left)) . One can see from the plots that there is a second order phase transition to a phase with no chiral condensate. In Fig 4.2c (Left) and 4.2d (Left) we show embeddings at the critical value of $\widetilde{d}$ and above it respectively. At very large density the solutions become the usual spike embeddings of the $\mathcal{N} = 2$ theory at zero magnetic field.

We are not yet done though since there are also Minkowski embedding with zero density but constant chemical potential. These can have lower energy and be the preferred vacuum at a given value of chemical potential - that is, they are important in the Grand Canonical Ensemble. The relevant analysis is in Fig 4.3a (Fig 4.3b-e will be explained in the next section). On the left it shows the three possible types of embedding of the D7 for a given chemical potential at zero temperature. The black curve is the Minkowski embedding (with $\widetilde{d} = 0$), the blue the chiral symmetry breaking spike embedding (with $\widetilde{d} \neq 0$) and the red the chiral symmetry preserving black hole embedding (with $\widetilde{d} \neq 0$). Strictly speaking there is a fourth embedding which lies along the $\tilde{\rho}$ axis and has constant $A_t = \mu$ - its energy is equal for all $\tilde{\mu}$ to that of the red embedding at $\tilde{\mu} = 0$ and is never preferred over the red embedding with density, so we will ignore it hence forth. The trajectory of the three key embeddings in the $\widetilde{d} - \tilde{\mu}$ space is shown in the middle plot (note that again these two variables are thermodynamical conjugate variables). Finally on the right the grand potential is computed. Clearly at low chemical potential the Minkowski embedding is preferred and $\widetilde{d} = 0$. There is a critical value of $\tilde{\mu} = 0.470$ at which a transition occurs to the spike embedding. This transition looks naively first order since it is a transition between a Minkowski embedding and a black hole embedding. However, we can see that the Grand Potential appears smooth and the quark

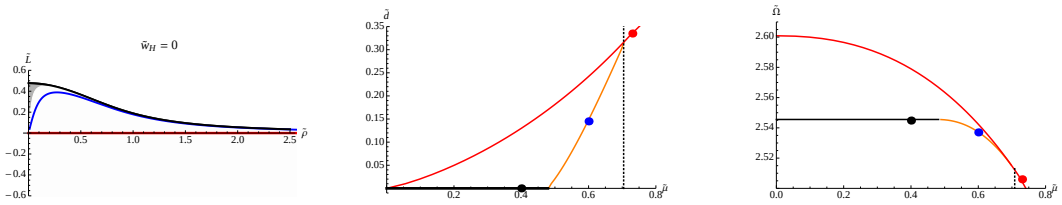

(a) Zero temperature - $\widetilde{w}_H = 0$. The second order meson melting transition and then the second order chiral restoration transition are apparent.

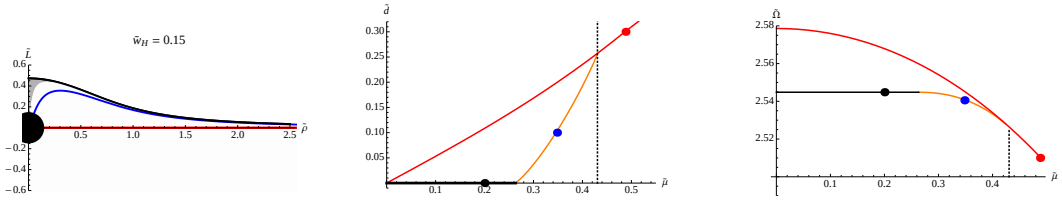

(b) Low temperature - $\widetilde{w}_H = 0.15$. The zero temperature structure remains.

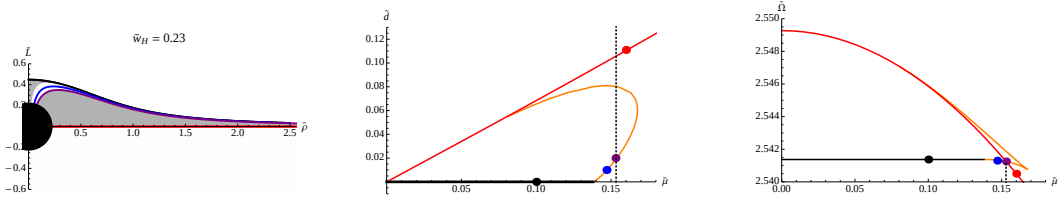

(c) Above the first tri-critical point - $\widetilde{w}_H = 0.23$. The meson melting transitions remains second order but the chiral symmetry restoration transition is first order.

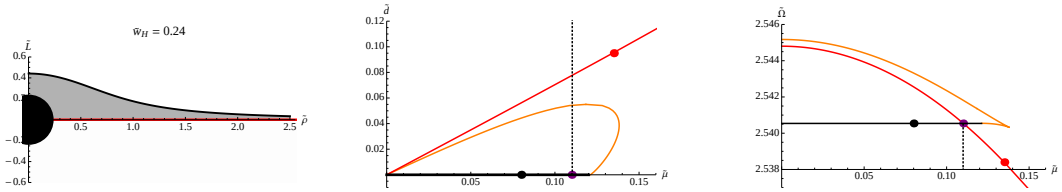

(d) Above the second tri-critical point - $\widetilde{w}_H = 0.24$. There is now only a single first order transition for meson melting and chiral symmetry restoration.

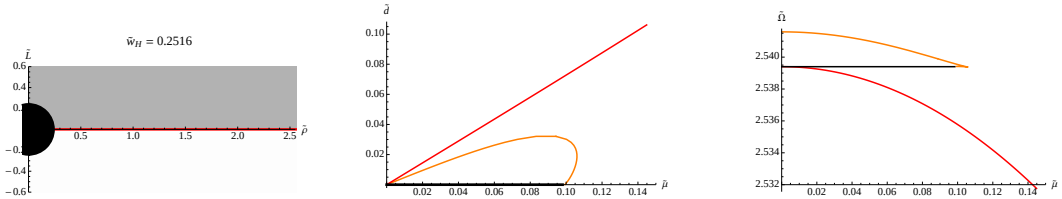

(e) High temperature - $\widetilde{w}_H = 0.2516$. The ground state preserves chiral symmetry for all values of $\tilde{\mu}$.

Figure 4.3: The D7 brane embeddings (Left), their corresponding $\widetilde{d} - \widetilde{\mu}$ diagrams (Middle), and the grand potentials (Right) for massless quarks in the presence of a magnetic field at a variety of temperatures that represent slices through the phase diagram Fig 4.5. (Parameters are scaled or $B = 1/2R^2$ in terms of parameters without tilde.)

density is continuous, which is shown again in Fig.4a. The solid lines in Fig 4.4a are calculated from (4.17), which is based on the holographic dictionary. The dotted lines are obtained by numerically differentiating the grand potential ($\widetilde{d} = -\frac{\partial\widetilde{\Omega}}{\partial\widetilde{\mu}}$), which comes from a thermodynamic relation. This is a nontrivial consistency check

of the holographic thermodynamics as well as our calculation [75, 76, 82].

Further, in Fig 4.4b we plot the behaviour of the quark condensate through this transition. The density and quark condensate are both smooth and the transition looks clearly second order. Here we have tested the smoothness numerically at better than the 1% level. Whether there is some other order parameter that displays a discontinuity is unclear but it would be surprising that any order parameter were smooth, were the transition first order. We conclude the transition is second order (or so weakly first order that it can be treated as second order). This second order nature of the transition from a Minkowski to a spiky embedding has been shown also in the $B = 0, \widetilde{m} \neq 0$ case at zero temperature analytically [58] and numerically [59].

Finally, above the chemical potential corresponding to the meson melting transition ($\widetilde{\mu} = 0.470$), non-zero density is present and the physics already described in the Canonical Ensemble occurs, which turns out to be equivalent to the results from the current Grand Canonical Ensemble. Both Ensemble predict the second order transition to the flat embedding at the same point, $\widetilde{\mu} = 0.708$ or $\widetilde{d} = 0.3197$, which is the chiral symmetry restoration point. Notice that for the Canonical Ensemble we used ($\widetilde{m}$,$\widetilde{c}$) conjugate variables on constant $\widetilde{d}$ slices, while for the Grand Canonical Ensemble we used ($\widetilde{\mu}$,$\widetilde{d}$) conjugate variables on constant $\widetilde{m} = 0$ slices. This agreement from different approaches is another consistency check of our calculation.

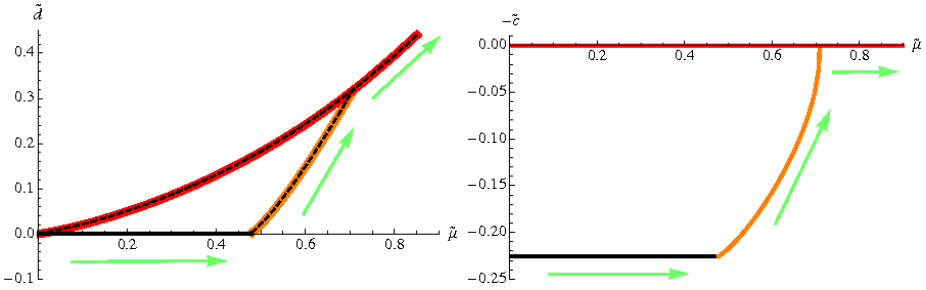

(a) Density: the solid lines are calculated from (4.17) and the dotted lines are obtained by numerically differentiating the grand potential ($\widetilde{d} = -\frac{\partial\widetilde{\Omega}}{\partial\widetilde{\mu}}$).

(b) The quark condensate.

Figure 4.4: Plots of the order parameters vs chemical potential at zero temperature and finite B. Both are continuous across the Minkowski to spiky embedding transition($\widetilde{\mu} \sim 0.47$). The green arrows indicate the changes of phase.

On the gauge theory side of the dual, the description is as follows. At zero density there is a theory with chiral symmetry breaking and bound mesons. As the chemical potential is increased $\widetilde{d}$ remains zero and the quark condensate remains unchanged. Then there is a second order transition to finite density (to a spike like embedding) which is presumably associated with meson melting induced by the medium. At a higher density there is then a further second order transition to a phase with zero quark condensate.

Finally, we note that in paper [83] an alternative ground state was proposed for a chiral symmetry breaking theory at finite density. They proposed that the string spike might end on a wrapped D5 brane baryon vertex in the center of the geometry. We have not considered that possibility here but it will be investigated in detail in chapter 7. The magnetic field induced chiral symmetry breaking provides a system in which this could be cleanly computed without the worries of the hard wall present in that geometry.

4.5 The phase diagram in the grand canonical ensemble

We have identified a first order phase transition from a chiral symmetry breaking phase with meson bound states to a chirally symmetric phase with melted mesons in our massless theory in the presence of a magnetic field with increasing pure temperature. On the finite density axis the meson melting transition is second order and separate from another second order chiral symmetry restoring phase transition. Clearly there must be at least one critical point in the temperature chemical potential phase diagram. We display the phase diagram of the massless theory, which we will discuss the computation of, in Fig 4.5.

To construct the phase diagram we have plotted slices at fixed temperature and varying chemical potential. We display the results in Fig 4.3a-e where we show the embeddings (Left) relevant at different temperatures, their trajectories in the $\widetilde{d}-\widetilde{\mu}$ plane (Middle) and the grand potential (Right).

The phase diagram agrees with our previous results: At zero chemical potential we

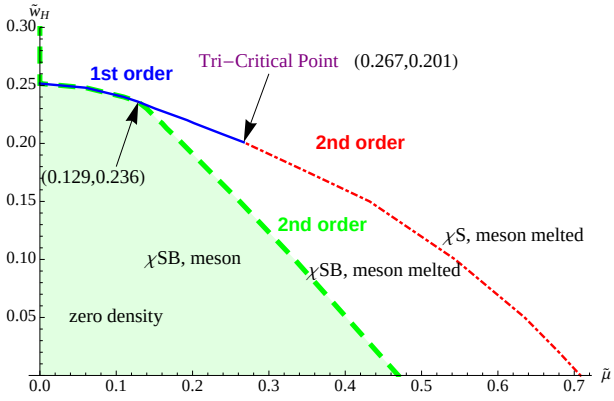

Figure 4.5: The phase diagram of the $\mathcal{N} = 2$ gauge theory with a magnetic field. The temperature is controlled by the parameter $\tilde{w}_H$ and chemical potential by $\tilde{\mu}$. (Parameters are scaled or $B = 1/2R^2$ in terms of parameters without tilde.)

have the transition point $\widetilde{w}_H = 0.2516$. At zero temperature we have the transition point at $\widetilde{\mu} = 0.708$, which corresponds to $\widetilde{d} = 0.3197$. We also identify $\widetilde{\mu} = 0.470$ as the position of the second order transition to a meson melted phase with non-zero $\widetilde{d}$ and chiral condensate $\widetilde{c}$.

The dotted green line is the line along which $\widetilde{d} = 0$ and corresponds to the second order meson melting transition from a Minkowski embedding to a black hole embedding. The transition generates density continuously from zero. The quark condensate also smoothly decreases from its constant value on the Minkowski embedding. We display the continuous behaviour of the quark condensate across the transition in Fig 4.6. Note this means that the slope of the embedding at the UV boundary is continuous through the transition even though the embedding in the IR is discontinuous and topology changing. Again we have checked the smoothness of these parameters numerically to better than the 1% level.

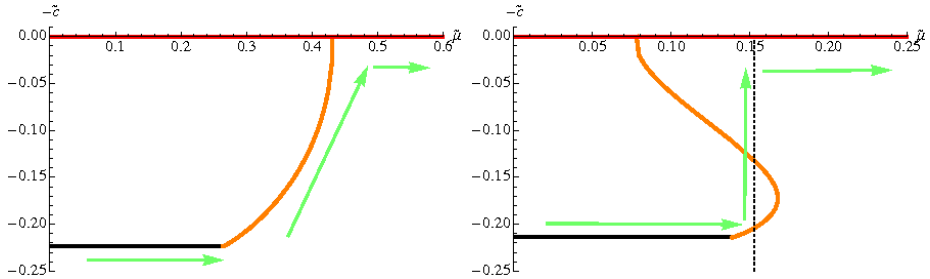

(a) $\widetilde{w}_H = 0.15$ (b) $\widetilde{w}_H = 0.23$

Figure 4.6: Quark condensate vs chemical potential at finite B. Both are continuous across the Minkowski (black) to black hole (orange) embedding transition. At $\widetilde{w}_H = 0.23$ the black hole (orange) to black hole(red) transition is discontinuous.

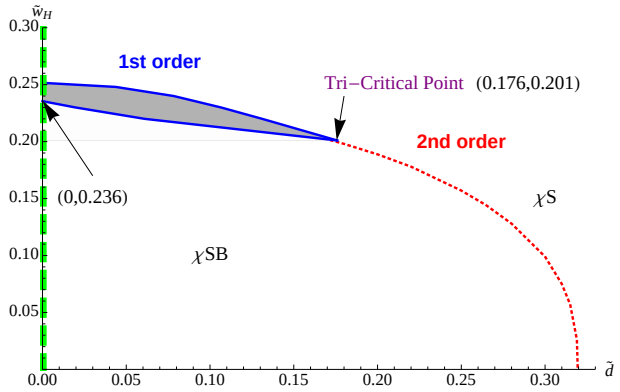

Figure 4.7: The phase diagram of the $\mathcal{N} = 2$ gauge theory with a magnetic field. The temperature is controlled by the parameter $\tilde{w}_H$ and the density by $\widetilde{d}$. (Parameters are scaled or $B = 1/2R^2$ in terms of parameters without tilde.)

The blue line corresponds to a first order transition and the red dotted line is a second order transition in density, chiral condensate etc. The red dotted line is rather special in that this is a phase boundary only at $\widetilde{m} = 0$. This is because this phase boundary is related to the spontaneous breaking of chiral symmetry which only exists at $\widetilde{m} = 0$. At finite $\widetilde{m}$ it must be a cross over region as we will discuss further in section 4.7

The diagram then displays two tri-critical points. It is straightforward to identify where the points lie numerically. The chiral symmetry tri-critical point where the first and second order chiral symmetry restoration transitions join lies at the point $(\widetilde{\mu}, \widetilde{w}_H) = (0.267, 0.201)$. The second tri-critical point where the meson melting transitions join is at $(\widetilde{\mu}, \widetilde{w}_H) = (0.129, 0.236)$.

4.6 The Phase Diagram in the canonical ensemble

We can study the phase diagram also in the canonical ensemble. It is shown in Fig 4.7 and has the same information as Fig 4.5. The pale green region in Fig 4.5 lies in the green dotted line along the $\tilde{w}_H$ axis of Fig 4.7. The chiral symmetry breaking region enclosed by the red, green and blue lines in each figure map onto each other. Similarly the high temperature and density region to the upper right of all the lines in both plots map onto each other. The two double blue lines and the area between them in Fig 4.7 correspond to the single blue line in Fig 4.5, which is natural since

the blue line in Fig 4.5 is a first order transition line and the density change is discontinuous. Thus the gray region in Fig 4.7 is an unstable density region which hides in the phase boundary in Fig 4.5. That region may only be reached by super-cooling or super-heating since it is unstable. The true ground state at those densities and temperatures should be a mixture of the black hole and Minkowski embedding in analogy with the liquid-gas mixture between the phase transition's of water [59]. It's not clear how to realize that mixture in a holographic set-up.

4.7 Finite mass

We next describe the evolution of the phase diagram with quark mass. If we move away from zero quark mass then the second order chiral symmetry restoration phase transition at T=0 but growing chemical potential becomes a cross over transition. This can be seen in Fig 4.2 where for $\widetilde{m} \neq 0$ the non-zero value of the condensate can be seen to change smoothly with changing $\widetilde{\mu}$ and there is no jump in any order parameter. The (chiral) tri-critical point becomes a critical point. However, the other transition lines survive the introduction of a quark mass.

In Fig 4.8. we plot the phase diagram for various quark mass, $\widetilde{m}$, at constant B. The colors represent different quark masses - $\widetilde{m} = 0, 1, 1.5, 2, 3$ from bottom to top are black, red, orange, green, and blue. The solid lines are for finite, fixed B. To show the influence of the magnetic field we also display the $B = 0$ solution as the dotted lines. The gray line shows the motion of the critical points.

In general the magnetic field shifts the transition line up and right, meaning that the magnetic field makes the meson more stable against the temperature/density meson dissociation effect. This is important at small $\widetilde{m}$ but negligible at large $\widetilde{m}$ as expected.

Both critical points survive the introduction of a finite $\widetilde{m}$, even though it looks like there is no critical point in Fig 4.8a. Zooming in on the appropriate region at small chemical potential reveals the two critical point structure as shown in Fig 4.8b. Their positions, as $\widetilde{m}$ changes, are marked by the gray line in Fig 4.8a. The one line

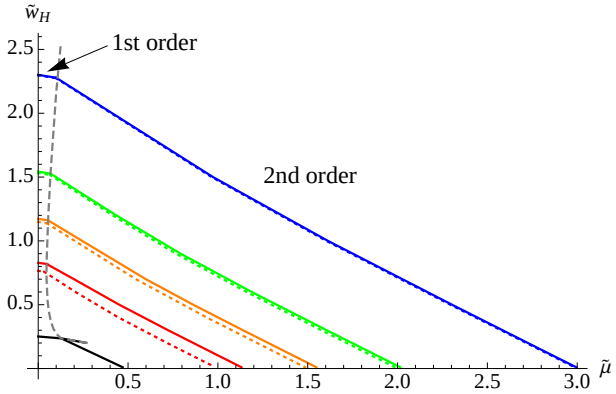

(a) The curves correspond to $\widetilde{m} = 0(\text{black}), 1(\text{red}), 1.5(\text{orange}), 2(\text{green}), 3(\text{blue})$ from bottom to top. The gray line is the path of the critical points.

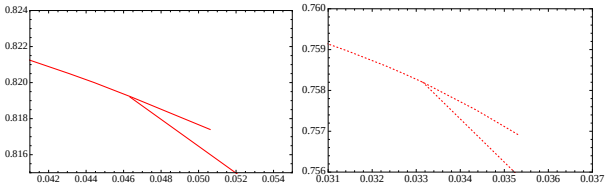

(b) A zoom into figure (a) to show the critical point structure. at small chemical potential. Here we show the detail of $\widetilde{m} = 1$ case, but a similar structure exists for every case.

Figure 4.8: The phase diagram at finite current quark mass with finite B (solid lines) and zero B (dotted lines).

represents the two critical points which are indistinguishable close on the scale of Fig 4.8a. The chiral symmetry critical point moves very close to the other critical point even for a very small mass ($\widetilde{m} \sim 0.01$). The interpretation of the critical points and the phase boundaries are the same as in the $\widetilde{m} = 0$ case in the previous section.

Notice that the black hole to black hole transition exists even in the B=0 case as shown in Fig 4.8b(Right), so it is not purely due to the magnetic field. Nevertheless this transition seems not to have been reported in the previous works [57, 59]. We believe that this is because the transition line between the two critical points is too small to be resolved on the scale of Fig 4.8a, which agrees qualitatively with the figures in [59]. In order to find those transitions we had to slice the temperature down to order 10^{-3} as shown on the vertical axis in Fig 4.8b(Right). Any coarser graining would miss it.

The final surprise relative to the previous work is that the meson melting transition below the critical point appears second order in our work even in the infinite mass limit. To emphasize this we show a number of plots in the $B = 0$ theory in Fig 4.9.

Since the scaled variables (4.15) cannot be used at $B = 0$, (4.19) and (4.17) read in terms of the original coordinates:

$$\begin{aligned}\bar{\Omega}(w_H, \bar{\mu}) &:= \frac{-S}{N_f T_{D7} \mathrm{Vol}} \\ &= \int_{\rho_H}^{\infty} d\rho \, \frac{w^4 - w_H^4}{w^4} \sqrt{\frac{(1 + (L')^2)}{K}} \left(\frac{w^4 + w_H^4}{w^4} \right)^2 \rho^6, \end{aligned} \tag{4.20}$$

where

$$\bar{\mu} = \int_{\rho_H}^{\infty} d\rho \, \bar{d} \, \frac{w^4 - w_H^4}{w^4 + w_H^4} \sqrt{\frac{1 + (L')^2}{K}}, \tag{4.21}$$

$$K = \left(\frac{w^4 + w_H^4}{w^4} \right)^2 \rho^6 + \frac{w^4}{(w^4 + w_H^4)} \bar{d}^2, \tag{4.22}$$

$$\bar{\mu} := \sqrt{2}^3 \pi \alpha' A_t(\infty), \quad \bar{d} := \frac{\sqrt{2}^3}{N_f T_{D7} 2\pi\alpha'} d. \tag{4.23}$$

By the same procedures as in the previous sections we get Fig 4.9. Compared to Fig 4.3, the left column of Fig 4.9 is the chiral condensate instead of the embedding configurations. In Fig 4.3 there is always a red black hole embedding, which corresponds to the flat embedding at zero quark mass. It is not present at finite quark mass.

At very low temperature the transition is Minkowski to black hole and *second order* in the condensate and density(Fig 4.9a). As the temperature goes up a *new* black hole to black hole transition pops up by developing a 'swallow tail' in the grand potential - this transition is first order in the condensate and density(Fig 4.9b). As temperature rises the 'swallow tail' grows continually and eventually "swallows" the *second order* Minkowski to black hole transition (Fig 4.9 c,d). *i.e.* At higher temperature the *second order* Minkowski to black hole transition enters an unstable regime and plays no role any more. Instead only the *first order* Minkowski to black hole transition is manifest. Finally the Minkowski embedding becomes unstable

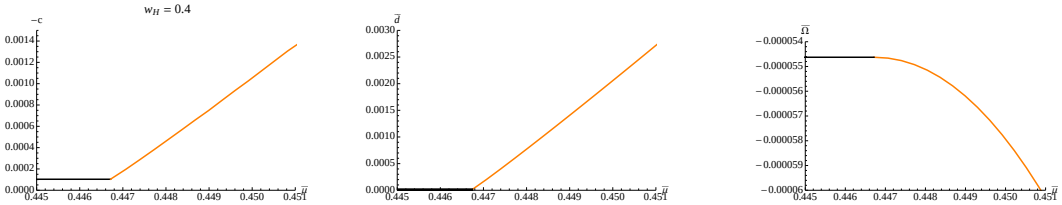

(a) $w_H = 0.4$. At $\bar{\mu} \sim 0.4467$ there is a Minkowski to black hole embedding transition, which is second order in both chiral condensation and density.

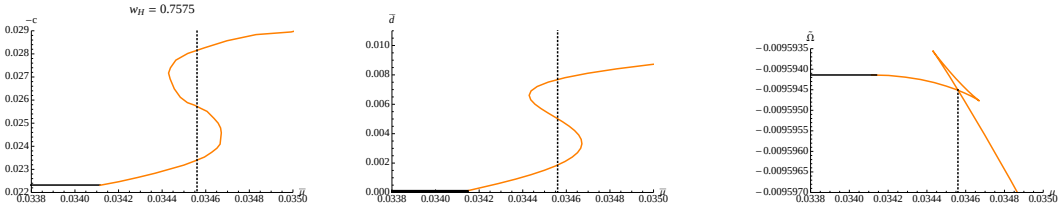

(b) $w_H = 0.7575$. There are two transitions. The first ($\bar{\mu} \sim 0.0341$) is a Minkowski to black hole transition and second order in condensation and density. The second ($\bar{\mu} \sim 0.03455$) is a black hole to black hole transition and first order.

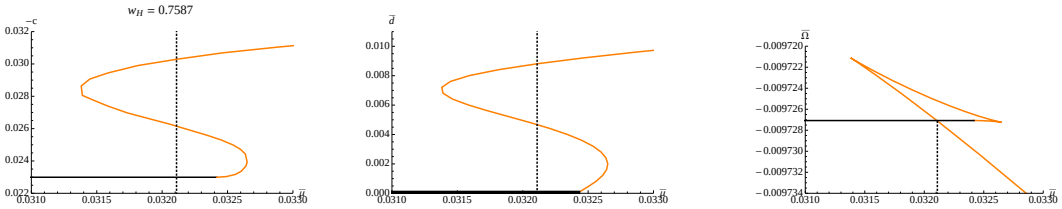

(c) $w_H = 0.7587$. At $\bar{\mu} \sim 0.0321$ there is a Minkowski to black hole embedding transition, which is first order in both chiral condensation and density.

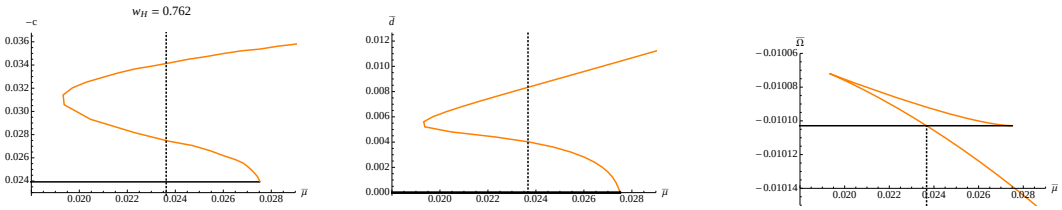

(d) $w_H = 0.762$. At $\bar{\mu} \sim 0.0235$ there is a Minkowski to black hole embedding transition, which is first order in both chiral condensation and density.

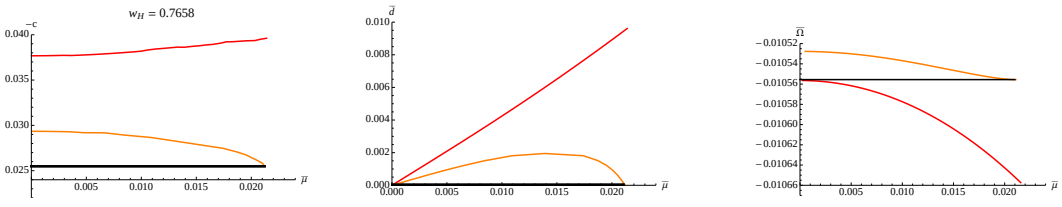

(e) Above $w_H = 0.7658$ only a black hole embedding (Red) is stable configuration.

Figure 4.9: Chiral condensation (Left), density (Middle) and the grand potentials (Right) for massive quarks ($m = 1$) at $B = 0$ at a variety of temperatures that represent slices through the phase diagram Fig 4.8a.

compared to the black hole embedding(Fig 4.9e). At an even higher temperature the Minkowski embedding is not allowed and only a black hole embedding is available (Not shown in Fig 4.9).

These results all match with our work at finite B and increasing mass, confirming

those results and our phase diagrams already presented.

4.8 Comparison to QCD

We have computed the phase diagram for a particular gauge theory using holographic techniques. There are many differences between our theory and QCD: the theory has super partners of the quarks and glue present; it is at large N and small N_f, so quenched (and we have only computed for degenerate quarks to avoid complications involving the non-abelian DBI action); the theory has deconfined glue for all non-zero temperature; the theory has a distinct meson melting transition. In spite of these differences the phase diagram for the chiral condensate shows many of the aspects of the QCD phase diagram so we will briefly make a comparison here.

The QCD phase diagram is in fact not perfectly mapped out since there have only recently been lattice computations attempting to address finite density [20]. The phase structure also depends on the relative masses of the up, down and strange quarks. The standard theoretical picture [18–20] for physical QCD is shown in Fig 4.10a. At zero chemical potential the transition with temperature is second order (or a cross over with massive quarks). At zero temperature there is a first order transition with increasing chemical potential (ignoring any superconducting phase). These transitions are joined by a critical point. Comparing to our theory in Fig 4.5 we see that the transitions' orders are reversed and the pictures look rather different.

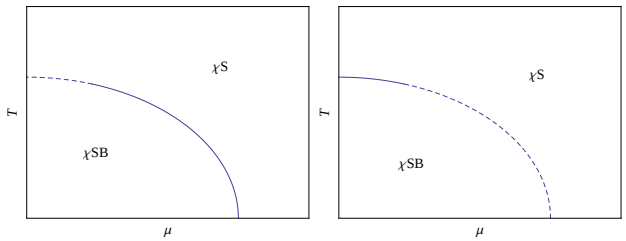

(a) Standard scenario (b) Exotic Scenario

Figure 4.10: Two possible phase diagrams for QCD with the observed quark masses. (a) is the standard scenario found in most of the literature but a diagram as different as (b) remains potentially possible according to the work in [20]. We have not included any color superconducting phase here at large chemical potential.

In fact though as argued in [20] the picture could be very different in QCD. At zero quark mass the finite temperature transition is first order and whether it has changed to second order depends crucially on the precise physical quark masses. Similarly whether the finite density transition is truly first order or second order depends on the exact physical point in the $m_{u,d}$, m_s, μ, T volume. Arguments can even be made for a phase diagram matching that in Fig 4.10b which then matches the structure of the chiral symmetry restoring phase diagram of the theory we have studied. For the true answer in QCD we must wait on lattice developments. Clearly our model will not match QCD's phase diagram point by point in $m_{u,d}$, m_s, μ, T volume but it provides an environment in which clear computation is possible for structures that match some points in that phase space.

Finally, we note a more general point that seems to emerge from the analysis. The introduction of a chemical potential weakens the first order nature of the transitions in our analysis. This matches with results found in QCD on the lattice. The weakening of the first order phase transition is demonstrated for the chiral transition in the light quark mass regime [84, 85], and is shown for the deconfinement transition in the heavy quark mass regime [86, 87].

Chapter 5

Phase diagram of the D3/D5 system in a magnetic field and a BKT transition

5.1 Introduction

In the previous chapter holographic methods where used, specifically a D3/D7 system, for the study of the phase structure of a 3+1d gauge theory with quarks in the fundamental representation in the presence of a magnetic field. That field theory was studied as a loose analogue of QCD as it exhibits confinement and chiral symmetry breaking.

Interest has also turned to the D3/D5 system [94–100] that describes fundamental representation matter fields on a 2+1d defect within a 3+1d gauge theory. This system may have some lessons for condensed matter systems. In [92] an analysis of the D3/D5 system at finite density (d) and at zero temperature (T) revealed that the chiral symmetry breaking transition with increasing magnetic field (B) is not second order but similar to a Berezinskii-Kosterlitz-Thouless (BKT) transition [101] (see also the holographic example in [93, 102]). In a BKT transition the order parameters across the transition grow as $\exp(-a/\sqrt{\nu_c - \nu})$, where a is a constant

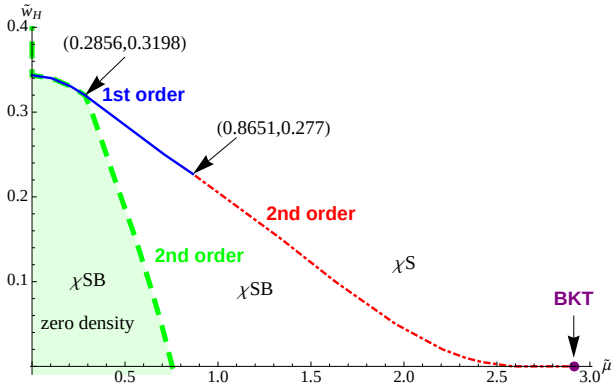

Figure 5.1: The phase diagram for the D3/D5 system. $\tilde{w}_H$ measure the temperature of the theory whilst $\tilde{\mu}$ is the chemical potential. The dashed line is a second order transition associated with the formation of quark density and meson melting. The dotted line is a second order transition for chiral symmetry restoration. In the D3/D5 case that transition ends at a BKT transition point. The continuous line is the merged first order transition. The position of critical points are marked.

and $\nu = d/B$. (ν_c the critical value for the transition). For small T the authors of [92] showed the BKT transition returns to a second order nature. This difference from the D3/D7 case is surprising so it seems worth fleshing out the entire phase diagram for the theory to see if other surprises are present. In this chapter we present that analysis - much of the computation matches that in the D3/D7 system which was presented in chapter 4. Here we very briefly present the formalism and the conclusions. We display the resulting phase diagram for massless matter fields in Fig 5.1b. Clearly much of the structure is similar to the D3/D7 case (see Fig 4.5) but the second order boundary of the chiral symmetry breaking phase is distorted by the presence of the BKT transition.

5.2 The holographic description

The $\mathcal{N}$=4 super Yang-Mills gauge theory at finite temperature has a holographic description in terms of an AdS_5 black hole geometry (with N D3 branes at its core) [46–48]. The geometry can be written as

$$\begin{aligned} ds^2 &= \frac{w^2}{R^2}(-g_t dt^2 + g_x d\vec{x}^2 + g_x dy^2) \\ &\quad + \frac{R^2}{w^2}(d\rho^2 + \rho^2 d\Omega_2^2 + dL^2 + L^2 d\bar{\Omega}_2^2), \end{aligned} \tag{5.1}$$

where $\vec{x}$ is two dimensional, y will be the D3 coordinate not shared by our D5, we have split the transverse six plane into two three planes each with a radial coordinate ρ, L and a two sphere, $R^4 = 4\pi g_s N \alpha'^2$ and

$$g_t := \frac{(w^4 - w_H^4)^2}{2w^4(w^4 + w_H^4)}, \qquad g_x := \frac{w^4 + w_H^4}{2w^4}. \tag{5.2}$$

The temperature of the theory is given by the position of the horizon, $w_H = \pi R^2 T$ We include our 2+1d defect with fundamental matter fields by placing a probe D5 brane in the D3 geometry. The probe limit corresponds to the quenched limit of the gauge theory. The D5 probe can be described by its DBI action

$$S_{DBI} = -T_{D5} \int d^6\xi \sqrt{-\det(P[G]_{ab} + 2\pi\alpha' F_{ab})}, \tag{5.3}$$

where $P[G]_{ab}$ is the pullback of the metric and F_{ab} is the gauge field living on the D5 world volume. We will use F_{ab} to introduce a constant magnetic field (eg $F_{12} = -F_{21} = B$) [65] and a chemical potential associated with baryon number $A_t(\rho) \neq 0$ [56, 75, 76, 103] We embed the D5 brane in the $t, \vec{x}, \rho$ and Ω_2 directions of the metric but to allow all possible embeddings must include a profile $L(\rho)$ at constant $y, \bar{\Omega}_2$. The full DBI action we will consider is then

$$S = \int d\xi^6 \mathcal{L}(\rho) = \left(\int_{S^2} \epsilon_2 \int dt d\vec{x} \right) \int d\rho \; \mathcal{L}(\rho), \tag{5.4}$$

where ϵ_2 is a volume element on the 2-sphere and

$$\begin{aligned} \mathcal{L} \;:=\; & -N_f T_{D5} \frac{\rho^2}{2\sqrt{2}} \left(1 - \frac{w_H^4}{w^4}\right) \\ & \times \sqrt{\left(1 + (\partial_\rho L)^2 - \frac{2w^4(w^4 + w_H^4)}{(w^4 - w_H^4)^2} (2\pi\alpha' \partial_\rho A_t)^2\right)} \\ & \times \sqrt{\left(\left(1 + \frac{w_H^4}{w^4}\right) + \frac{4R^4}{w^4 + w_H^4} B^2\right)}. \end{aligned} \tag{5.5}$$

Since the action is independent of A_t, there is a conserved quantity $d \left(:= \frac{\delta S}{\delta F_{\rho t}}\right)$ and we can use the Legendre transformed action

$$\widetilde{S} = S - \int d\xi^6 F_{\rho t} \frac{\delta S}{\delta F_{\rho t}} = \left(\int_{S^2} \epsilon_2 \int dt d\vec{x} \right) \int d\rho \; \widetilde{\mathcal{L}}(\rho), \tag{5.6}$$

where

$$\widetilde{\mathcal{L}} := -N_f T_{D5} \frac{(w^4 - w_H^4)}{2\sqrt{2}w^4} \sqrt{K(1 + (\partial_\rho L)^2)}, \tag{5.7}$$

$$K := \left(\frac{w^4 + w_H^4}{w^4}\right)\rho^4 + \frac{4R^4B^2}{w^4 + w_H^4}\rho^4 + \frac{4w^4}{(w^4 + w_H^4)}\frac{d^2}{(N_f T_{D5} 2\pi\alpha')^2}. \tag{5.8}$$

To simplify the analysis we note that we can use the magnetic field value as the intrinsic scale of conformal symmetry breaking in the theory - that is we can rescale all quantities in (5.7) by B to give

$$\widetilde{\mathcal{L}} = -N_f T_{D5} (R\sqrt{B})^3 \frac{\widetilde{w}^4 - \widetilde{w}_H^4}{\widetilde{w}^4} \sqrt{\widetilde{K}(1 + \widetilde{L}'^2)}, \tag{5.9}$$

$$\widetilde{K} = \left(\frac{\widetilde{w}^4 + \widetilde{w}_H^4}{\widetilde{w}^4}\right)\widetilde{\rho}^4 + \frac{1}{\widetilde{w}^4 + \widetilde{w}_H^4}\widetilde{\rho}^4 + \frac{\widetilde{w}^4}{(\widetilde{w}^4 + \widetilde{w}_H^4)}\widetilde{d}^2, \tag{5.10}$$

where the dimensionless variables are defined as

$$(\widetilde{w}, \widetilde{L}, \widetilde{\rho}, \widetilde{d}) := \left(\frac{w}{R\sqrt{2B}}, \frac{L}{R\sqrt{2B}}, \frac{\rho}{R\sqrt{2B}}, \frac{d}{(R\sqrt{B})^2 N_f T_{D5} 2\pi\alpha'}\right). \tag{5.11}$$

In all cases the embeddings become flat at large ρ taking the form

$$\widetilde{L}(\widetilde{\rho}) \sim \widetilde{m} + \frac{\widetilde{c}}{\widetilde{\rho}}. \tag{5.12}$$

In the absence of temperature, magnetic field and density the regular embeddings are simply $L(\widetilde{\rho}) = \widetilde{m}$, which is the minimum length of a D3-D5 string, allowing us to identify it with the quark mass as shown. $\tilde{c}$ should then be identified with the quark condensate.

We will classify the D5 brane embeddings by their small $\widetilde{\rho}$ behavior. If the D5 brane touches the black hole horizon, we call it a black hole embedding, otherwise, we call it a Minkowski embedding. We have used Mathematica to solve the equations of motion for the D5 embeddings resulting from (5.9). Typically in what follows, we numerically shoot out from the black hole horizon (for black hole

embeddings) or the $\widetilde{\rho}=0$ axis (for Minkowski embeddings) with Neumann boundary condition for a given $\widetilde{d}$. Then by fitting the embedding function with (5.12) at large $\widetilde{\rho}$ we can read off $\widetilde{m}$ and $\widetilde{c}$.

The Hamilton's equations from (5.6) are $\partial_\rho d = \frac{\delta \widetilde{S}}{\delta A_t}$ and $\partial_\rho A_t = -\frac{\delta \widetilde{S}}{\delta d}$. The first simply means that d is the conserved quantity. The second reads as

$$\partial_{\widetilde{\rho}} \widetilde{A}_t = \widetilde{d}\, \frac{\widetilde{w}^4 - \widetilde{w}_H^4}{\widetilde{w}^4 + \widetilde{w}_H^4} \sqrt{\frac{1+(\widetilde{L}')^2}{\widetilde{K}}}, \tag{5.13}$$

where $\widetilde{A}_t := \frac{\sqrt{2}2\pi\alpha' A_t}{R\sqrt{2B}}$.

There is a trivial solution of (5.13) with $\widetilde{d}=0$ and constant $\widetilde{A}_t$ [59]. The embeddings are then the same as those at zero chemical potential. For a finite $\widetilde{d}$, $\tilde{A}_t'$ is singular at $\widetilde{\rho}=0$ and requires a source. In other words the electric displacement must end on a charge source. The source is the end point of strings stretching between the D5 brane and the black hole horizon. The string tension pulls the D5 branes to the horizon resulting in black hole embeddings [56]. For such an embedding the chemical potential($\widetilde{\mu}$) is defined as

$$\begin{aligned} \widetilde{\mu} &:= \lim_{\widetilde{\rho}\to\infty} \widetilde{A}_t(\widetilde{\rho}) \\ &= \int_{\widetilde{\rho}_H}^{\infty} d\widetilde{\rho}\; \widetilde{d}\, \frac{\widetilde{w}^4 - \widetilde{w}_H^4}{\widetilde{w}^4 + \widetilde{w}_H^4} \frac{\sqrt{1+(\widetilde{L}')^2}}{\sqrt{\widetilde{K}}}, \end{aligned} \tag{5.14}$$

where we fixed $\widetilde{A}_t(\widetilde{\rho}_H)=0$ for a well defined A_t at the black hole horizon.

The generic analysis below with massless quarks and B, T and μ all switched on involve four types of solution of the Euler Lagrange equations. All of these approach the $\tilde{\rho}$ axis at large ρ to give a zero quark mass. Firstly, there are Minkowski embeddings that avoid the black hole so have a non-zero condensate $\widetilde{c}$ - these solutions have $\tilde{d}=0$ so $\tilde{A}_t=\mu$. Secondly, there can be generic black hole solutions with both of $\widetilde{c}$ and $\widetilde{d}$ none zero. Finally there are solutions that lie entirely along the $\tilde{\rho}$ axis so that $\widetilde{c}=0$ but with $\widetilde{d}$ either zero or non zero. In fact the flat embeddings with $\widetilde{d}=0$ are always the energetically least preferred but the other three all play a part in the phase diagram of the theory.

To compare these solutions we compute the relevant thermodynamic potentials. The Euclideanized on shell bulk action can be interpreted as the thermodynamic potential of the boundary field theory. The Grand potential ($\widetilde{\Omega}$) is associated with the action (5.5) while the Helmholtz free energy ($\widetilde{F}$) is associated with the Legendre transformed action (5.6):

$$\begin{aligned}\widetilde{F}(\widetilde{w}_H,\widetilde{d}) &:= \frac{-\widetilde{S}}{N_f T_{D5}(R\sqrt{B})^3\mathrm{Vol}} \\ &= \int_{\widetilde{\rho}_H}^{\infty} d\widetilde{\rho}\ \frac{\widetilde{w}^4-\widetilde{w}_H^4}{\widetilde{w}^4}\sqrt{(1+(\widetilde{L}')^2)}\sqrt{\widetilde{K}}, \qquad (5.15)\\ \widetilde{\Omega}(\widetilde{w}_H,\widetilde{\mu}) &:= \frac{-S}{N_f T_{D5}(R\sqrt{B})^3\mathrm{Vol}} \\ &= \int_{\widetilde{\rho}_H}^{\infty} d\widetilde{\rho}\ \frac{\widetilde{w}^4-\widetilde{w}_H^4}{\widetilde{w}^4}\sqrt{(1+(\widetilde{L}')^2)}\frac{\widetilde{K}(\widetilde{d}=0)}{\sqrt{\widetilde{K}}}, \qquad (5.16)\end{aligned}$$

where Vol denote the trivial 5-dimensional volume integral except $\widetilde{\rho}$ space, so the thermodynamic potentials defined above are densities, strictly speaking. Since $\widetilde{K}\sim\widetilde{\rho}^4$, both integrals diverge as $\widetilde{\rho}^2$ at infinity and need to be renormalized.

5.3 Chiral symmetry restoration by temperature

The chiral symmetry restoration transition by temperature is first order [72] (a transition related to the thermal transition for non-zero mass at B=0 [77–81]). The transition on the gravity side is between a Minkowski embedding that avoids the black hole to an embedding that lies along the $\tilde{\rho}$ axis ending on the black hole. Fig 5.2 shows the $(-\widetilde{c},\widetilde{m})$ diagram for some temperatures ($\widetilde{w}_H=0.25, 0.3435, 0.45$ from the bottom). The solid lines are the black hole embeddings and the dotted lines are Minkowski embeddings. Since we are interested in the case $\widetilde{m}=0$, the condensate is the intersect of the curves with the vertical axis. As temperature goes up the condensate moves from the lower dot to the middle curve continuously, then jumps at $\widetilde{w}_H=0.3435$ to the origin (zero condensate), which corresponds to the chiral symmetric phase. It is also the transition from a Minkowski (dotted line) to a black hole embedding (solid line). This jump can be seen by a Maxwell construction: $\widetilde{m}$ and $\widetilde{c}$ are conjugate variables and the two areas between the middle curve and the

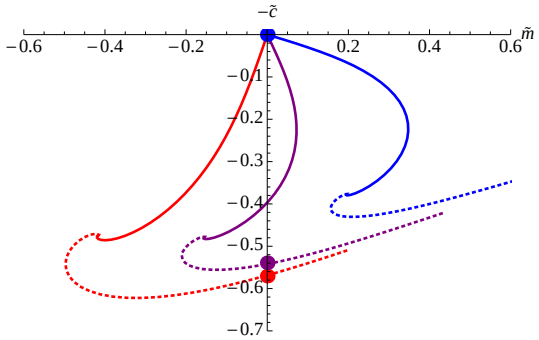

Figure 5.2: A plot of the condensate vs the quark mass to show the first order phase transition at zero chemical potential induced by temperature. The solid line corresponds to the black hole embedding and the dotted line to a Minkowski embedding. From bottom to top the curves correspond to temperatures $\widetilde{w}_H = 0.25, 0.3435, 0.45$.

axis are equal at the transition point. See [72] for more details.

This transition as well as restoring chiral symmetry also corresponds to the melting of bound states of the defect quarks since the Minkowski embedding has stable linearized mesonic fluctuation whilst the black hole embedding has a quasi-normal mode spectrum [61–64].

5.4 Chiral symmetry restoration by density

At zero temperature we find two phase transitions with increasing chemical potential.

At low chemical potentials the preferred embedding is a Minkowski embedding with $\tilde{A}_t = \mu$ so there is no quark density. There is then a transition to a black hole embedding with non-zero quark density, $\widetilde{d}$. This transition, whilst appearing first order in terms of the brane embeddings, displays second order behaviour in all field theory quantities such as the condensate or density (which grows smoothly from zero). The transition also corresponds to the on set of bound state melting since the black hole embedding has quasi-normal modes rather than stable fluctuations.

The chiral symmetry transition induced by density at zero temperature is distinct and also a continuous transition. It has been shown to be of the BKT type for this D3/D5 case [92] as opposed to a mean-field type second order transition as seen in the D3/D7 case in chapter 4 and [91].

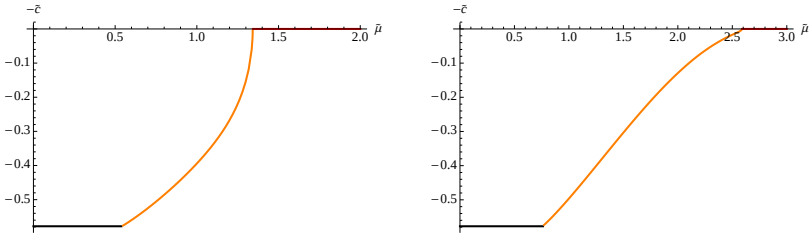

(a) $\widetilde{w}_H = 0.15$

(b) $\widetilde{w}_H = 10^{-5}$

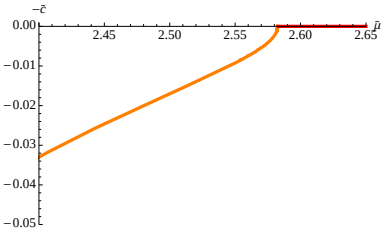

(c) $\widetilde{w}_H = 10^{-5}$ near the critical point

Figure 5.3: Plots of the condensate vs chemical potential on fixed temperature slices, showing the phase structure of the theory. Figure (b) and (c) show that at low temperature the BKT transition becomes second order.

The chiral symmetric phase corresponds to the trivial embedding, $L = 0$. Chiral symmetry breaking is signaled by the instability of small fluctuation around the $L = 0$ embedding. The Free energy (5.15) with (5.9) at zero T reads

$$\widetilde{F} \sim \sqrt{1+\widetilde{L}'^2}\sqrt{\widetilde{\rho}^4 + \frac{\widetilde{\rho}^4}{\widetilde{w}^4} + \widetilde{d}^2}, \tag{5.17}$$

which can be expanded up to the quadratic order in $\widetilde{L}$ as

$$\widetilde{F} \sim -\frac{1}{2}\sqrt{1+\widetilde{\rho}^4+\widetilde{d}^2}\widetilde{L}'^2 + \frac{\widetilde{L}^2}{\widetilde{\rho}^2\sqrt{1+\widetilde{\rho}^4+\widetilde{d}^2}}. \tag{5.18}$$

At $\widetilde{\rho} \gg 1$, $\frac{\widetilde{L}}{\widetilde{\rho}}$ behaves as a scalar with $m^2 = -2$ in AdS_4, while at small $\widetilde{\rho} \ll 1$ and $\widetilde{\rho} \ll \widetilde{d}$ it behaves as a scalar with $m^2 = -\frac{2}{1+\widetilde{d}^2}$ in AdS_2. The Breitenlohner-Freedman (BF) bound of AdS_2 is $-\frac{1}{4}$, so below $\widetilde{d}_c = \sqrt{7}$ the BF bound is violated and the embedding $\widetilde{L} = 0$ is unstable [92]. This critical density corresponds to the critical chemical potential $\widetilde{\mu} \sim 2.9$ as can be computed from (5.14). In [92] it was shown that the condensate scales near this transition as

$$-\widetilde{c} \sim -e^{-\pi\sqrt{\frac{1+\widetilde{d}^2}{\widetilde{d}_c^2-\widetilde{d}^2}}}, \tag{5.19}$$

which corresponds to BKT scaling [101]. This transition is an example of the analysis in [102] where it was shown that if a scalar mass in a holographic model could be tuned through the BF bound a BKT transition would be seen at the critical point.

5.5 Phase diagram in μ-T plane

To compute the full phase diagram we work on a series of constant T slices. We have found the four relevant embeddings discussed above and found those that minimize the relevant thermodynamic potential. The methods and analysis followed is exactly the same as the one in chapter 4, so not many details are given here. Fig 5.3 shows some example plots of the dependence of the condensate on the density on fixed T slices. It shows that the Minkowski embedding with $\widetilde{d} = 0$ is preferred at low $\tilde{\mu}$, a black hole embedding with growing $\widetilde{d}$ at intermediate $\tilde{\mu}$, before finally a transition to a flat embedding occurs at high chemical potential.

Qualitatively the phase diagram, shown in Fig 5.1, is almost the same as the D3/D7 case (see Fig 4.5) - the two second order transitions at zero temperature converge at two critical points to form the first order transition identified at zero density. The only difference is induced by the chiral phase transition at zero T. Comparing to the D3/D7 case we see there is a long tail near zero T, the end point of which corresponds to the BKT transition. However even infinitesimal temperature turns it into mean-field type second order transition [92, 93]. In Fig 5.3(b),(c) we plot the condensate against μ at a very low temperature ($\widetilde{w}_H = 10^{-5}$)to show the second order nature.

Chapter 6

Towards a Holographic Model of the QCD Phase Diagram

The QCD phase diagram is notoriously difficult to compute. Firstly, the physics associated with deconfinement or chiral symmetry restoration is strongly coupled where we traditionally do not know how to compute. Secondly, at finite density lattice gauge theory, the first principles simulation of the theory on supercomputers, suffers a "sign problem" that means Monte Carlo methods break down. In fact with light quarks there is no clear order parameter for deconfinement so we will concentrate on the chiral transition. Progress has been made by identifying effective theories of the transitions and through lattice computations at low density. [104] and section 2.6 provides a review of the standard picture of the QCD phase diagram.

It is interesting to ask whether holographic models can in principle describe a phase diagram like that of real QCD. An example of a holographic model of 3+1d strongly coupled theory has been explored in chapter 4, without having any success in reproducing the standard phase diagram of QCD. In this chapter we will follow a more phenomenological approach in order to study a holographic model of quark fields, in an attempt to reproduce key features of the QCD phase diagram.

Quarks can be introduced into the AdS/CFT Correspondence through probe

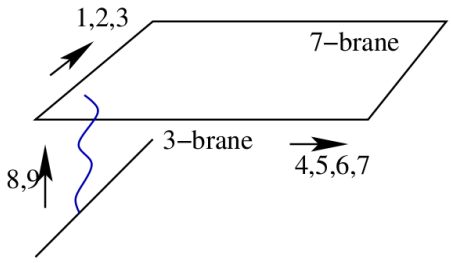

Figure 6.1: A schematic of the D3/D7 showing our conventions. The D3-D3 strings generate the $\mathcal{N} = 4$ theory, the D3-D7 string represent the quarks and D7-D7 strings describe mesonic operators.

branes [39, 51–54] and a number of systems with chiral symmetry breaking have been developed [42, 65, 77, 106–108]. True QCD can not be described holographically because the holographic dual, if it exists, is not known and is probably very complicated (and strongly coupled, at least, in the UV). The analysis followed here is therefore in the spirit of AdS/QCD [109, 110], a phenomenological modeling of the QCD phase diagram. If one could model the phase diagram correctly one might hope to then predict other features of the theory such as time dependent dynamics during transitions and so forth.

The models developed in this chapter will be in the context of the simplest brane construction of a 3+1d gauge theory with quarks which is the D3/D7 system of Fig 6.2 [39, 51–54]. The basic gauge theory is large N, $\mathcal{N} = 4$ super Yang-Mills with N_f quark fields. On the gauge theory side the D7 branes, that provide the quarks, are not backreacted on the geometry but instead the probe approximation [51] is adapted, which corresponds to the quenched approximation in the field theory side. The theory has a $U(1)$ symmetry under which a fermionic quark anti-quark condensate has charge 2 and plays the role of $U(1)$ axial [77]. Although the theory does not have a non-abelian chiral symmetry (as for example the Sakai Sugimoto model does [42]) this is not important in the quenched approximation since the dynamics of the formation of the quark condensate is flavour independent. The model is very simple to work with having a background geometry that is just $\mathrm{AdS}_5 \times S^5$ and the gauge theory is 3+1d at all energy scales.

So called top down models of this type exist which exhibit chiral symmetry breaking. Supergravity solutions exist that correspond to the AdS space being

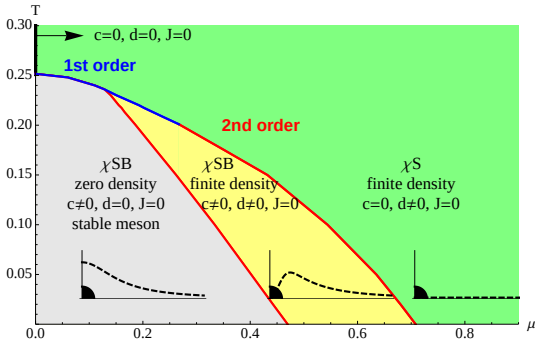

Figure 6.2: The phase diagrams of the massless $\mathcal{N} = 2$ gauge theory with a magnetic field. First order transitions are shown in blue, second order transitions in red. The temperature is controlled by the parameter T, chemical potential by μ and electric field by E. The inset diagrams are representative probe brane embeddings (dotted lines), where a black disk represents a black hole.

deformed in reaction to a running coupling introduced by a non-trivial dilaton profile [77, 107]. In cases where the coupling grows in the infra-red (IR), breaking the conformal symmetry, chiral symmetry breaking is induced. These models have very specific forms for the running coupling and are typically singular somewhere in the interior. At the string theory level a full interpretation is lacking.

A yet simpler and completely computable case (top-down) with chiral symmetry breaking is provided by introducing a background magnetic field associated with $U(1)$ baryon number [65]. Such a background source can be described by a gauge field on the surface of the D7 brane. A chiral condensate is induced. Very simplistically one can think of the B-field as introducing a scale that breaks the conformal symmetry as the strong coupling scale $\Lambda_{\rm QCD}$ does in QCD allowing the strong dynamics to form the quark condensate. In chapter 4 (see also [111–114]) we have explored the phase structure of the theory with magnetic field . The phase diagram of the theory is shown in Fig 6.2. The chiral restoration transition was found to be first order with temperature and second order with density. A tricritical point lies between these regimes.

In paper [116] a similar, to chapter 4, top down analysis was performed but instead of having a magnetic field inducing chiral symmetry breaking, a running dilaton geometry was used. The geometry is that of [117] in which there is a non-zero profile for both the dilaton and axion fields in AdS. The field theory is the $\mathcal{N} = 4$ gauge theory with a vev for both $\mathrm{Tr}F^2$ and $\mathrm{Tr}F\tilde{F}$ which preserves supersymmetry

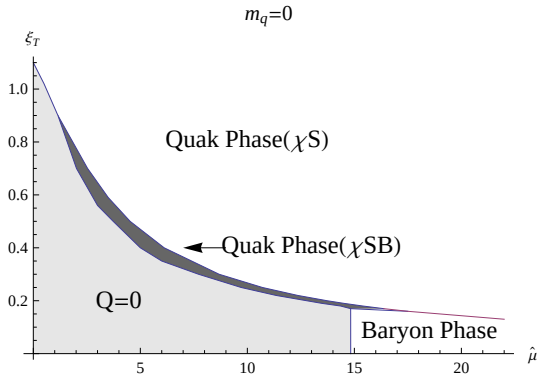

Figure 6.3: The phase diagram of the massless axion/dilaton gauge theory in [116].

at zero temperature but displays confinement. A D7 was introduced in a supersymmetry breaking fashion and chiral symmetry breaking is observed. The temperature density chiral transformation was first order throughout the plane and is shown in Fig 6.3. It shows the same three phases as the magnetic field case. An extra component of the analysis in [116] was to note that in the confining geometry with a running dilaton a baryonic phase was also present. A baryon vertex is described by a D5 brane wrapped on the S^5 of the $\mathrm{AdS}_5 \times S^5$ space. More about holographic baryons will be explained in chapter 7. Finally, the phase diagram of this setup (Fig 6.3) is certainly unlike QCD.

The phase structures mentioned above are very interesting and surprisingly complex but do not match the expectations in QCD. In QCD, a second order transition with temperature and a first order transition with density to the chirally symmetric phase is expected (standard picture).

In this chapter, we want to work in a much more generic framework to ask what phase structures it is possible to get in the holographic description and to try to force ourselves onto a representation of the QCD phase diagram. We will therefore take a bottom up approach within the model and allow ourselves to dial the running of the gauge coupling by hand. We will have a dilaton profile that smoothly transitions from a UV conformal regime to an IR conformal regime through a step of variable height and width. Such an ansatz allows one to consider runnings that range from precocious growth in the IR to more walking like dynamics [118]. A similar ansatz was used in [108] to study the impact of walking

on meson physics and as a mechanism for generating inflation [119]. Here, in a completely new analysis of the phase structure of these models, we find that with the simple step ansatz we can move from a totally first order transition in the phase plane to a configuration similar to that we obtained with a B field (a first order transition with temperature but second order with density). With this ansatz we can not achieve a second order transition with temperature.

The model directly suggests other phenomenological generalizations though. In particular, if we think of the running dilaton profile as a short cut for including the back reaction due to the quark fields/D7 brane [1], then it is natural to break the $SO(6)$ symmetry of AdS_5 in the dilaton in the same fashion as the D3/D7 system's geometry. This allows us an extra phenomenological freedom to distort the dilaton or black hole horizon. These simple changes do allow us to reproduce a wide range of phase diagrams including QCD-like ones as we will show below. We will discuss the simple geometric reasons for the emergence of first or second order transitions in these different scenarios.

Our conclusions derived from this anaysis is that holographic model has no intrinsic problem with mimicking the QCD phase diagram and these systems may therefore be phenomenologically useful in the future.

6.1 The Model

First let us review the gravity dual description of the symmetry breaking behaviour of our strongly coupled gauge theory.

Dp-branes are p dimensional membrane like objects to which the ends of open strings are tied. The weak coupling picture for our D3/D7 set up is shown in Fig 6.2 [39, 51–54] - there are N D3 branes and the lightest string states with both ends on the D3 generate the adjoint representation fields of the $\mathcal{N} = 4$ gauge theory. Strings stretched between the D3 and the D7 are the quark fields lying in the

[1] In [120], D3-D7 solutions at finite temperature and chemical potential, with the inclusion of dynamical flavor effects, have been derived and studied as full-fledged top-down models. They will be the first step towards the top-down study of phase transitions in D3-D7 systems with dynamical flavors.

fundamental representation of the $SU(N)$ group (they have just one end on the D3).

In the strong coupling limit the D3 branes in this picture are replaced by the geometry that they induce. We will consider a gauge theory with a holographic dual described by the Einstein frame geometry $\mathrm{AdS}_5 \times S^5$

$$\mathrm{d}s^2 = \frac{r^2}{R^2}\mathrm{d}x_4^2 + \frac{R^2}{r^2}\left(\mathrm{d}\varrho^2 + \varrho^2\mathrm{d}\Omega_3^2 + \mathrm{d}w_5^2 + \mathrm{d}w_6^2\right), \tag{6.1}$$

where we have split the coordinates into the x_{3+1} of the gauge theory, the ϱ and Ω_3 which will be on the D7 brane world-volume and two directions transverse to the D7, w_5, w_6. The radial coordinate, $r^2 = \varrho^2 + w_5^2 + w_6^2$, corresponds to the energy scale of the gauge theory. The radius of curvature is given by $R^4 = 4\pi g_s N \alpha'^2$ with N the number of colours. The $r \to \infty$ limit of this theory is dual to the $\mathcal{N} = 4$ super Yang-Mills theory where $g_s = g_{\mathrm{UV}}^2$ is the constant large r asymptotic value of the gauge coupling.

In addition we will allow ourselves to choose the profile of the dilaton as $r \to 0$ to represent the running of the gauge theory coupling, $e^{\phi} \equiv \beta$, where the function $\beta \to 1$ as $r \to \infty$. An interesting phenomenological case is to consider a gauge coupling running with a step of the form [108, 119]

$$\beta(r) = A + 1 - A\tanh\left[\Gamma(r - \lambda)\right]. \tag{6.2}$$

Of course in this case the geometry is not back reacted to the dilaton and the model is a phenomenological one in the spirit of AdS/QCD [109, 110]. This form introduces conformal symmetry breaking at the scale $\Lambda = \lambda/2\pi\alpha'$ which triggers chiral symmetry breaking. The parameter A determines the increase in the coupling across the step.

We will introduce a single D7 brane probe [51] into the geometry to include quarks - by treating the D7 as a probe we are working in a quenched approximation although we can reintroduce some aspects of quark loops through the running coupling's form if we wish (or know how). This system has a $U(1)$ axial symmetry on the quarks, corresponding to rotations in the w_5-w_6 plane, which will be broken

by the formation of a quark condensate.

In the true vacuum at $T = 0$ the brane will be static. We must find the D7 embedding function e.g. $w_5(\varrho), w_6 = 0$. The Dirac Born Infeld (DBI) action in Einstein frame is given by

$$\begin{aligned} S_{D7} &= -T_7 \int \mathrm{d}^8\xi e^{\phi}\sqrt{-\mathrm{det}P[G]_{ab}} \\ &= -\overline{T}_7 \int \mathrm{d}^4x\ d\varrho\ \varrho^3\beta\sqrt{1+(\partial_\varrho w_5)^2}, \end{aligned} \tag{6.3}$$

where $T_7 = (2\pi)^{-7}\alpha'^{-4}g_{\mathrm{UV}}^{-1}$ and $\overline{T}_7 = 2\pi^2 T_7$ when we have integrated over the 3-sphere on the D7. The equation of motion for the embedding function is therefore

$$\partial_\rho\left[\frac{\beta\varrho^3\partial_\varrho w_5}{\sqrt{1+(\partial_\varrho w_5)^2}}\right] - 2w_5\varrho^3\sqrt{1+(\partial_\varrho w_5)^2}\frac{\partial\beta}{\partial r^2} = 0. \tag{6.4}$$

The UV asymptotic of this equation, provided the dilaton returns to a constant so the UV dual is the $\mathcal{N} = 4$ super Yang-Mills theory, has solutions of the form

$$w_5 = m + \frac{c}{\varrho^2} + \cdots, \tag{6.5}$$

where we can interpret m as the quark mass ($m_q = m/2\pi\alpha'$) and c is proportional to the quark condensate.

The embedding equation (6.4) clearly has regular solutions $w_5 = m$ when g_{YM}^2 is independent of r - the flat embeddings of the $\mathcal{N} = 2$ Karch-Katz theory [51]. Equally clearly if $\partial\beta/\partial r^2$ is none trivial in w_5 then the second term in (6.4) will not vanish for a flat embedding.

There is always a solution $w_5 = 0$ which corresponds to a massless quark with zero quark condensate ($c = 0$). In the pure $\mathcal{N} = 2$ gauge theory with $\beta = 1$ this is the true vacuum. In the symmetry breaking geometries this configuration is a local maximum of the potential.

If the coupling is larger near the origin then the D7 brane will be repelled from the origin [2]. The parameter Γ spreads the increase in the coupling over a region in r of

[2] In fact there is a competition between the increased action from the D7 entering the region with larger dilaton and the derivative cost of the D7 bending to avoid it. This leads to a critical value of

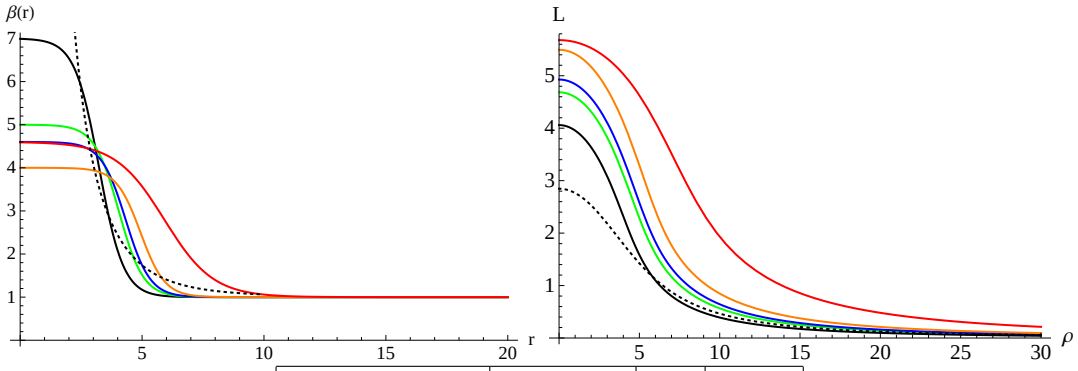

	Γ	A	λ
Black	1	3	3.240
Green	1	2	4.045
Blue	1	1.8	4.325
Orange	1	1.5	4.940
Red	0.5	1.8	5.882
Black(Dotted)	B = 35.6	-	-

Figure 6.4: Example coupling flows (6.2) (top) and the induced D7 brane embeddings/quark self energy (bottom) with the parameter choices shown in the table.

order Γ^{-1} in size.

We display the embeddings for some particular cases in Fig 6.4. Note that we have chosen parameters here that make the vacuum energy of the theory the same in each case. The vacuum energy is given by minus the DBI action evaluated on the solution. In fact this energy is formally divergent corresponding to the usual cosmological constant problem in field theory. As usual we will subtract the UV component of the energy to renormalize.

The symmetry breaking of these solutions is visible directly [77]. The $U(1)$ symmetry corresponds to rotations of the solution in the w_5-w_6 plane. An embedding along the ϱ axis corresponds to a massless quark with the symmetry unbroken (this is the configuration that is preferred at high temperature and it has zero condensate c). The symmetry breaking configurations though map onto the flat case at large ϱ (the UV of the theory) but bend off axis breaking the symmetry in the IR.

One can interpret the D7 embedding function as the dynamical self energy of the quark, similar to that emerging from a gap equation [108]. The separation of the

A to trigger chiral symmetry breaking. For example for $\lambda = 1.7$ and $\Gamma = 1$ $A_c = 2.1$. In this chapter we will consider only super-critical values of A.

D7 from the ϱ axis is the mass at some particular energy scale given by ϱ.

6.1.1 Temperature

Temperature can be included in the theory by using the AdS-Schwarzschild black hole metric. In Einstein frame we have

$$\mathrm{d}s^2 = -\frac{K(r)}{R^2}\mathrm{d}t^2 + \frac{R^2}{K(r)}\mathrm{d}r^2 + \frac{r^2}{R^2}\mathrm{d}\vec{x}_3^2 + R^2 d\Omega_5^2, \tag{6.6}$$

where

$$K(r) = r^2 - \frac{r_H^4}{r^2}, \qquad r_H = \pi R^2 T. \tag{6.7}$$

Witten identified this as the thermal description of the gauge theory in [47]. The parameter r_H is of dimension one in the field theory and preserves the $SO(6)$ symmetry so is identified as shown with temperature T. The black hole is the natural candidate since it has intrinsic thermodynamic properties such as entropy and temperature.

We make the coordinate transformation [77]

$$\frac{rdr}{(r^4 - r_H^4)^{1/2}} \equiv \frac{dw}{w}, \qquad 2w^2 = r^2 + \sqrt{r^4 - r_H^4}, \tag{6.8}$$

with $\sqrt{2}w_H = r_H$, such that the metric becomes

$$\mathrm{d}s^2 = \frac{w^2}{R^2}(-g_t\mathrm{d}t^2 + g_x\mathrm{d}\vec{x}^2) + \frac{R^2}{w^2}(\mathrm{d}\rho^2 + \rho^2\mathrm{d}\Omega_3^2 + \mathrm{d}L^2 + L^2\mathrm{d}\Omega_1^2), \tag{6.9}$$

where

$$\begin{aligned} &g_t = \frac{(w^4 - w_H^4)^2}{w^4(w^4 + w_H^4)}, \quad g_x = \frac{w^4 + w_H^4}{w^4}, \\ &w = \sqrt{\rho^2 + L^2}, \quad \rho = w\sin\theta, \quad L = w\cos\theta. \end{aligned} \tag{6.10}$$

Now we have to transform β also:

$$e^{\phi} = \beta\left(\frac{w^4 + w_H^4}{w^2}\right) \tag{6.11}$$

and therefore

$$\beta = A + 1 - A \tanh\left[\Gamma\left(\sqrt{\frac{(\rho^2+L^2)^2+w_H^4}{\rho^2+L^2}} - \lambda\right)\right]. \tag{6.12}$$

Note that for $w_H \to 0$: $w \to r$, $\rho \to \varrho$ and $L \to w_5$, if we set $w_6 = 0$.

6.1.2 Chemical Potential

The DBI action for the D7 brane naturally includes a surface gauge field which holographically describes the quark bilinear operators $\bar{q}\gamma^\mu q$ and their source, a background $U(1)$ baryon number gauge field [55, 56, 75]. We introduce a chemical potential through the $U(1)$ baryon number gauge field which enters the DBI action in Einstein frame as

$$S_{D7} = -T_7 \int \mathrm{d}^8\xi e^{-\phi}\sqrt{-\det\left(e^{\phi/2}P[G]_{ab} + (2\pi\alpha')F_{ab}\right)}.$$

We allow a chemical potential through $A_t(\rho) \neq 0$. So the Action becomes

$$\begin{aligned} S_{D7} &= \int d^4x\, d\rho\, \mathcal{L} \\ &= -\overline{T}_7 \int d^4x\, d\rho\, \beta(\rho)\rho^3 \sqrt{g_t g_x^3\,(1+L'^2) - \frac{g_x^3}{\beta(\rho)}\tilde{A}_t'^2}. \end{aligned} \tag{6.13}$$

where $\tilde{A}_t' = (2\pi\alpha')A_t'$. In our convention of the metric this is

$$\mathcal{L} = -\overline{T}_7\beta(\rho)\rho^3\ \left(1 - \frac{w_H^4}{w^4}\right)\left(1 + \frac{w_H^4}{w^4}\right)\sqrt{(1+L'^2) - \frac{w^4\left(w^4+w_H^4\right)}{\left(w^4-w_H^4\right)^2}\frac{\tilde{A}_t'^2}{\beta(\rho)}}. \tag{6.14}$$

Now we can Legendre transform the action as we have a conserved quantity, the density, $d\left(=\frac{\delta S_{D7}}{\delta A_t'}\right)$.

$$\tilde{S}_{D7} \;=\; S_{D7} - \int \mathrm{d}^8\xi A_t' \frac{\delta S_{D7}}{\delta A_t'} \;=\; \left(\int_{S3}\epsilon_3 \int \mathrm{d}^4x\right)\int \mathrm{d}\rho\ \tilde{\mathcal{L}},$$

where

$$\begin{aligned} \tilde{\mathcal{L}} &= -\overline{T}_7 \frac{\left(w^4 - w_H^4\right)}{(w^4)}\sqrt{1+L'^2} \\ &\sqrt{\left(\frac{w^4 d^2\beta(\rho)}{\left((2\pi\alpha')^2\overline{T}_7^2\left(w^4+w_H^4\right)\right)} + \frac{\rho^6\left(w^4+w_H^4\right)^2}{w^8}\beta(\rho)^2\right)}. \end{aligned} \tag{6.15}$$

We can redefine $d = (2\pi\alpha')\overline{T}_7\tilde{d}$ to give the simpler expression

$$\tilde{\mathfrak{L}} = -\overline{T}_7 \frac{\left(w^4 - w_H^4\right)}{\left(w^4\right)} \sqrt{1+L'^2} \sqrt{\left(\frac{w^4\tilde{d}^2\beta(\rho)}{\left(w^4+w_H^4\right))} + \frac{\rho^6\left(w^4+w_H^4\right)^2}{w^8}\beta(\rho)^2\right)}. \tag{6.16}$$

By varying the Lagrangian with respect to A_t', we get an expression for $\tilde{d}(\tilde{A}_t')$ which we can invert for an expression for $\tilde{A}_t'(\tilde{d})$

$$\tilde{A}_t' = \tilde{d}\frac{\left(w^4 - w_H^4\right)}{\left(w^4+w_H^4\right)}\sqrt{1+L'^2}\sqrt{\frac{1}{\frac{\tilde{d}^2}{\beta(\rho)}\frac{w^4}{\left(w^4+w_H^4\right)} + \rho^6\left(\frac{w^4+w_H^4}{w^4}\right)^2}}. \tag{6.17}$$

This can be used to find the chemical potential $\mu = \frac{\tilde{\mu}}{(2\pi\alpha')}$

$$\tilde{\mu} = \int_{\rho_H}^{\infty} \mathrm{d}\rho\, \tilde{d}\frac{\left(w^4 - w_H^4\right)}{\left(w^4+w_H^4\right)}\sqrt{\frac{(1+L'^2)}{\frac{\tilde{d}^2}{\beta(\rho)}\frac{w^4}{\left(w^4+w_H^4\right)} + \rho^6\left(\frac{w^4+w_H^4}{w^4}\right)^2}}, \tag{6.18}$$

where $\tilde{\mu}(\rho \to \rho_H) = 0$.

The free energy can be found by integrating the Legendre transformed Lagrangian, the grand potential by integrating the original Lagrangian, where we replace $\tilde{A}_t'(d)$.

$$F = -\frac{\tilde{S}_{D7}}{\overline{T}_7} = \int_{\rho_H}^{\infty} \mathrm{d}\rho\, \frac{\left(w^4 - w_H^4\right)}{\left(w^4\right)}\beta(\rho)\sqrt{1+L'^2} \sqrt{\frac{\tilde{d}^2}{\beta(\rho)}\frac{w^4}{\left(w^4+w_H^4\right)} + \frac{\rho^6\left(w^4+w_H^4\right)^2}{w^8}}.$$

The grand potential is

$$\Omega = -\frac{S_{D7}}{\overline{T}_7} = \int_{\rho_H}^{\infty} \mathrm{d}\rho\, \beta(\rho)\frac{w^4 - w_H^4}{w^4}\rho^6\left(\frac{w^4+w_H^4}{w^4}\right)^2 \sqrt{\frac{(1+L'^2)}{\frac{\tilde{d}^2}{\beta(\rho)}\frac{w^4}{\left(w^4+w_H^4\right)} + \rho^6\left(\frac{w^4+w_H^4}{w^4}\right)^2}},$$

where we need to note that $F(\rho \to \infty) = \Omega(\rho \to \infty) = \rho^3$, so we need to subtract $\frac{1}{4}(\Lambda_{UV})^4$ from both integrals to renormalize them.

6.2 Analysis and results

The methodology to study the phase diagram of our model is straight-forward if laborious. We will work throughout in the massless quark limit. We can think of the scale λ in the dilaton ansatz as our intrinsic scale of the theory and so we will leave that fixed. Then for each choice of parameters in the dilaton profile (A, Γ) we analyze the theory on a grid in T and μ space.

For each point on the T, μ grid we seek three sorts of embedding. The flat embedding $L = 0$ exists in all cases and describes the theory with $m = 0$ and $c = 0$. We use (6.18) to compute the d-μ relation for these embeddings.

We can also seek curved embeddings that miss the black hole. These solutions must have $d = 0$ but are consistent for any value of μ. Here we use the equation of motion for L from (6.16) and numerically shoot from an initial condition at $\rho = 0$ with vanishing ρ derivative, $L'(0) = 0$. We seek solutions that approach $L = 0$ at

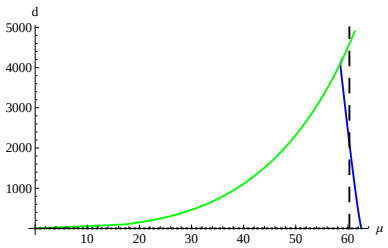

(a) $T = 0.4, A = 30, \Gamma = 0.1, \lambda = 1.715$ - shows a single first order transition.

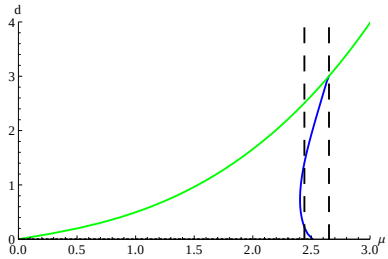

(b) $T = 0.3, A = 3, \Gamma = 1, \lambda = 1.715, \tilde{\alpha} = 3$ - shows a first order transition followed by a second order transition as μ increases.

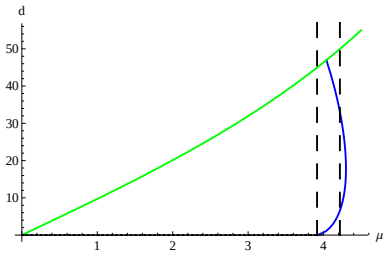

(c) $T = 1.55, A = 30, \Gamma = 1, \lambda = 1.715$ - shows a second order transition followed by a first order transition as μ increases.

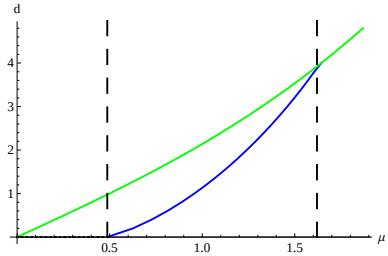

(d) $T = 0.7, A = 3, \Gamma = 1, \lambda = 1.715, \tilde{\alpha} = 3$ - shows two second order transitions.

Figure 6.5: Plots of density d versus chemical potential μ. The top lighter line (green) in each case corresponds to the flat embedding; the horizontal line (black) along the axis is a chiral symmetry breaking (Minkowski) embedding; the near vertical dark line (blue) is a black hole embedding. Transition points are shown by the dotted vertical lines.

large ρ. These configurations have a non-zero condensate parameter c.

Finally we can look for solutions that end on the black hole horizon. To find these we fix the density d and shoot out from all points along the horizon seeking a solution that approaches $L = 0$ at large ρ. We then use (6.18) to compute μ from the solution. In this way we can fill out the T,μ grid. The condensate can again be extracted from the large ρ asymptotics of the embedding.

After finding as many such solutions as exist at each point the easiest method to identify the transition points is to plot the density against μ on fixed T lines. The transitions and their order are then manifest. We display four sample plots in Fig 6.5 taken from scenarios below showing the four cases of the chiral transition and the meson melting transition being respectively first or second order in all combinations.

6.2.1 Dependence on the change in coupling

Let us first consider how the phase diagram depends on the height of the step in the gauge coupling function β. We fix λ (the intrinsic scale of the theory) and also $\Gamma = 1$ and explore the phase structure as a function of A. We display the results for three choices of A in Fig 6.6.

In these and all our future phase diagrams the regions shown are similar to that in Fig 6.2 we will simply display the phase boundaries and their order henceforth.

As mentioned in footnote 2 above there is a critical value of A for chiral symmetry breaking to occur. A conformal theory can not break a symmetry since it offers no scale for that symmetry breaking to occur at. In fact some finite departure from conformality is needed to break the chiral symmetry. For these choices of λ, Γ the critical A is $A_c = 2.1$. We work above this value throughout.

At low A there is a single transition for chiral symmetry restoration and meson melting which is first order for all T and μ. On the gravity side this is a transition between the curved embedding that misses the black hole and the flat embedding. In this case an embedding ending on the black hole never plays a role.

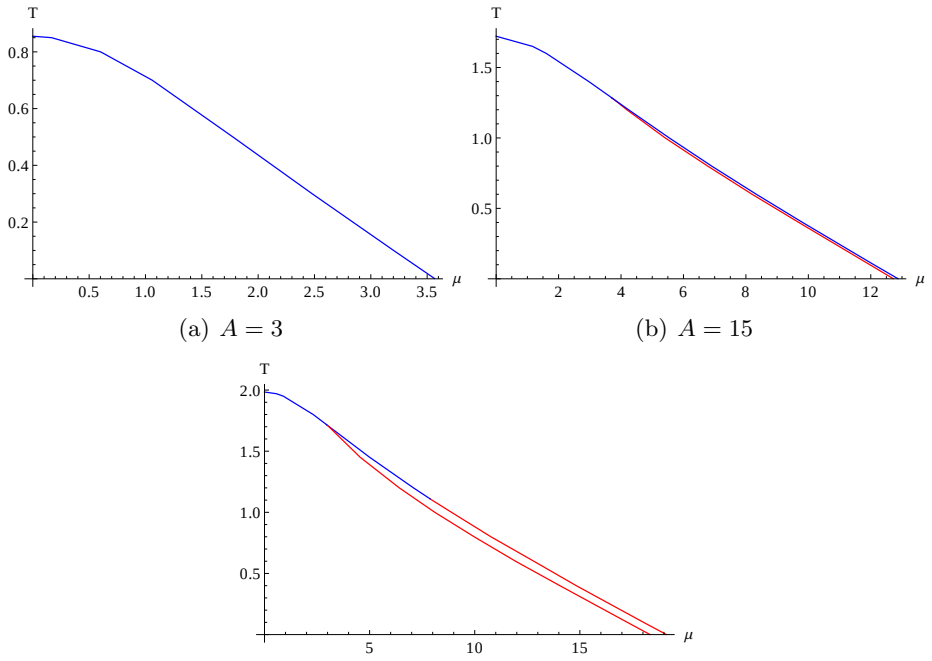

(a) $A = 3$ (b) $A = 15$

(c) $A = 30$

Figure 6.6: Plots for three possible phase diagrams for the choices $A = 3, 15, 30$. Large (small) A gives second (first) order transition at low T. $\Gamma = 1, \lambda = 1.715$.

For larger A, a new phase with chiral symmetry breaking but melted mesons develops. There is a regime now in which the curved embedding ending on the black hole is energetically favoured. The transition from the chiral symmetry breaking phase to this new phase is second order. The chiral symmetry restoration phase remains first order.

At very large A the chiral restoration transition becomes second order at high density. This latter phase resembles that of the theory with chiral symmetry breaking induced by a magnetic field [65]. In fact the B field case can be thought of as our case but with a choice of β given by

$$\beta = \sqrt{1 + \frac{B^2 w^4}{(w^4 + w_H^4)^2}}. \tag{6.19}$$

It is the black dotted curve ($w_H = 0$) in Fig 6.4 - it is not surprising therefore that we see similar phase structure here (and indeed that we do provides strength to our analysis which is capturing the behaviour of top down models).

For very large A the step becomes very sharp and there is little change relative to

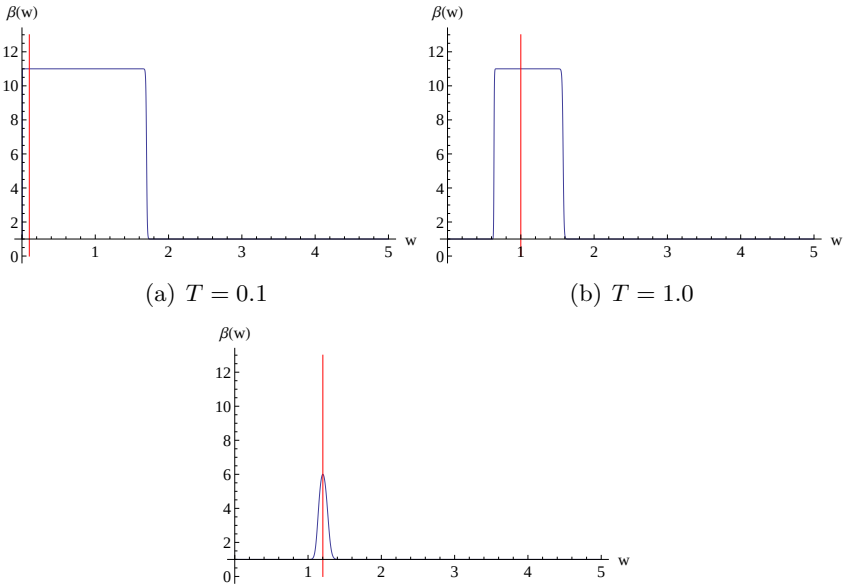

(a) $T = 0.1$

(b) $T = 1.0$

(c) $T = 1.20208 = \frac{\lambda}{\sqrt{2}}$. Dilaton is almost screened. The residual effect is due to finite Γ effect.

Figure 6.7: Plots for parameter choices $A = 5, \Gamma = 100, \lambda = 1.7$. The blue lines show the value of the coupling β. The red line shows the position of the horizon. The final plot corresponds to the point of the first order transition.

our phase diagram in Fig 6.6(c). In particular the thermal transition always remains first order.

The behaviour we are seeing here can be readily explained from the D7 perspective. First of all the zero density transition with temperature is first order for a simple reason. The D7 embedding breaks chiral symmetry at zero temperature because it prefers to avoid the action cost of entering the region in which the dilaton is large. As temperature is introduced through a small horizon the interior of the space is "eaten" but the D7 embedding remains oblivious to this change since it never reaches down to small r. As temperature rises the point of transition is when the horizon moves through the scale λ where the dilaton step is. Once the region with a large dilaton is eaten by the black hole the preferred D7 embedding is the flat one.

In Fig 6.7 we show an extreme case of this behaviour explicitly. Here we have taken Γ very large so that the transition in the dilaton between the low and high value is very sharp. We plot the β profile against our radial parameter w and mark in red the position of the black hole horizon. Note that in the w coordinates the region where β is large depends on the temperature (it doesn't in the original r

coordinate). The dilaton effective radius λ_* is

$$\lambda_* = \sqrt{\frac{\lambda^2 + \sqrt{\lambda^4 - 4T^4}}{2}}, \tag{6.20}$$

where the argument of tanh in (6.12) vanishes. So, as T increases λ_* decreases. When T becomes $T_c = \frac{\lambda}{\sqrt{2}}$, $\lambda_* = T_c$ the dilaton is perfectly screened by the black hole horizon. (i.e. If $T = 0$, $\lambda_* = \lambda$. If $T = \frac{\lambda}{\sqrt{2}}$, $\lambda_* = \frac{\lambda}{\sqrt{2}}$). The point of the first order transition is where the horizon screens the dilaton.

When density is introduced the story can become more complex. The action is (6.16) where it can be seen from the first of the two terms in the square root that including d increases the action. This increase can be beneficial though if the second term with β can be reduced. It is possible to reduce the β term if the D7 enters the region where β is large at small ρ. This means that the situation can arise where curving off the axis and then spiking on to the axis can be the lowest action state. This is typically more likely where β is largest in the interior space and the most savings can be made entering that region at low ρ. As we have seen at large values of A embeddings that spike onto the horizon do play a role introducing an extra phase.

It is only possible to have second order transitions if all three phases we have described are present. In the D7 description the D7 must move from a curved embedding that avoids the black hole to a configuration that spikes onto the black hole to a flat embedding smoothly.

6.2.2 Dependence on the speed of running

The parameter Γ controls the period in ρ or RG scale over which the change in the coupling A occurs. It allows us to naively go from a precociously running theory to a walking theory (although the change in the parameter A over that period may enter into what is meant by walking versus running too).

In Fig 6.8 we show the phase diagram as a function of Γ at fixed λ and A. We start at $\Gamma = 1$ with a configuration already discussed that has all three phases present

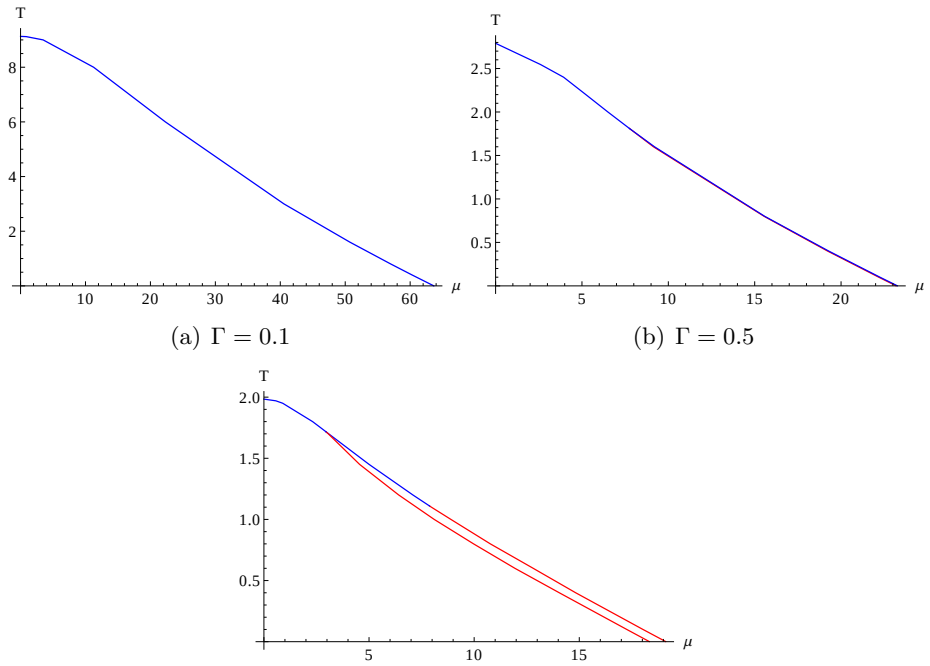

(a) $\Gamma = 0.1$ (b) $\Gamma = 0.5$

(c) $\Gamma = 1$

Figure 6.8: Example plots of three possible phase structures for $A = 30, \lambda = 1.715$ and varying Γ. Large (small) Γ gives a second (first) order transition at low T.

and second order transitions at high density. As Γ is reduced so that the step function in the dilaton becomes broader the first order nature of the transitions reasserts itself. By $\Gamma = 0.1$ the mixed phase with chiral symmetry breaking but melted mesons is no longer preferred at any temperature or chemical potential value - there is a single first order transition.

In conclusion then moving towards a walking theory by either increasing the width of the running or decreasing the magnitude of the increase in the coupling both move us towards a first order chiral transition. Stronger or quicker running favours a second order transition at low temperature, high density.

6.3 Breaking the ρ-L symmetry

Our goal is to attempt to reproduce a phase diagram comparable to that of QCD in our holographic model. So far we have failed to generate a second order transition with temperature at zero density which is a key part of the QCD picture.

We have a further natural freedom within our holographic model to exploit though.

Our running dilaton is in someway supposed to represent the backreaction of the quark fields on the strongly interacting gauge dynamics to allow us to model theories with more interesting dynamics than the conformal $\mathcal{N} = 4$ gauge fields. We introduce quarks through D7 branes that break the $SO(6)$ symmetry of the five sphere of the original AdS/CFT Correspondence down to $SO(4) \times SO(2)$. Our metric and ansatz for the running coupling (6.2) though respected the full $SO(6)$ symmetry. It seems reasonable to make use of the broken symmetry to introduce a further free parameter into our model.

The most successful scenario we have found is to introduce our explicit $L - \rho$ symmetry breaking parameter, α through the blackening factors of the metric

$$g_t = \frac{(w^4 - w_H^4)^2}{w^4(w^4 + w_H^4)}, \qquad g_x = \frac{w^4 + w_H^4}{w^4}, \tag{6.21}$$

with

$$w^2 \to \rho^2 + \frac{1}{\alpha} L^2 \,, \quad \alpha > 1. \tag{6.22}$$

We show the α dependence of our model in Fig 6.9. We start from a model with a

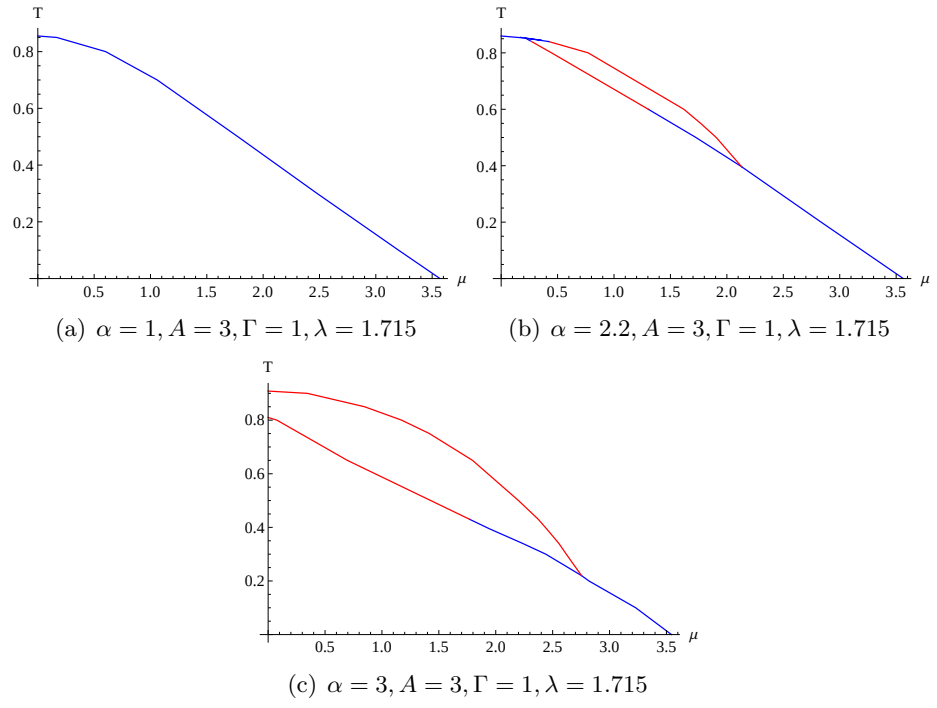

(a) $\alpha = 1, A = 3, \Gamma = 1, \lambda = 1.715$ (b) $\alpha = 2.2, A = 3, \Gamma = 1, \lambda = 1.715$

(c) $\alpha = 3, A = 3, \Gamma = 1, \lambda = 1.715$

Figure 6.9: Sample phase diagrams for theories with none zero α.

first order transition throughout the phase plane. As we increase α a region with melted mesons but chiral symmetry breaking develops, associated with second order transitions. It then spreads to the zero chemical potential axis

The reason for the onset of second order transitions with just temperature is simply understood. We have deformed the black hole horizon into an ellipse whose major axis is along the L axis. The area of enlarged dilaton remains circular in the ρ-L plane. Thus there are temperature periods in which the area of the ρ-L plane with a large dilaton is covered except for a small piece that emerges from the horizon near the ρ axis. If the value of the dilaton is sufficiently large in that uncovered area to encourage the D7 to avoid it, but the horizon on the L axis has met the zero temperature D7 embedding, then a second order transition to a black hole embedding is likely. Since in the absence of the rise in the dilaton the flat embedding would now be preferred the D7 settles on the horizon so it just misses the raised dilaton area. As the black hole grows further the embedding is likely to track down onto the axis smoothly as the raised dilaton area is finally eaten. This intuition is indeed matched by the solutions as shown in Fig 6.9.

The bottom phase diagram in Fig 6.9 achieves our goal of reproducing a chiral transition that is second order with temperature but first order with density.

6.4 Summary

In this chapter we have converted the D3 probe-D7 system, that holographically describes $\mathcal{N} = 4$ super Yang-Mills theory with quenched $\mathcal{N} = 2$ quark multiplets, to a phenomenological description of strongly coupled quark matter. We introduced a simple unback-reacted profile for the dilaton that describes a step of variable height and width in the running coupling of the gauge theory - (6.2). This breaks the conformal symmetry of the model and introduces chiral symmetry breaking. We have then studied the temperature and chemical potential phase structure of the model.

The phase diagrams consist of three phases - a chirally symmetric phase at large

temperature and density; a chirally broken phase with non-zero quark density at intermediate values of T and μ; and a chiral symmetry broken phase with zero quark density at low T and μ. Fig 6.2 shows these phases and their holographic analogue in a previously studied case where chiral symmetry was broken by an applied magnetic field. Here we showed that a small wide step in the gauge coupling's running gives rise to a single first order transition between the chiral symmetric and the broken phase (see Fig 6.6). If the step is made larger in height or thinner then the chirally broken phase with non-zero density also plays a role. Here the transitions at low temperature with chemical potential can be second order. These results match known results in top down models in the presence of magnetic fields to induce the symmetry breaking.

We were interested in reproducing phase diagrams with the structure believed to exist in QCD. To do this we made use of the broken $SO(6)$ symmetry of the gravity dual in the presence of D7 branes. Were the branes backreacted the dilaton and geometry would reflect this symmetry breaking. We introduced a further phenomenological parameters α in the black hole blackening factor. This models allowed us to control which volumes of the holographic space have a large dilaton value within, which the D7 branes prefer to avoid. Using this one extra parameter we were able to generate phase diagrams like those in QCD with a chiral restoration transition that was second order with temperature but first order with density (see Fig 6.9).

The ease with which such a variety of phase structures could be obtained is very encouraging for the idea of phenomenologically modeling the QCD phase diagram holographically. Further, the phenomenological parameters we introduced are very natural in this context and it seems likely that top down models with such phase structures should be possible as a result.

Chapter 7

The Baryonic Phase in Holographic Descriptions of the QCD Phase Diagram

7.1 Introduction

In this chapter we will continue our attempts to find a holographic description of the QCD phase diagram. Our studies are based on the previous chapters, with new elements added that allow a new holographic baryon phase to be included in the phase diagram of the strongly coupled gauge theory under consideration.

The QCD phase diagram is characterised by the quark and baryon densities and the chiral condensate. It is therefore sensible to continue exploring the same simple holographic model that was used in previous chapters and which encodes the physics of quarks and chiral symmetry breaking, the D3/D7 system [39, 51–54]. This system describes the SU(N_c) $\mathcal{N} = 4$ super Yang-Mills theory with N_f quark hypermultiplets. In the quenched approximation the theory is conformal and on the gravity side is described by probe D7 branes in $AdS_5 \times S^5$. The theory is 3+1 dimensional at all energy scales and has a conformal UV in which the identification of the operator matching between the field theory and the gravity description is

clear.

The simplest example of chiral symmetry breaking in the D3/D7 system is found by imposing a background magnetic field [65]. We have in detail consider this scenario in chapter 4. In chapter 6 we have explored an alternative way of inducing chiral symmetry breaking in these type of holographic setups, the introduction of a non trivial running dilaton. We introduced a phenomenological model in which we treated the running of the gauge coupling/dilaton profile as a free function. This was inspired by the fact that the DBI action for the probe with the magnetic field present is equivalent to the same theory with a particular choice of unbackreacted dilaton. Using an ansatz which steps between a conformal UV and a conformal IR with a larger coupling value we could reproduce phase diagrams like that for the magnetic field case but also a wider set of phase diagrams.

Although the phase diagram of the magnetic field case is interesting it does not overlap with expectations in QCD, where the finite temperature transition is believed to be second order and the finite density transition first order. In the dilaton running case, to describe phase diagrams that looked like the QCD case we used a further phenomenological freedom. The D3/D7 system if backreacted would display an $SO(4)\times SO(2)$ symmetry in the directions transverse to the D3 rather than the SO(6) symmetry of $\mathrm{AdS}_5 \times S^5$ space. We therefore allowed ourselves to introduce a parameter breaking the symmetry in that fashion in the emblackening factor of the black hole providing temperature. With this extra freedom we could produce the phase diagram in Fig 6.9(c) which maps more closely to that expected in QCD. The high T and low μ transition can therefore be fitted well. Here we turn our interest to the phase structure in the low T, high μ regime.

In [116] the phase diagram was studied for the holographic description of a theory with a running dilaton. The background has an induced vev for both TrF^2 and $Tr\tilde{F}F$; in the gravity dual these scalar solutions satisfy the equations of motion whilst leaving a pure AdS background. Quarks are again introduced using a D7 probe. The phase diagram is shown in Fig 7.1a and shows the same three phases as the cases already discussed. The chiral transition is first order throughout the plane.

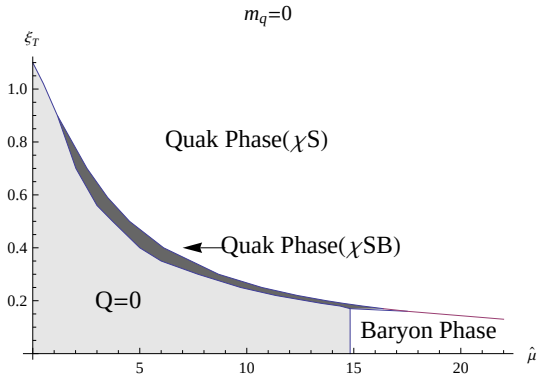

(a) The phase diagram of the massless axion/dilaton gauge theory in [116] showing a baryonic phase.

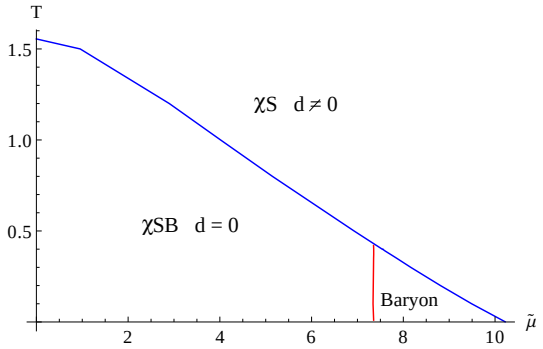

(b) The QCD-like phase diagram for a step function dilaton computed in this chapter: $A = 10, \lambda = 1.715$

Figure 7.1: Example holographic phase diagrams (see the appropriate references for conventions): red lines are first order transitions and blue second order. Phases are labelled by whether chiral symmetry is broken or not and whether there is a quark density, d, present. In each case the vertical axis is the size of the black hole in the geometry which measures the temperature T.

The extra key component of the analysis in [116] was to note that in the geometry with a running dilaton a baryonic phase was also present. A baryon vertex is described by a D5 brane wrapped on the S^5 of the $AdS_5 \times S^5$ space [83, 125–129]. In the pure $\mathcal{N} = 4$ theory such vertices shrink to zero size. However in the running dilaton geometry the large IR value of the dilaton stabilizes the D5 embedding. Solutions exist that link the D5 to the D7 brane embedding with a balancing force condition. These configurations describe the gauge theory with finite baryon density rather than finite quark density. The D7 bends off axis to meet the D5 and so the phase has chiral symmetry broken. This phase sets in at a particular finite chemical potential value and then persists to infinite chemical potential (as shown in Fig 7.1a) which is certainly unlike the equivalent phase in QCD (the phase diagram is very similar to that found in the Sakai Sugimoto model in [130]).

In QCD the transition to the baryon phase from low μ is known to be first order at zero and small T and ends at some critical point. In fact the low T phase is characterized by "droplets" (nuclei) due to the inter-nucleon interactions. Nucleons in the D3/D7 system presumably also interact but in [116] and here we will not include these interactions. The first order behaviour of the transition from droplets to constant baryon density is therefore not surprisingly missing but a second order change of phase is observed. It is worth stressing again that since the field theory is at strong coupling there is no secure field theory technique to analyze the transition from the baryonic phase to the quark density phase and holography gives us unique insights.

The goal of this chapter is to combine the approaches of the chapter 6 with [116]. We will investigate the baryonic phase in the model with phenomenological freedom in the running coupling. As we had hoped, we will show that these models can possess a baryonic phase and that, for regions of parameter space, it can be in the finite region one would expect it to be in for QCD. Our dilaton ansatz transitions between two conformal regions. In each of those conformal regimes, as in the $\mathcal{N} = 2$ Karch Katz theory, the baryon vertices are free to shrink. Around the transition radius though there is an extra cost to the D5s shrinking further since they must encounter the larger dilaton value within. The result is a set of stable D5 configurations when the change in dilaton between the two conformal regimes is sufficiently large. These configurations are present for low temperatures where the black hole horizon has not "eaten" the D5s but not present at large temperatures. The D7 branes that introduce the quark fields can end on the D5 baryon vertex when they are available. The D7 branes also prefer not to enter the interior of the geometry with a large dilaton value. Thus if the dilaton is sufficiently large inside the D5 radius they will prefer to join the D5. For very large interior dilaton values this occurs for all values of chemical potential and the baryonic phase exists out to infinite chemical potential as in the analysis of [116] (in that model the dilaton actually diverges in the IR). However we find that if the change in the dilaton is more modest across the transition then whether the D7 energetically prefer to join the D5 or end on the black hole horizon must be calculated and depends on the

parameters. In particular we do find ranges of parameter space where the baryonic phase lives in the regime shown in Fig 7.1b corresponding to the region expected in QCD. This is the main result of this chapter which we will explore in detail.

Finally, we briefly explore the link between confinement and the baryonic phase. The quark anti-quark potential can be computed by drooping a string into the AdS interior [121, 122]. The step dilaton profile induces a linear potential between a quark and an anti-quark when the step size is sufficiently large. The transition from a Coulomb potential to linear confinement qualitatively happens at the same value of the step size that induces a baryonic phase in the theory at finite chemical potential as one might expect.

7.2 The Holographic Model

We seek to describe a strongly coupled gauge theory with quenched quark fields using the D3/probe-D7 system. A running coupling will be imposed on the theory through a radial dilaton profile. Finite temperature will be included through an AdS-Schwarzchild geometry and baryon number / chemical potential via a gauge field in the probe D7 DBI action. The final ingredient will be to also allow D5 configurations wrapped on the S^5 of the geometry to represent baryon density. We review each of these steps in turn:

7.2.1 The Background

Our geometry will be the AdS-Schwarzschild black hole metric in Einstein frame which reads

$$\mathrm{d}s^2 = \frac{r^2}{R^2}\left(-f\mathrm{d}t^2 + \mathrm{d}\vec{x}_3^2\right) + \frac{R^2}{r^2}\frac{\mathrm{d}r^2}{f} + R^2\mathrm{d}\Omega_5^2, \tag{7.1}$$

where R is the AdS radius ($R^4 = 4\pi g_s N_c \alpha'^2$) and f is the emblackening factor

$$f(r) = 1 - \frac{r_H^4}{r^4}, \qquad r_H = \pi R^2 T, \tag{7.2}$$

with the temperature T. There is also the self-dual RR five-form $G_{(5)}$

$$G_{(5)} = (1 + *)\mathrm{d}t \wedge \mathrm{d}\vec{x} \wedge \mathrm{d}(g_{xx}). \tag{7.3}$$

We will impose an unbackreacted dilaton profile in the AdS-Schwarzschild geometry to allow us to explore a range of gauge coupling runnings in the gauge theory. In particular we will use the simple step-function form

$$e^{\phi} = A + 1 - A \tanh(r - \lambda), \tag{7.4}$$

where the dimensionless constant A is the change in the value of the gauge coupling, or e^{ϕ}, from the UV to the IR. The step is centred at the radial position λ, which corresponds approximately to the energy scale Λ_{QCD}, in the gauge theory. It is important to stress here that this ansatz does not satisfy the supergravity equations and we are instead moving to a phenomenological model in the spirit of AdS/QCD [109, 110], although retaining the key ingredients of the dynamics of chiral symmetry breaking from the top down D3/D7 systems. Our hope is that with this ansatz we still capture the key elements of the dependence of chiral symmetry breaking on the way in which conformal symmetry breaking is introduced. The step ansatz is convenient because it returns the theory to $\mathcal{N} = 4$ SYM in the UV and allows us to vary the strength of conformal symmetry breaking.

The rescaling of the radius (r) coordinate [77]

$$\frac{dr}{r\sqrt{f}} \equiv \frac{dw}{w} \implies w = \frac{1}{\sqrt{2}}\sqrt{r^2 + \sqrt{r^4 - r_H^4}}, \quad r = \sqrt{\frac{w^4 + w_H^4}{w^2}}, \tag{7.5}$$

with $\sqrt{2}w_H = r_H$, makes the $\mathbb{R}^6$ structure in the transverse space explicit:

$$\mathrm{d}s^2 = \frac{w^2}{R^2}(-g_t \mathrm{d}t^2 + g_x \mathrm{d}\vec{x}^2) + \frac{R^2}{w^2}(\mathrm{d}w^2 + \mathrm{d}\Omega_5^2), \tag{7.6}$$

where

$$g_t = \frac{(w^4 - w_H^4)^2}{w^4(w^4 + w_H^4)}, \quad g_x = \frac{w^4 + w_H^4}{w^4}. \tag{7.7}$$

	AdS-Black hole					S^5				
coordinate	t	x^1	x^2	x^3	r, w	S^5				
Background D3	•	•	•	•						
					$\mathbb{R}^4$				$\mathbb{R}^2$	
coordinate	t	x^1	x^2	x^3	ρ	S^3			L	S^1
Flavour D7	•	•	•	•	•	•	•	•		
					$\mathbb{R}$	S^5				
coordinate	t	x^1	x^2	x^3	ξ	θ	S^4			
Baryon vertex D5	•					•	•	•	•	•

Table 7.1: The brane profile showing the coordinates we use: the background D3, the compact D5 and the probe D7

7.2.2 D7 flavour brane and quark phase

We include a small number (N_f) of quark flavours by placing probe D7 branes into the background we have constructed. For this purpose, it is convenient to parameterize $\mathbb{R}^6$ so that $\mathbb{R}^4 \times \mathbb{R}^2$ is explicit (see the middle of Table 7.1):

$$\mathrm{d}w^2 + w^2\mathrm{d}\Omega_5^2 = \mathrm{d}\rho^2 + \rho^2\mathrm{d}\Omega_3^2 + \mathrm{d}L^2 + L^2\mathrm{d}\Omega_1^2, \tag{7.8}$$

where the D7 brane lies in the $(t, \vec{x}, \rho, \Omega_3)$ directions and L and ρ are related to $w, \tilde{\theta}$

$$w = \sqrt{\rho^2 + L^2}, \quad \rho = w\cos\tilde{\theta}, \quad L = w\sin\tilde{\theta}, \tag{7.9}$$

where $0 \leq \tilde{\theta} \leq \pi/2$ and is different from $0 \leq \theta \leq \pi$ in the bottom of Table 7.1.

The action for a D7 brane is given by the DBI action without the Wess-Zumino term

$$S_{D7} = -T_7 \int \mathrm{d}^8\xi e^{-\phi}\sqrt{-\det(e^{\frac{\phi}{2}}P[G]_{\alpha\beta} + (2\pi\alpha')F_{\alpha\beta})}, \tag{7.10}$$

where $T_{D7} = \frac{1}{g_{UV}^2(2\pi)^7\alpha'^4}$ and

$$e^{\phi} = A + 1 - A\tanh\left[\left(\sqrt{\frac{(\rho^2+L^2)^2 + w_H^4}{\rho^2+L^2}} - \lambda\right)\right]. \tag{7.11}$$

We add a chemical potential to our system by allowing
$\tilde{A}_t \equiv 2\pi A_t(\rho) \neq 0$ [55, 57, 75, 76], and assume that the D7 brane embedding profile is non trivial in ρ only, $L = L(\rho)$. The action becomes:

$$S_{D7} = \overline{T}_{D7}\int \mathrm{d}^4x\mathrm{d}\rho\mathcal{L}_{D7}, \tag{7.12}$$

$$\mathcal{L}_{D7} = -e^{\phi}\rho^3\sqrt{g_t g_x^3(1+L'^2)-\frac{g_x^3}{e^{\phi}}\tilde{A}_t'^2}, \tag{7.13}$$

where $\overline{T}_{D7} = T_{D7}N_f\Omega_3$.

Since A_t is a cyclic coordinate, there is the conserved charge defined by

$$\tilde{d} \equiv \frac{\partial\mathcal{L}_{D7}}{\partial\tilde{A}_t'}, \tag{7.14}$$

in terms of which, the Wick-rotated (Euclidean, $t \to -it_E$) Legendre transformed action ($\tilde{A}_t' \to \tilde{d}$) is defined by

$$\begin{aligned} S_{D7}^{E,LT} &= \overline{T}_{D7}\int \mathrm{d}t_E\mathrm{d}\vec{x}\int \mathrm{d}\rho\mathcal{L}_{D7}^{E,LT}, \\ \mathcal{L}_{D7}^{E,LT} &= \tilde{A}_t'\tilde{d} - \mathcal{L}_{D7} \\ &= e^{\phi}\frac{w^4-w_H^4}{w^4}\sqrt{1+L'(\rho)^2}\sqrt{\left(\frac{w^4+w_H^4}{w^4}\right)^2\rho^6+\frac{w^4}{w^4+w_H^4}\frac{\tilde{d}^2}{e^{\phi}}}, \end{aligned} \tag{7.15}$$

where the following relation obtained from (7.14) is used.

$$\tilde{A}_t' = \tilde{d}\frac{w^4-w_H^4}{w^4+w_H^4}\sqrt{\frac{1+L'^2}{\left(\frac{w^4+w_H^4}{w^4}\right)^2\rho^6+\frac{w^4}{w^4+w_H^4}\frac{\tilde{d}^2}{e^{\phi}}}}. \tag{7.16}$$

We solve the equation of motion for $L(\rho)$ minimizing the action (7.15) for a given $\tilde{d}$. The equation is second order and we impose two boundary conditions: $L(\infty) = m$ and the IR ($\rho \to \rho_H$) regularity. Asymptotically at large ρ the embedding field L takes the form $L = m + c/\rho^2 + ...$ with m and c proportional to the quark mass and condensate bilinear. By plugging the classical solution $L(\rho)$ into (7.16), we also get the solution A_t, for which the large ρ behaviour is $\tilde{A}_t = \tilde{\mu} - \frac{\tilde{d}}{2\rho^2} + ...$ with $\tilde{\mu}$ and $\tilde{d}$ proportional to the chemical potential and quark density. To compute the chemical potential, $\tilde{\mu}$, we simply integrate the right hand side of (7.16), i.e.

$$\tilde{\mu} = \int_{\rho_H}^{\infty}\mathrm{d}\rho\,\tilde{d}\,\frac{w^4-w_H^4}{w^4+w_H^4}\sqrt{\frac{1+L'^2}{\left(\frac{w^4+w_H^4}{w^4}\right)^2\rho^6+\frac{w^4}{w^4+w_H^4}\frac{\tilde{d}^2}{e^{\phi}}}}\,, \tag{7.17}$$

where $\tilde{A}_t(\rho_H) = 0$ by a regularity condition at horizon.

The field theory free energy density ($\mathcal{F}$) is holographically identified as

$$\mathcal{F} = \overline{T}_{D7} \int_{\rho_H}^{\infty} \mathrm{d}\rho \, \mathcal{L}_{D7}^{E,LT}\Big|_{\mathrm{on-shell}} , \tag{7.18}$$

where $\mathcal{L}_{D7}^{E,LT}$ is written in (7.15). The field theory grand potential density (Ω) is identified with the Euclidean original action before the Legendre transformation:

$$\begin{aligned} \Omega &= \overline{T}_{D7} \int_{\rho_H}^{\infty} \mathrm{d}\rho \, \mathcal{L}_{D7}^{E}\big|_{\mathrm{on-shell}} \\ &= \overline{T}_{D7} \int_{\rho_H}^{\infty} \mathrm{d}\rho\rho^6 e^{\phi} \frac{w^4 - w_H^4}{w^4} \left(\frac{w^4 + w_H^4}{w^4}\right)^2 \sqrt{1 + L'^2} \\ &\quad \sqrt{\frac{1}{\left(\frac{w^4+w_H^4}{w^4}\right)^2 \rho^6 + \frac{w^4}{w^4+w_H^4} \frac{\tilde{d}^2}{e^{\phi}}}} . \end{aligned} \tag{7.19}$$

In both cases, we added the counterterm $\sim -\frac{1}{4\rho_{\mathrm{cut-off}}^4}$ to renormalize the actions.[1]

7.2.3 D5 Baryon Vertex

The D7 world volume gauge field (dual to the chemical potential) has to be sourced by strings (quarks in the gauge theory). The string endpoints on the D7 world volume are point charges and the world volume gauge field A_t couples to this point source. The other end of the strings must end on either the black hole horizon or another brane. In the previous section, we considered the first case: the D7 brane touches the black hole horizon and the source for the gauge field is behind the horizon. Now we turn to the latter case.

Baryons, bound states of N_c quarks, are described in $\mathrm{AdS}_5 \times S^5$ by a baryon vertex, a D5 brane wrapped on the five sphere with N_c fundamental strings attached to it. This idea was first introduced in [125]. A baryon should correspond to an object made from N quarks or open strings ending on the D7 brane. Normally a fundamental string cannot end on some new *compact* brane since the fundamental string end points act as electric charges for the $U(1)$ gauge field living on the

[1] Since we consider only the massless case, $L(\infty) \to 0$, the counter term is simple. In general, the counter term is a function of m and c.

D-brane worldvolume. However, these charges can be cancelled in the case of a wrapped D5 by the RR field flux. This is possible because of the coupling $\int A \wedge F_{(5)} \sim N \int dt A_0$ where A is the world volume gauge field and $F_{(5)}$ is the RR 5-form field: $F_{(5)}$ induces N units of electric charge on the D5 brane. In other words, N fundamental strings have to be attached to the compact D5 brane wrapping S^5 in the bulk, and the other end points of strings will attach to the N_f D7 probe branes. This compound object is widely identified as the "holographic baryon". Therefore, it is natural to consider such a baryon vertex as a source of strings coupling to the A_t world volume field of the D7 brane. Note in the field theory dual to the D3/D7 system baryon states made purely from N valence quarks presumably match the structure of those in QCD - the additional super-partner states will only enter as sea states and the hope is that these effects do not modify the quantitative physics we will see. Of course a precise understanding of these states in these theories is again not possible on the field theory side and we rely on holography to describe them.

For a D5 brane baryon vertex configuration, it is more useful to parameterize $\mathbb{R}^6$ as

$$\mathrm{d}w^2 + w^2 \mathrm{d}\Omega_5^2 = \mathrm{d}\xi^2 + \xi^2 \left(\mathrm{d}\theta^2 + \sin\theta^2 \mathrm{d}\Omega_4^2\right), \tag{7.20}$$

rather than (7.8), since the D5 brane will lie in the (t, Ω_4) directions with a non-trivial profile $\xi(\theta)$. See the bottom of Table 7.1. We renamed w to ξ, to make clear that the radial coordinate is a function of θ here, which is different from $w(\rho) = \sqrt{L(\rho)^2 + \rho^2}$ in the D7 brane case. Furthermore, θ here is also different from $\tilde{\theta}$ in the D7 brane case as noted below (7.9). The plots in the following section show the D7 and D5 brane embeddings simultaneously in one plot, which is not, strictly speaking, correct because of these different coordinate systems. The superposition of the two pictures, which only match where the two branes join, is though helpful to understand the solutions.

The action for the D5 baryon vertex in the string frame is given by the DBI and the

Wess-Zumino term:

$$S_{D5} = -T_{D5}\int \mathrm{d}^6\xi e^{-\phi}\sqrt{-\det(P[G]_{\alpha\beta}+(2\pi\alpha')F_{\alpha b})} + T_{D5}\int \mathrm{d}^6\xi \mathcal{A}_{(1)}\wedge G_{(5)}, \quad (7.21)$$

where $T_{D5} = \frac{1}{g_{UV}^2(2\pi)^5 a'^3}$ and $\mathcal{A}_{(1)}$ is the world volume gauge field one-form on the D5 brane, which is different from A_t introduced on the D7 brane. In (7.20) the dilaton reads

$$e^{\phi} = A + 1 - A\tanh\left[\left(\sqrt{\frac{\xi^4+w_H^4}{\xi^2}}-\lambda\right)\right]. \quad (7.22)$$

Note that the Wess-Zumino term contributes to the action as well due to the coupling of the worldvolume gauge field $\mathcal{A}_{(1)}$ with the background five-form $G_{(5)}$ (7.3). A nontrivial temporal gauge field $\mathcal{A}_t(\theta)$ couples to N_c charge on the D5 brane. With assumptions $\xi = \xi(\theta)$ and $\mathcal{A}_t = \mathcal{A}_t(\theta)$, the action is given by:

$$\begin{aligned} S_{D5} &= \overline{T}_{D5}\int \mathrm{d}t\mathrm{d}\theta\mathcal{L}_{D5}, \\ \mathcal{L}_{D5} &= -\sin\theta^4\left(\sqrt{e^{\phi}}\sqrt{\frac{(\xi^4-w_H^4)^2}{\xi^4(\xi^4+w_H^4)}(\xi^2+\xi'^2)-\frac{1}{e^{\phi}}\tilde{\mathcal{A}}_t'^2}-4\tilde{\mathcal{A}}_t\right), \end{aligned}$$

where $\overline{T}_{D5} = R^4\Omega_4 T_{D5}$. Note that we extract R^4 to make $\mathcal{L}_{D5}$ dimensionless.

The equation of motion for the gauge field $\mathcal{A}_t(\theta)$ takes the form:

$$\partial_\theta\tilde{D}(\theta) = 4\sin\theta^2\,, \quad (7.23)$$

where the conjugate momentum $\tilde{D}$ of $\tilde{\mathcal{A}}_t$ is defined by

$$\tilde{D}(\theta) = \frac{\delta\mathcal{L}_{D5}}{\delta\tilde{\mathcal{A}}_t'} = \frac{\tilde{\mathcal{A}}_t'\sin^4\theta}{\sqrt{e^{\phi}}\sqrt{\frac{(\xi^4-w_H^4)^2}{\xi^4(\xi^4+w_H^4)}(\xi^2+\xi'^2)-\frac{\tilde{\mathcal{A}}_t'^2}{e^{\phi}}}}. \quad (7.24)$$

The general solution of (7.23) is:

$$\tilde{D}(\theta) = \frac{3}{2}(\nu\pi-\theta+\frac{3}{2}\sin\theta\cos\theta+\sin\theta^3\cos\theta), \quad (7.25)$$

where $0\le\nu\le 1$ is the integration constant and it is related to the number of fundamental strings attached to each pole [126]. For our purposes we choose $\nu = 0$

which is the case that all the fundamental strings emerge from only one pole of the baryon vertex which we choose to be $\theta = \pi$. Using (7.24) we can rewrite our Euclidean baryon vertex Lagrangian as:

$$\mathcal{L}^E_{D5} = \sqrt{e^{\phi}}\sqrt{\frac{(\xi^4 - w_H^4)^2}{\xi^4(\xi^4 + w_H^4)}(\xi^2 + \xi'^2)}\sqrt{\tilde{D}(\theta)^2 + \sin^8\theta}\,, \tag{7.26}$$

where $\tilde{D}(\theta)$ is defined in (7.25) with $\nu = 0$. This is for one Baryon vertex. The holographic energy density of many non-interacting free baryon vertex system at finite density n_B is

$$n_B \overline{T}_{D5} \int \mathrm{d}\theta \mathcal{L}^E_{D5}, \tag{7.27}$$

where $n_B = \frac{n_q}{N_c}$ and n_q is the quark density. Note here we have introduced a translationally invariant density of baryons in the field theory directions and we will not consider crystal like structures which in any case are only possible in the presence of inter-nucleon interactions.

7.2.4 Baryon phase: D7 + D5 branes

The baryon phase is constructed by connecting a D7 flavour brane and D5 baryon vertices by strings between them. It can be shown that the strings' tension is so strong that they tend to shrink to a point [116], which makes the D7 flavor brane and D5 baryon vertices meet at a point. Therefore, ignoring strings, we start with the D7 - n_B D5 combined system. Its free energy density is

$$\mathcal{F}_B = \overline{T}_{D7}\int_0^{\infty} \mathrm{d}\rho \mathcal{L}^{E,LT}_{D7} + \frac{n_q}{N_c}\overline{T}_{D5}\int_0^{\pi}\mathrm{d}\theta\mathcal{L}^E_{D5} \tag{7.28}$$

$$= \overline{T}_{D7}\left(\int_0^{\infty}\mathrm{d}\rho\mathcal{L}^{E,LT}_{D7} + \frac{2}{3\pi}\tilde{d}\int_0^{\pi}\mathrm{d}\theta\mathcal{L}^E_{D5}\right) \tag{7.29}$$

$$\equiv \overline{T}_{D7}(\tilde{\mathcal{F}}_{D7} + \tilde{\mathcal{F}}_{D5}), \tag{7.30}$$

where $\frac{n_q}{2\pi\alpha'\overline{T}_{D7}} = \tilde{d}$ since n_q is identified with $\frac{1}{V_3}\frac{\delta S_{D7}}{\delta A_t(\infty)}$ (V_3 is the three dimensional volume). Let us consider, at a fixed finite density $\tilde{d}$, the configuration of the D7 brane with a fixed boundary value $L(\infty) = m$ and the D5 brane with a fixed $\xi(0) = \xi_0$. The two brane embeddings have to meet at $\rho = 0$ and $\theta = \pi$, i.e.

$L(0) = \xi(\pi) \equiv w_0$. There are infinitely many configurations satisfying this condition, parameterized by w_0. To find out the lowest energy configuration, we vary the total free energy

$$\begin{aligned}\delta\mathcal{F}_B \sim &\int_0^\infty \mathrm{d}\rho(\mathrm{EOM_L})\delta L + \left.\frac{\partial\mathcal{L}^{E,LT}_{D7}}{\partial L'}\delta L\right|_0^\infty \\ &+ \frac{2}{3\pi}\tilde{d}\int_0^\pi (\mathrm{EOM}_\xi)\delta\xi + \left.\frac{2}{3\pi}\tilde{d}\frac{\partial\mathcal{L}^{E}_{D5}}{\partial\xi'}\delta\xi\right|_0^\pi \\ \sim &-\left.\frac{\partial\mathcal{L}^{E,LT}_{D7}}{\partial L'}\delta L\right|_{\rho=0} + \left.\frac{2}{3\pi}\tilde{d}\frac{\partial\mathcal{L}^{E}_{D5}}{\partial\xi'}\delta\xi\right|_{\theta=\pi},\end{aligned} \tag{7.31}$$

where the EOM_L and EOM_ξ are the equations of motion of L and ξ respectively. They vanish since we consider only the solutions of the equation piecewise. $\delta L(\infty) = \delta\xi(0) = 0$ by our boundary condition. At the matching point, $\delta L = \delta\xi$, so the condition is reduced to

$$\left.\frac{\partial\mathcal{L}^{E,LT}_{D7}}{\partial L'}\right|_{\rho=0} = \left.\frac{2}{3\pi}\tilde{d}\frac{\partial\mathcal{L}^{E}_{D5}}{\partial\xi'}\right|_{\theta=\pi} \quad\Rightarrow\quad L'(0) = \frac{\xi'(\pi)}{\xi(\pi)}, \tag{7.32}$$

which is called a force balancing condition [83, 116].

In the baryon phase, the chemical potential has an extra contribution from D5 branes

$$\tilde{\mu} \equiv \frac{1}{\overline{T}_{D7}}\frac{\partial\mathcal{F}_B}{\partial\tilde{d}} = \tilde{\mu}_{D7} + \frac{2}{3\pi}\int_0^\pi \mathrm{d}\theta\mathcal{L}^{E}_{D5}, \tag{7.33}$$

where $\tilde{\mu}_{D7}$ means (7.17) now integrated from the D5/D7 join to infinity. Note the extra term from the D5 originates from (7.29) where there is an extra coefficient of $\tilde{d}$.

However, both in the quark phase and the baryon phase, the grand potential is computed as a D7 brane Euclidean on-shell action, which is written explicitly in (7.19). The D5 brane action does not explicitly contribute in the baryon phase because

$$\begin{aligned}\tilde{\Omega}_B \equiv \frac{\Omega_B}{\overline{T}_{D7}} &= \tilde{\mathcal{F}}_B - \tilde{\mu}\tilde{d} \\ &= \tilde{\mathcal{F}}_{D7} + \tilde{\mathcal{F}}_{D5} - \left(\tilde{\mu}_{D7} + \frac{2}{3\pi}\int_0^\pi \mathrm{d}\theta\mathcal{L}^{E}_{D5}\right)\tilde{d} \\ &= \tilde{\mathcal{F}}_{D7} - \tilde{\mu}_{D7}\tilde{d}\,.\end{aligned} \tag{7.34}$$

However, the D5 brane still implicitly contributes by changing the classical embedding solution. In the following section, we will drop the subscripts B and $D7$. In this phase, the physical objects which carry $U(1)$ charge are baryon vertices. Each baryon is a bound system of N quarks and N $U(1)$ charges are associated with the D5 vertex. Therefore, this phase can be interpreted as a nuclear matter system or quark-confined phase. Without a baryon vertex, the $U(1)$ charge is carried by single unconnected strings, which correspond to quark matter.

7.3 Phase diagram in grand canonical ensemble

We will explore the phase diagram of the model with massless quarks. The phase diagram, neglecting the baryon vertex, was explored in chapter 6. The scale λ is the only conformal symmetry breaking scale in the model and so its value can be scaled (for numerical work we take $\lambda = 1.715$ to match previous work). The phase structure depends on the value of the parameter A that determines how much the dilaton changes between the UV and the IR.

For each point in the phase diagram one numerically seeks all possible D7 embedding solutions that asymptote to $L = 0$ at large ρ. There is always the flat solution $L(\rho) = 0$. There can also be "Minkowski" solutions that end at $\rho = 0$ with $L'(0) = 0$. Finally there can be embeddings that end on the black hole horizon. It is convenient to fix the density d and then determine μ from (7.17). The grand potentials of the solutions are then compared to determine the preferred phase.

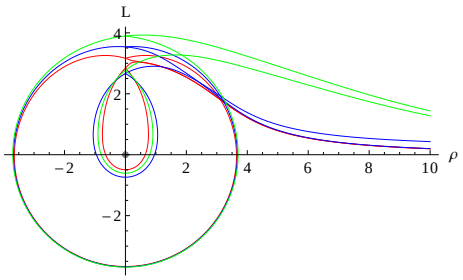

Figure 7.2: Examples of the baryon vertex solutions and their behaviour as we increase density - for these parameters there are two vertices for each value of density. The energetically preferred one is always that with the largest radius. The red lines corresponds to $d = 0.01$, blue $d = 5$ and green $d = 1000$. Parameters $w_H = 0.1, A = 10, \lambda = 1.715$.

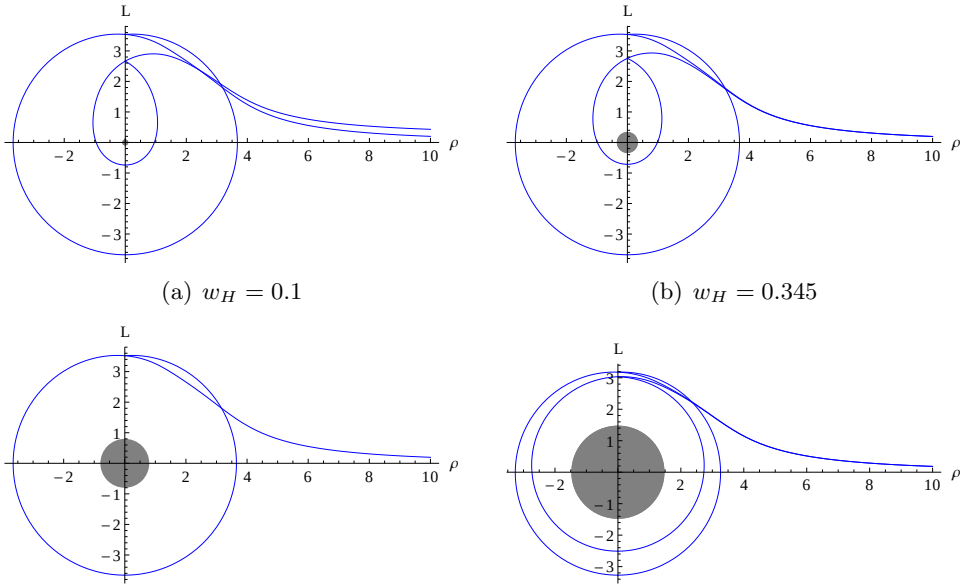

(a) $w_H = 0.1$ (b) $w_H = 0.345$

(c) $w_H = 0.8$ (d) $w_H = 1.5$

Figure 7.3: Behavour of the baryon vertex with temperature for fixed density. There is always one baryon vertex for the temperatures considered and typically two as shown. The energetically preferred one is always the one with the largest radius. Parameters $d = 5, A = 10, \lambda = 1.715$.

For $A < 2.1$ the model is always in the chirally symmetric phase. The massless D7 embedding is $L(\rho) = 0$ at all temperatures and density. To induce chiral symmetry breaking the cost of entering the interior volume with the enlarged dilaton must outweigh the cost of bending off axis. For $A > 2.1$ such chiral symmetry breaking is preferred at low T and μ. In the parameter regime $2.1 < A < 15$ the phase diagram divides into a chiral symmetric phase at high T, μ and a region with chiral symmetry breaking at low T, μ. The transition between is first order throughout the phase diagram. For $A > 15$ the D7 embeddings that end on the black hole play a role in the phase structure at high μ and the phase diagram mutates to the form shown in Fig 6.6(b)(c). The extra phase has non-zero quark number and chiral symmetry breaking. The transitions between the phases at high density become second order (the transition with T at $\mu = 0$ remains first order no matter how large A).

In addition to these embeddings we can now seek linked D5-D7 configurations as well with the same massless asymptotic boundary condition on the D7. Some examples of these configurations are shown in Fig 7.2 and Fig 7.3. The D5s are all stabilized for radii of order λ. Note that each of these figures corresponds to a translationally invariant constant density of baryons in the field theory. The

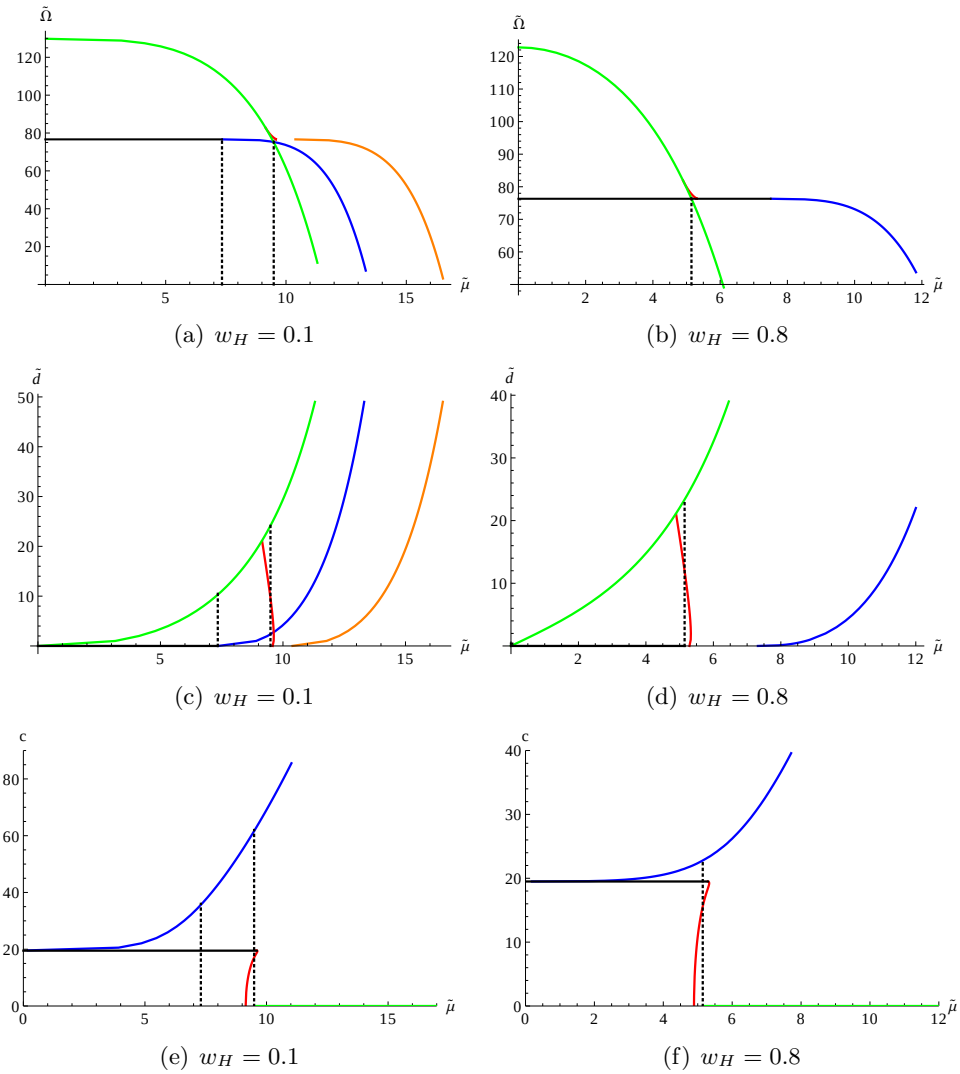

(a) $w_H = 0.1$ (b) $w_H = 0.8$

(c) $w_H = 0.1$ (d) $w_H = 0.8$

(e) $w_H = 0.1$ (f) $w_H = 0.8$

Figure 7.4: Plots showing the variation of a number of order parameters through the transition regions. The colour coding is - Green:flat embedding, Black: Minkowski embedding, Blue: large radius baryon vertex, Orange: small radius baryon vertex, Red: black hole embedding. Parameters: $A = 10, \lambda = 1.715, \Gamma = 1$. Top: the grand canonical potential vs chemical potential, Middle: d-μ plot, Bottom: condensate c vs μ.

structure shown is in the holographic and S^5 directions of the gravity description. The precise shapes presumably encode information about the inter-baryon quark wave functions and the relative role of the various R-charged super partners in the sea. There is certainly no deep understanding of the relations in the literature though so we shall simply accept these configurations and compute their energy to see which phase is preferred under various conditions.

Generally the number of baryon vertex solutions (linked D5/D7 solutions with massless boundary conditions on the D7) vary with the parameters A, d and T. For

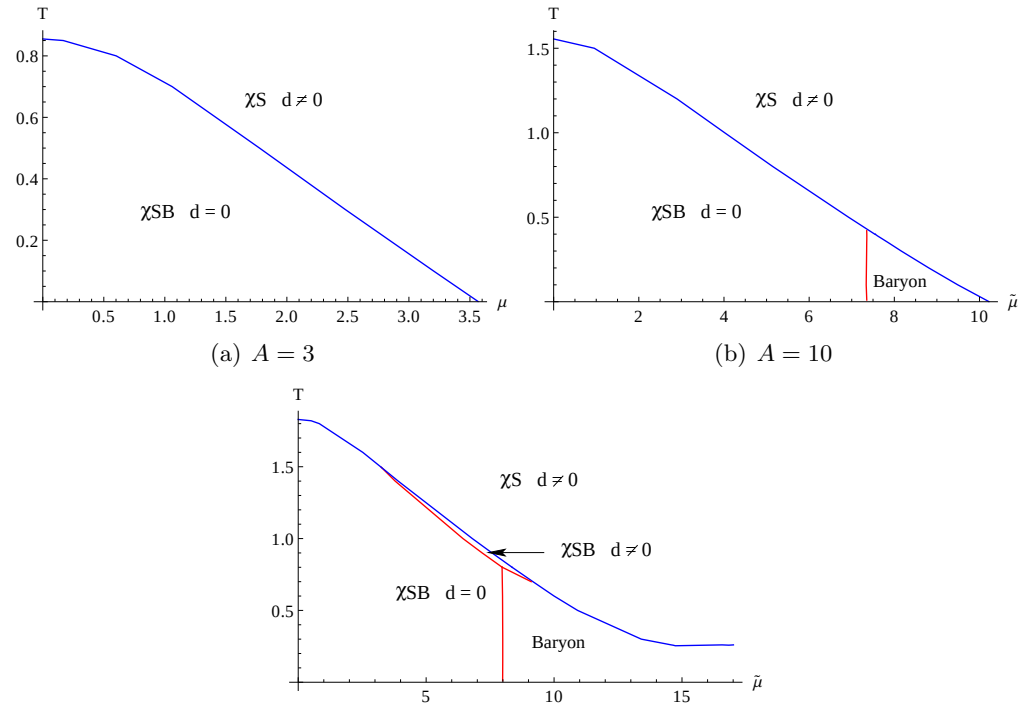

(a) $A = 3$ (b) $A = 10$

(c) $A = 20$

Figure 7.5: Phase diagrams as a function of the parameter A in the dilaton profile. The temperature T is in units of w_H. Transitions marked in blue are first order, those in red second order. The phases are labelled by whether chiral symmetry is broken (χS or χSB) and whether there is a baryon (Baryon) or quark density ($d \neq 0$). In the language of gravity side, "χSB and $d = 0$" means the curved Minkowski embedding, "χS and $d \neq 0$" means the flat embedding, "χSB and $d \neq 0$" means the curved black hole embedding, "Baryon" means the curved embedding contacting the baryon vertex.

some parameter sets we don't have any baryon vertex solutions (for small A's and densities). In Fig 7.2 we show an example of a parameter set where we have two baryon vertex solutions. Regardless of the number of baryon vertex solutions, we have always found that the energetically favoured solution is the one with the largest radius at the south pole. As we increase A the number of solutions increases and the D5 embeddings grow in radius. The baryon vertex solutions also change with density. Starting from very small density and increasing density the baryon vertex increases its radius rapidly in the beginning before asymptoting to a slower growth for larger densities. At fixed density, increasing temperature typically generates a smaller baryon vertex due to the black hole attraction (Fig 7.3). At high enough temperature, the baryon vertex cannot exist because the size of the black hole horizon becomes larger than the size of the D5 brane. So only the quark phase exists at high temperature.

Our job now is to again compare the Grand Potential energies of all these configurations. Some examples of that process are shown in Fig 7.4(a,b). The points where transitions occur can be read from the energies and then checked against transitions in order parameters of the model. For example in Fig 7.4(c,d) we plot the quark density against the chemical potential where the transitions and their orders can also be seen. The parameter c determining the quark condensate is also shown in Fig 7.4(e,f).

After this work one can construct the full phase diagram, summarizing the physical content of Fig 7.4, which is shown in Fig 7.5 for three choices of the parameter A. For small A (but still above the threshold for there to be chiral symmetry breaking) the baryonic phase plays no role. The cost of entering the high A area is not large enough to discourage the flat embedding.

At intermediate A we see the baryonic phase enters at intermediate chemical potential and low T. Fig 7.5b looks similar to expectations in QCD for the position of the baryonic phase and this is the most significant result we present. Note that the transition to the baryonic phase from the vacuum phase is second order. In QCD it is expected to be first order at low temperature due to the interactions between the nucleons. At low μ the phase in QCD can be thought of as sparse liquid droplets of nucleons (ie nuclei) in the vacuum. When μ is sufficient to fill space with nucleons the droplets rearrange themselves into the hadron gas. The entropy change associated with the internuclear interactions in this rearrangement generates the first order behaviour. In our analysis such interactions are neglected so not surprisingly a simple second order transition results. Recent work on computing inter-baryon forces using holography are summarized in [131].

Finally for large A the baryonic phase is stable out to infinite chemical potential - the cost of entering the large A region is so great that the flat embedding is always less preferred than a D5 ending embedding. This matches the model of [116] in which the dilaton diverges at small radius (and also the Sakai Sugimoto phase diagram in [130]). The $A = 20$ diagram also displays a small phase region in which black hole embeddings are dominant corresponding to a chiral symmetry broken

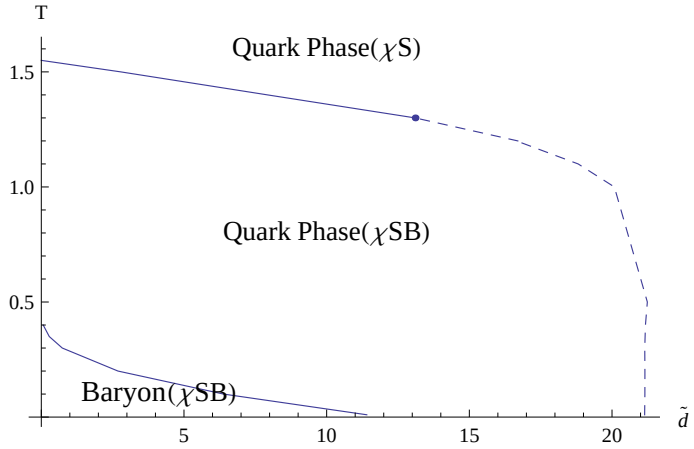

Figure 7.6: The canonical ensemble phase diagram for the case $A = 10$. The temperature T is in units of w_H. Transitions marked in blue are first order, those in red second order. The phases are labelled by whether chiral symmetry is broken and whether there is a baryon or quark density.

phase but with quark density.

7.4 The canonical ensemble

The phase diagram of our theory shows some additional structure in the canonical ensemble that is worth mentioning. We will work just in the case $A = 10$. Here we fix the density d rather than the chemical potential μ and we minimize the free energy rather than the grand potential. We display the phase diagram in Fig 7.6. The chiral symmetry breaking phase with $d = 0$ in the grand canonical ensemble lies entirely on the T axis in this plot. Interestingly though the canonical ensemble phase diagram includes a region with black hole embeddings (the chiral symmetry breaking, $d \neq 0$ phase) which is absent in the grand canonical ensemble. This is not a discrepancy. At the first order transitions in the grand canonical ensemble there is a jump in all order parameters including the quark density d - there must therefore be regions of the canonical ensemble phase diagram that are not present in the grand canonical ensemble and indeed are energetically unstable. On any given fixed T line the first order transition from either the Minkowski embedding or the baryon phase to the symmetric phase "leaps" over the black hole embedding phase of the canonical ensemble. As we saw in Fig 7.5(c) for $A = 20$ this third phase does play a small role in the phase diagram in the grand canonical ensemble.

7.5 Quark-antiquark potential

We found above that a larger dilaton step-size, A, makes a baryonic phase more stable, which implies that a large A triggers a confinement transition as well as chiral symmetry breaking. Therefore, it is interesting to study the confinement/deconfinement transition property by other methods. One of the standard tools is the Wilson-Polyakov loop, which can be obtained holographically by computing the on-shell Nambu-Goto action [117, 121, 122, 132, 133].

$$S_{NG} = \frac{1}{2\pi\alpha'}\int \mathrm{d}r e^{\phi/2}\sqrt{1+\left(\frac{r}{R}\right)^4 f(r)x'^2}, \tag{7.35}$$

where the static string worldsheet is parametrized as $x(r)$ and x is one of the field theory spacial direction. There are two types of solutions: a pair of parallel strings and a U-shaped string. In principle, the string end points can end on the deep IR bottom of the D7 probe brane. Such a non-trivial embedding is determined by the DBI action. However, in this work, we will simply consider the D7 brane infinitely far away from the horizon, which corresponds to an infinitely heavy quark.

For a pair of parallel strings, the embedding is simply

$$x(r) = \text{constant}, \tag{7.36}$$

and for a U-shaped strings, we have the conserved quantity (x is a cyclic coordinate)

$$c_0 \equiv \frac{e^{\phi(r)/2}}{\sqrt{\frac{r^4}{R^4}f(r)+1/x'^2}}\frac{r^4}{R^4}f(r) = \frac{e^{\phi(r_0)/2}r_0^2\sqrt{f(r_0)}}{R^2}, \tag{7.37}$$

where r_0 is the minimum value of r giving $x'(r_0)=\infty$. From (7.37) we have

$$x(r) = 2R^2\int_{r_0}^{r}\mathrm{d}r\frac{1}{r^2\sqrt{f(r)}\sqrt{e^{\phi(r)}r^4 f/(e^{\phi(r_0)}r_0^4 f(r_0))-1}}. \tag{7.38}$$

We can compute the on-shell action of the U-shaped string embedding (S_{NG}^{U}) by plugging (7.38) into (7.35). However, it is divergent because of the infinitely heavy quark mass contribution. We regularize the on-shell action by subtracting this

infinite mass, which is nothing but the on-shell action of a pair of parallel strings ($S^{\parallel}_{NG}$).

In summary, we define the quark-antiquark potential ($V_{q\bar{q}}(l)$) as

$$\begin{aligned} V_{q\bar{q}}(l) &\equiv \frac{S^{\rm U}_{NG} - S^{\parallel}_{NG}}{2\pi\alpha'} \\ &= 2\int_{r_0}^{\infty} {\rm d}r \frac{e^{\phi(r)/2}}{\sqrt{1 - e^{\phi(r_0)} r_0^4 f(r_0)/(e^{\phi}(r) r^4 f(r))}} - 2\int_{r_H}^{\infty} {\rm d}r e^{\phi(r)/2}, \end{aligned} \tag{7.39}$$

which is the function of $l \equiv x(\infty)$, the distance between the quark and antiquark. r_0 on the right hand side can be related to $l = x(\infty)$ by (7.38). Our numerical plots of $V_{q\bar{q}}$ for given parameter sets are shown in Fig 7.7.

Let us start with the case $A = 0$ which is just the well known $\mathcal{N} = 4$ theory, Fig 7.7(a). This is the case with a trivial dilaton, $e^{\phi} = 1$, which was studied first in [121, 122, 132, 133]. At zero T, the potential scales as $1/l$ (dotted line), which is a consequence of the conformality. At finite low T, the potential scales as $1/l(1 + \mathcal{O}((Tl)^4))$. Again the dependence on the Tl combination is due to the underlying conformal symmetry. The new feature at finite T is the existence of the phase transition from the bound quark antiquark pair to the free quark state, as the distance between quarks increases. In Fig 7.7(a) it corresponds roughly to the transition from the blue solid curve (a U-shape string) to the red horizontal line (a pair of parallel strings) near $l = 1.5$[2].

Now let us turn on A at a fixed T, Fig 7(b) ($w_H = 0.5$ and here again we set the scale in (7.4) at $\lambda = 1.715$). As A increases a linear potential starts forming, which is the characteristic feature of confinement. It is interesting that the linearity is very clear at $A = 10$, where there exists a stable baryon phase, see Fig 7.5(b)[3]. So, we see a rough correlation between our phase diagrams Fig 7.5 and $V_{q\bar{q}}$ (Fig 7.7). Fig 7.7(c) corresponds to Fig 7.5(a). The linearity is not clear in Fig 7.7(c) and it is

[2]In principle one should also take into account "graviton exchange" between the separated string worldsheets as was done carefully in [134] for large quark separation. This will modify the potential at large separation and will replace the phase transition shown at $l \sim 1.5$ with a cross-over. Since we focus on the dilaton effect at intermediate distance we don't consider that modification. If we considered it we could have a smoother cross over at larger distance, and also possibly, lose the additional first order transition in the inset of Fig 7.7(d).

[3]This linear potential was observed also in a similar setup with $e^{\phi} = 1 - q/r_H^4 \log\left(1 - r_H^4/r^4\right)$, where q plays the role of our A [117].

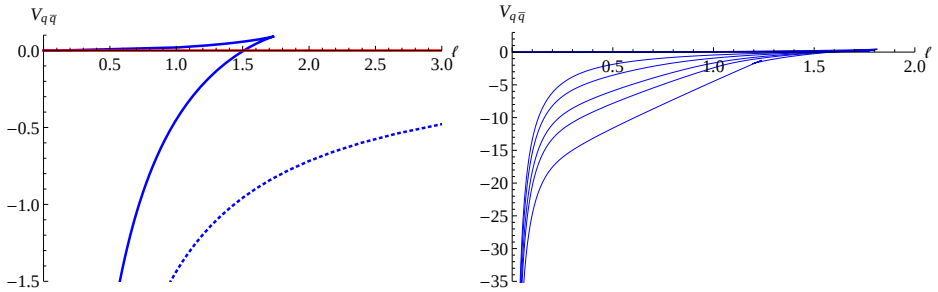

(a) $A = 0$, $w_H = 0$ (dotted line) and $w_H = 0.5$ (solid line)

(b) $w_H = 0.5$, $A = 0, 1, 3, 5, 10$ from top

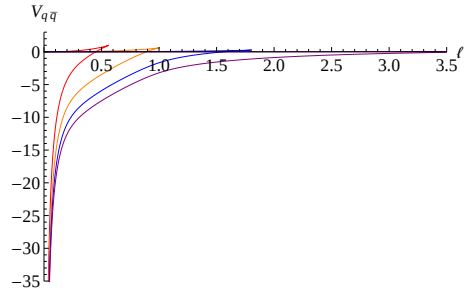

(c) $A = 3$, $w_H = 2, 1, 0.5, 0.2$ from top

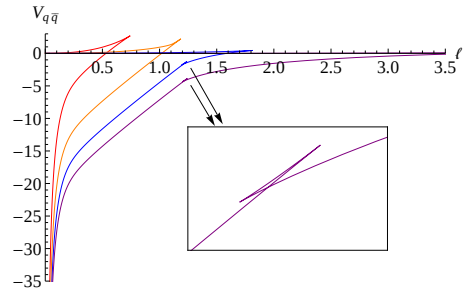

(d) $A = 10$, $w_H = 2, 1, 0.5, 0.2$ from top

Figure 7.7: Quark-antiquark potential ($\Gamma = 1, \lambda = 1.715$)

natural that we expect a deconfined phase and no stable baryons as shown in Fig 7.5(a). Fig 7.7(d) corresponds to Fig 7.5(b). At high temperature we tend to loose the linearity and there is no big difference from Fig 7.7(c) (deconfinement, no baryon). However at lower temperature, the linearity becomes stronger (confinement, baryon phase). So it is consistent with the phase diagram Fig 7.5(b).

There is one additional interesting feature at low temperature and large A. As shown in the insert of Fig 7.7(d), there is a first order phase transition between the linear potential and Coulomb-like potential. This is at odds with QCD, but makes good sense in our model. Our dilaton profile is a step function so there is a potential barrier localized at $r = \lambda$. As l increases, the string will extend inside, reduce r_0 and finally meet $r_0 = \lambda$, where a linear potential is built. If we further increase l, then the string finally will manage to get through the barrier at $r = \lambda$ and beyond that point, there is no friction against the string moving to lower r since the dilaton is constant. Therefore the potential becomes Coulomb-like again. We don't see this first order transition at high T, because at high T, the interval between r_H and λ is too short and there is no room for a "Coulomb" phase. i.e. After getting inside $r = \lambda$, the string should meet the black hole horizon very quickly.

The Coulomb-phase should not be present in QCD. We could easily cure this artifact by considering a continuously growing dilaton profile in the IR rather than the flat form. However, to keep the phase diagram seen in Fig 7.5(b), the dilaton should only increase mildly (For example, as $1/r^q$ as studied in [135]). If it is too strong, the phase diagram will be always the type of Fig 7.5(c), destroying our motivation for this work. However, a simpler explanation of the Coulomb phase is that it is a result of the quenched approximation. In reality we would expect $\bar{q}q$ pair production to break the string at separations before the Coulomb phase sets in for large A. For this reason these models still seem reasonable for QCD. In this section, our discussion has only been qualitative. More quantitative studies of the Wilson-Polyakov loop, together with other modifications of dilaton, would be interesting.

7.6 Summary

We have used the D3/D7 system to holographically study the phase diagram of a chiral symmetry breaking gauge theory as a function of the running coupling profile. We have included a running coupling through a phenomenological non-backreacted dilaton profile which steps between conformal UV and IR regimes. Here we have considered dependence on the height of the step. The model has previously been shown to have three phases : a chirally symmetric quark plasma at high T and μ; a chiral symmetry broken phase at small T and μ; and a more exotic chiral symmetry broken phase with quark density at intermediate T, μ for some parameter values. The order of these phase transitions depend on the height of the step. A first order transition to the chirally symmetric phase can be achieved for low step values. Previous work has also shown that the low μ transition with T can be made second order by phenomenologically tinkering with the shape of the AdS black hole horizon (in a way compatible with the spatial symmetry breaking of the D3/D7 system).

The crucial extra ingredient we have concentrated in this analysis is the low T and intermediate μ baryonic phase. Baryons can be introduced as D5 branes wrapped on the S^5 of the dual geometry and linked D7-D5 systems describe the hadronic

phase. In [116] such configurations were introduced in a geometry with a diverging dilaton in the IR. The resulting baryonic phase persisted though to arbitrarily high density unlike in QCD (but in a similar fashion to the equivalent phase diagram in the Sakai Sugimoto model [130]). Our intuition for our analysis was that in a model with a step function dilaton profile there would be no very large or small baryon vertices because in the two conformal regimes they would shrink away. The only D5 brane configurations would lie around the step and we could hope they would only play a role at intermediate μ. We indeed find, after careful numerical analysis, that this is the case for some range of the step size. Our model which best matches expectations for QCD in the low T regime is shown in Fig 7.5(b). The second order transition to this regime matches expectations in the absence of internuclear interactions which we neglected.

We have also made a qualitative link between the presence of the baryonic phase and the observation of linear confinement in Wilson loop computations in the background. The step function dilaton form generates both confinement and chiral symmetry breaking when the step size is large enough.

The phase diagrams we produce are not intended as predictions for QCD since the underlying physics model is somewhat different (e.g. the presence of super-partners) but they do demonstrate the wealth of behaviours possible in strongly coupled gauge theory. We can also hope for some universality and by finding models that match QCD's expectations for the phase structure it may be possible in the future to study phenomena beyond that structure using the models. For example in [114] the temporal behaviour of these systems, such as bubble formation, could be followed through a first order phase transition in a model of this type.

Chapter 8

Holographic Wilsonian Renormalization and Chiral Phase Transitions

8.1 Introduction

Recently a number of authors have proposed using renormalization ideas in the spirit of Wilson in holographic descriptions of strongly coupled gauge theories [136–143]. (For earlier discussions, see [144–149]) The radial direction in AdS like spaces is dual to energy scale in the field theory [46, 150–152] and one can imagine introducing a cut-off at some finite radius, splitting the supergravity solution in two. By integrating out the high energy regime an effective Wilsonian description should emerge. The precise matching of the radial direction to a gauge invariant measure of energy scale remains an open problem so a precise match to Wilsonian renormalization in the field theory will also remain imprecise but the spirit is clear.

In this chapter we wish to bring these ideas to bare on some explicit examples of theories with phase transitions. We wish to study how those transitions emerge in the Wilsonian language and will find examples of new transitions with changing

Wilsonian cut-off scale. We are also interested in deriving low energy effective actions near the transition points using this language.

In particular we will use the simple but highly instructive D3/D7 and D3/D5 systems [51]. The D3/D7 theory is the $\mathcal{N} = 4$ Super Yang-Mills theory in 3+1 dimension with $\mathcal{N} = 2$ quark hypermultiplets. In the D3/D5 case the hypermultiplets are restricted to a 2+1 dimension sub-surface of the gauge theory. In the quenched limit, when the number of quark flavours is small but the number of colours large, we can use the gauge/gravity dual consisting of probe D7(D5) branes in $AdS_5 \times S^5$. This system has been widely explored (For example in the D3/D7 case see chapter 4, [39, 55, 56, 65, 77, 91, 111, 112, 114, 119, 153] and references therein and chapter 5 and [92, 94–97] for the D3/D5 case) and we will make use of a number of known phenomena. In these systems the radial coordinate on the probe brane plays the role of the renormalization group (RG) scale in the field theory.

We will first introduce our methodology in the supersymmetric $\mathcal{N} = 2$ theory. That theory does not induce a chiral quark condensate (which would break supersymmetry were it present) but we can nevertheless attempt to find an effective potential for the quark condensate which should be minimized at zero. We will study its dependence on changing Wilsonian scale. This introduces the first subtlety which is the need to define holographic flows for non-vacuum, "off-shell", states in the field theory. In the UV, solutions of the Euler Lagrange equation for the D7 embedding exist for all values of the condensate. In fact we show analytically in this case that the D7 embeddings with non-zero condensate become complex at some finite AdS radius. At any fixed radius the solutions that are still real do not share the same boundary condition so formally one should not cut them off and compare their actions. To remedy this we consider a cut-off with explicit width i.e. effectively two close cut-offs. We use the naive UV solutions down to the the higher cut-off but then match them to classical embeddings between the two cut-offs that share the same IR boundary conditions. After making this construction one can then take the limit where the cut-offs come together. In this case that limit leaves us just evaluating the UV flow's action down to the cut-off as one naively expects, however it prepares the ground work for later more complicated cases. If the cut off

is taken too low then an embedding will become complex and computing the action is impossible. We interpret this as high energy states being integrated from the low energy effective theory - these states have energy above the cut off and are simply no longer present in the Wilsonian effective IR theory.

The precise meaning in the field theory of any cut-off we introduce of course is ambiguous but we presume there is some sensible mapping. Indeed there are also many distinct ways in which a cut-off can be introduced in the field theory from a sharp cut on UV modes to some smooth function suppressing the UV contributions. Using our prescription for the cut-off, we then evaluate the action of the D7 brane, which is just the free energy in the field theory. If we evaluate the UV component of that action above our cut-off we are simply determining the effective classical potential for the quark condensate that encapsulates the physics above that scale. This is the Wilsonian effective potential. The deep IR of this potential only contains the vacuum state with the condensate equal to zero since all other states are associated with complex embeddings - we can though freeze the energy of those states at the point they are integrated out (become complex) to generate an IR effective potential.

In the presence of a magnetic field, B, in the D3/D7 system a quark condensate is induced that breaks a $U(1)$ chiral symmetry [65]. In this system we again study the effective potential for the quark condensate with changing Wilsonian scale using the ideas so far developed. In the pure B case the resulting RG flow shows a novel second order transition to the symmetry breaking configuration as the Wilsonian scale is changed. This is an example of a strongly coupled Coleman Weinberg [154] style symmetry breaking. We also holographically compute the effective potential close to the transition and show it is mean field in nature. We plot the RG flow of the couplings of the Wilsonian effective potential. In the deep IR the effective potential for the condensate again develops gaps as embeddings become complex and are integrated from the low energy theory. The picture that emerges is satisfyingly Wilsonian. The bare UV theory has no symmetry breaking; at intermediate RG scales integrated out, UV, quantum effects enter the bare potential and display the symmetry breaking; in the deep IR all states but the true

vacuum are integrated from the low energy theory. The Wilsonian approach gives a sensible intuition.

The pure B theory can also be related immediately to the case of a B field and a perpendicular electric field, E [113, 155, 156]. These two theories essentially share the same action. The E field [69, 153, 157] tends to dissociate quark bound states and so disfavours chiral symmetry breaking [113]. We show that our previous results can be mapped to display the E dependence of the Wilsonian description.

We next turn our techniques to analyze the D3/D7 system with a magnetic field and chemical potential (see chapter 4, [91]). The chemical potential tends to induce a non-zero quark density which also disrupts the chiral condensate. Here the naive embedding flows for the D7 brane, describing different condensate values, all progress to the deep IR where they mostly end in a singular fashion. Previously those flows that end at the position of the D3 branes (the origin) have been picked out to describe the physical vacuum [56]. The picture is that fundamental strings, representing the quark density, link the D3 and D7 brane. They manifest as a spike in the D7 brane embedding to the origin. The fundamental strings are needed to source the D7 brane world volume gauge field that is dual to chemical potential. To compare the actions of these vacuum flows and the off shell configurations, the off shell configurations must be forced to have the same IR boundary conditions. We use our cut-off procedure to argue that in the deep IR the off-shell configuration should be completed with a spike of D7 brane to the origin. The natural extension of this procedure at non-zero cut-off values is that all configurations should be completed with a spike along the cut-off.

Having argued for this implementation of the cut-off we then analyze the Wilsonian effective potential of this theory at fixed B but varying density. Again we find a sensible Wilsonian description with the UV theory showing no symmetry breaking. Then, provided the density is sufficiently small, there is a transition with lowering cut-off scale to the chiral symmetry broken vacuum. This transition is in parts of parameter space first order and elsewhere second order and mean field. We can explicitly derive the effective potential through the transition. As the cut-off is

taken into the IR the second order behaviour dominates and we perform a fit to the mean field potential. In this case we do not see the degeneracy of the potential in the deep IR we described in the supersymmetric and pure B case - none of the embeddings become complex. This might reflect that our cut-off prescription is overly naive. We simply report on what we find in this case.

Finally we study the D3/D5 system [94–96] with a magnetic field and density, d, using our Wilsonian methodology. This system is of further interest because it is known to exhibit a holographic BKT transition (see Chapter 5, [92]) at which the condensate grows as $e^{-1/\sqrt{d_c-d}}$. Here we again display the density versus cut-off phase diagram, in which there are first order transition regimes, second order regimes and finally for the cut-off in the deep IR a BKT transition. Here we successfully derive an effective potential for the BKT transitions when the Wilsonian scale goes to zero.

8.2 Wilsonian Flow For the $\mathcal{N} = 2$ Theory

We will begin by exploring a Wilsonian analysis of the simplest model $\mathcal{N} = 2$ gauge theory which does not display chiral symmetry breaking. The $\mathcal{N} = 4$ gauge theory at zero temperature is described by the dual geometry ($\mathrm{AdS}_5 \times S^5$)

$$\mathrm{d}s^2 = \frac{r^2}{R^2}\mathrm{d}x_4^2 + \frac{R^2}{r^2}(\mathrm{d}\rho^2 + \rho^2\mathrm{d}\Omega_3^2 + \mathrm{d}L^2 + L^2\mathrm{d}\phi^2), \tag{8.1}$$

where $r^2 = \rho^2 + L^2$ and $R^4 = 4\pi g_s N\alpha'^2$.

Quenched ($N_f \ll N$) $\mathcal{N}$=2 quark superfields can be included through probe D7 branes in the geometry. The D3-D7 strings are the quarks. D7-D7 strings holographically describe mesonic operators and their sources. The D7 probe can be described by its DBI action

$$S_{\mathrm{DBI}} = -T_{D7}\int \mathrm{d}^8\xi\sqrt{-\det(P[G]_{ab} + 2\pi\alpha' F_{ab})}, \tag{8.2}$$

where $T_{D7} = (2\pi)^{-7}\alpha'^{-4}g_s^{-1}$ and $P[G]_{ab}$ is the pullback of the metric and F_{ab} is the

gauge field living on the D7 world volume. The Wess-Zumino term is irrelevant to our discussion.

The gauge field holographically describes the operator $\bar{q}\gamma^\mu q$ and its source, a background $U(1)$ gauge field for baryon number. We will use F_{ab} below to introduce a constant magnetic field (eg $F_{12} = -F_{21} = B/(2\pi\alpha')$) [65] but for the moment keep it zero.

We embed the D7 brane in the t, $\vec{x}$, ρ and Ω_3 directions of the metric but to allow all possible embeddings must include a profile $L(\rho)$ at constant Ω_1. The full DBI action we will consider becomes one dimensional:

$$S_{\rm DBI} = \mathcal{N} \int {\rm d}t{\rm d}\vec{x}{\rm d}\rho \, \mathcal{L}(L, L'; \rho), \tag{8.3}$$

where $\mathcal{N} = N_f T_{D7} 2\pi^2$ and

$$\mathcal{L} = -\rho^3 \sqrt{(1 + L'^2)}\,. \tag{8.4}$$

The Euler-Lagrange equation for the embedding is then

$$\partial_\rho \left(\frac{\rho^3 L'}{\sqrt{(1 + L'^2)}} \right) = 0. \tag{8.5}$$

At large ρ the classical solution from (8.3) behaves as

$$L(\rho) \sim m + \frac{c}{\rho^2} + \cdots, \tag{8.6}$$

where m is proportional to the quark mass and c to the quark condensate.

Numerically we can shoot into the IR from a UV solution with particular values of c and m. For the particular case $m = 0$ we show such flows in Fig. 8.1(a). All except the $c = 0$ solution appear to stop at some finite ρ. In this case we can find the analytic solution to investigate this in more detail. The real solution valid in $\rho \in (\rho_c, \infty)$, where $\rho_c = (2c)^{1/3}$ is

$$L(\rho) = m + \frac{c}{\rho^2} \, {}_2{\rm F}_1[1/3, 1/2, 4/3, 4c^2/\rho^6], \tag{8.7}$$

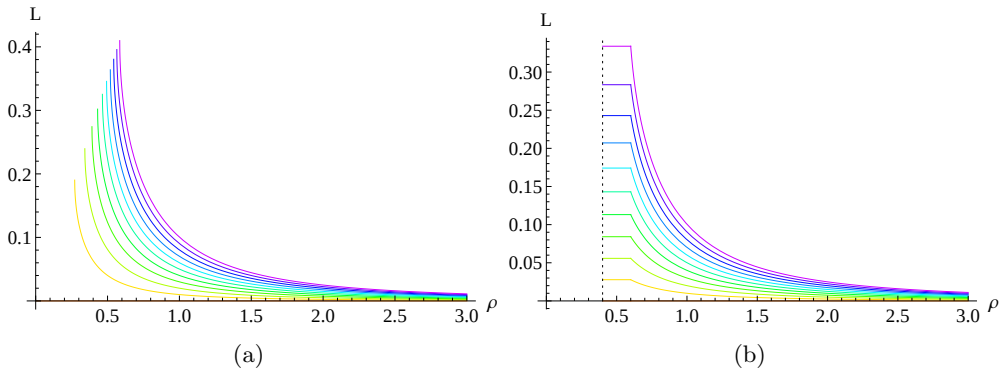

Figure 8.1: Plots of D7 embeddings in the $\mathcal{N} = 2$ theory. (a) Full embedding solutions for $m = 0$. (b) The embeddings interrupted by a two scale cut off.

with

$$L'(\rho) = \frac{2c}{\sqrt{\rho^6 - 4c^2}}. \tag{8.8}$$

From (8.8) we can see that the gradient of the embedding becomes complex at $\rho_c = (2c)^{1/3}$. These results match very well to the numerical results in Fig 8.1(a) and provide an explicit form for the behaviour at ρ_c. The only solution that survives to $\rho = 0$ is the flow with $c = 0$.

One would naively like to plot the effective potential $V(c)$ generated by the holographic flows to show the $c = 0$ solution is the minimum. However, since all but one flow (c=0) become ill-defined this is confusing. Understanding why there is no IR effective potential provided by holography is one of our goals. We will adopt the recently suggested idea that we should approach the holographic description in a Wilsonian manner. In particular we will introduce a cut-off in ρ, the holographic direction for quark physics (i.e. the radial direction on the D7 brane), which we will call ϵ and study the theory as a function of changing that cut-off.

Thus specifically to convert the "off-shell" flows, with non-vacuum values of the quark condensate, into kosher flows we will interrupt them with a cut-off at an intermediate value of ρ. In the UV we find the Euler Lagrange equation solutions with large ρ asymptotics c/ρ^2 and solve down to the cut-off. A technical issue arises at this point though. The flows ending on the cut-off do not share the same IR boundary conditions since they meet the cut-off at arbitrary angles. Formally one should not compare their actions in a Euler-Lagrange analysis.

To cure this let us imagine a more general structure for our cut-off in which it has finite width. We introduce two cut-offs in ρ, ϵ_- and ϵ_+. In the UV from infinite ρ down to ϵ_+ we use the flows in Fig 8.1(a). Then we match these flows to flows beginning at ϵ_- with $L'(\epsilon_-) = 0$ and ending at ϵ_+ at the same point as the UV flows. We pick this boundary condition at ϵ_- because it naturally matches on to the boundary condition of the regular flows as $\epsilon_- \to 0$ ie $L'(0) = 0$. We show example flows in Fig 8.1(b). Now all of our flows have the same IR and UV boundary conditions.

Having introduced this cut-off structure it is actually most natural to remove it by taking $\epsilon_+ \to \epsilon_-$. In this example the flows between ϵ_- and ϵ_+ simply become short straight lines whose action vanishes as the two cut-offs coincide. This digression therefore is just to justify that one can effectively consider the UV flows down to the common ϵ to share IR boundary conditions and directly compare their action sensibly. In other words we assume a small change to the flows at the cut-off that bends them to satisfy $L'(\epsilon) = 0$ but assume this doesn't make a large change to the action. Here this seems rather trivial but we shall see much more structure emerge in the later example with density.

We now proceed in this case with the single cut-off ϵ. For each choice of ϵ we can plot a potential (density) given by

$$V_{\text{eff}}(c) = -\int_{\epsilon}^{\infty} d\rho \; \mathcal{L}(\rho), \tag{8.9}$$

which is nothing but a Euclidean on-shell action (8.3) normalized by $\mathcal{N}$ and a field theory volume (so it is a density.). These actions diverge in the UV but the difference between them determines which is preferred (or they can be regulated by adding a holographic counter term $\sim \Lambda^4/4$, where Λ is a UV cut-off to be set to ∞ at the end). A minus sign comes from Euclideanization. To regulate these flows we will always compute the difference in action from the flat embedding $L = 0$ with the equivalent cut-off ϵ. The $L = 0$ embedding will therefore always lie at $V = 0$ in our plots. The potential should be viewed as the potential energy incurred for a particular value of the condensate from scales above the cut-off ϵ. In other words

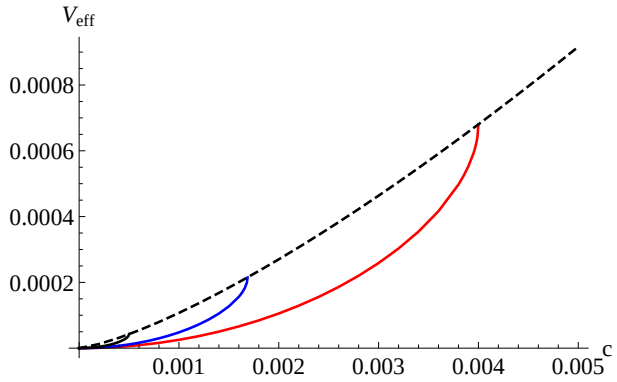

Figure 8.2: Plots of the effective potential against the parameter c in the $\mathcal{N} = 2$ theory. Plots for $\epsilon = 0.2, 0.15, 0.1$ (red,blue,black) from right to left. The dotted curve is the extended IR effective potential with the values of the action frozen at the point the embeddings become complex.

this potential is the equivalent of the potential in the "bare" Lagrangian written down for the theory at the given cutoff which should be used in conjunction with quantum (or holographic) behaviour below the cut-off. This is exactly the Wilsonian paradigm.

8.2.1 Wilsonian Potentials

Using the methodology described above we can now plot the Wilsonian effective potential for the quark condensate as a function of cut off scale ϵ. We show this in Fig 8.2. Reassuringly $c = 0$ is the minimum of the potential at all values of the cut off as we would expect in the supersymmetric theory.

The finite extent of the plots in c is a result of solutions with larger c having gone complex before reaching the cut off at ϵ. We interpret the removal of states with large values of the condensate from the effective potential as a sign that these states can not be reached with the energy available in the IR theory. This seems to match well with a Wilsonian approach and explains the degeneracy if $\epsilon \to 0$. In the examples below we will simply omit states that are not in the low energy theory in this sense. One could though simply freeze the potential value at the point where the embedding becomes complex and retain that value for lower choices of the cut off. We plot that version of the IR effective potential for the $\mathcal{N} = 2$ system as the dotted curve in Fig 8.2 - again it is minimized at $c = 0$.

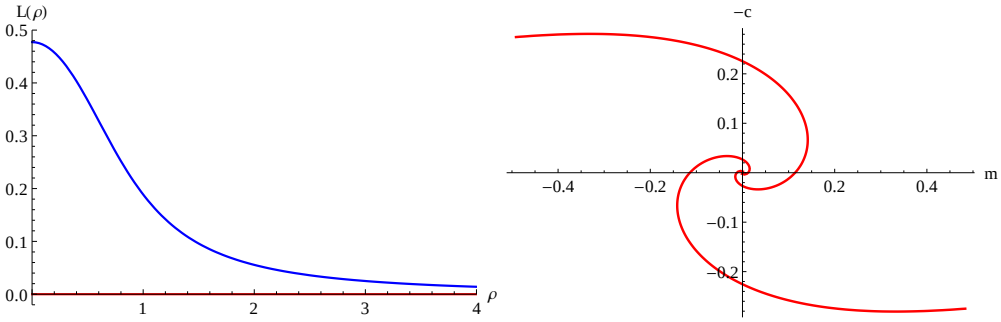

(a) (b)

Figure 8.3: In (a) we show the flat and vacuum embeddings of the D7 brane probe in $AdS_5 \times S^5$ with a magnetic field ($B = 1$). In (b) we plot the quark condensate against mass extracted from embeddings such as those in (a).

8.3 Wilsonian Flow for a Chiral Condensate

We will now move on to study more interesting examples of gauge theories that induce chiral symmetry breaking in the IR. We next look at the $\mathcal{N} = 2$ theory with an applied magnetic field which induces a chiral condensate [65]. We introduce the B field through the D7 brane world volume gauge field in (8.2). We now have

$$\mathcal{L} = -\rho^3 \sqrt{(1 + L'^2)} \sqrt{\left(1 + \frac{R^4}{(L^2 + \rho^2)^2} B^2\right)}. \tag{8.10}$$

At large ρ the asymptotic solution is again given by (8.6) and we can again interpret m, c as the quark mass and condensate. In the absence of B the theory is conformal so it is natural to write all dimensionful parameters in units of $\sqrt{B}$, the intrinsic conformal symmetry breaking scale, which we do for our numerical work (i.e. put $B = 1$).

The solutions of the Euler-Lagrange equations for the embedding $L(\rho)$ are well known (chapter 4, [65]) and we show two[1] regular solutions with $m = 0$ and with $L'(0) = 0$ in Fig 8.3(a) - numerically one shoots out from $\rho = 0$ to find these. More generally one can seek such solutions for any mass m and read off the condensate c from the large ρ asymptotics. In Fig 8.3(b) we show a plot of c vs m for the regular embeddings. It has the spiral structure discussed in [65]. The Fig 8.3(a) solutions

[1] In principle there are infinite number of meta-stable solutions corresponding to the spiral structure in Fig 8.3(b). However, we omit them since they are always meta-stable not a ground state.

are the $c = 0$ flat embedding and the largest c solution with $m = 0$. The vacuum energy of these configurations can be found by integrating minus the holographic action over the ρ coordinate. These actions diverge in the UV but the difference between them determines which is preferred (or they can be regulated by adding a holographic counter term $\sim \Lambda^4/4 + B^2/2 \log \Lambda$, where Λ is a UV cut-off to be set ∞ at the end). The curving configuration shown, with the quark condensate, is the preferred state and the flat embedding is a local maximum of the effective potential.

8.3.1 Wilsonian Effective Potentials

As in the previous example we would like to plot the effective potential $V(c)$ generated by the holographic flows to show the solutions we have found are the turning points. To describe off-shell states we find numerical solutions of the embedding equation for massless quarks that look like c/ρ^2 at large ρ and shooting into the interior. We plot these flows in Fig 8.4(a), where it can be seen that most fail to reach the L axis or a deep IR cut-off. We expect that these are associated to the embedding becoming complex by continuity to the $c >> B^{3/2}$ curves, although here we do not have analytic solutions.

To proceed we again introduce a cut off. In Fig 8.4(b) we show such a cut off with the two scale structure, ϵ_+, ϵ_- that allows us to make the flows all share the same $L'(\epsilon_-) = 0$ boundary condition. As with the pure supersymmetric case we can take $\epsilon_- \to \epsilon_+$ limit trivially here, having a single cut off ϵ at which we end the flows. We

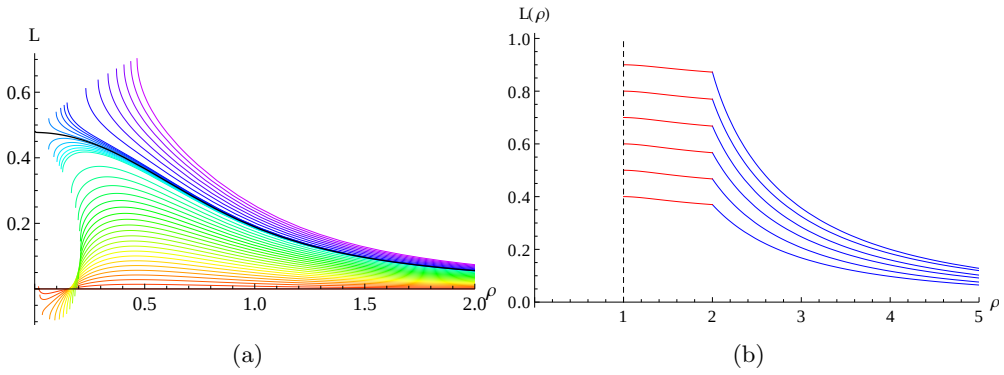

(a) (b)

Figure 8.4: (a) Plots of the D7 embeddings against ρ for several asymptotic values of the quark condensate at zero quark mass with a magnetic field ($B = 1$). (b) Those flows interrupted by a two scale cut-off ($\epsilon_- = 1$ and $\epsilon_+ = 2$ here) used to give the flows the same IR boundary condition.

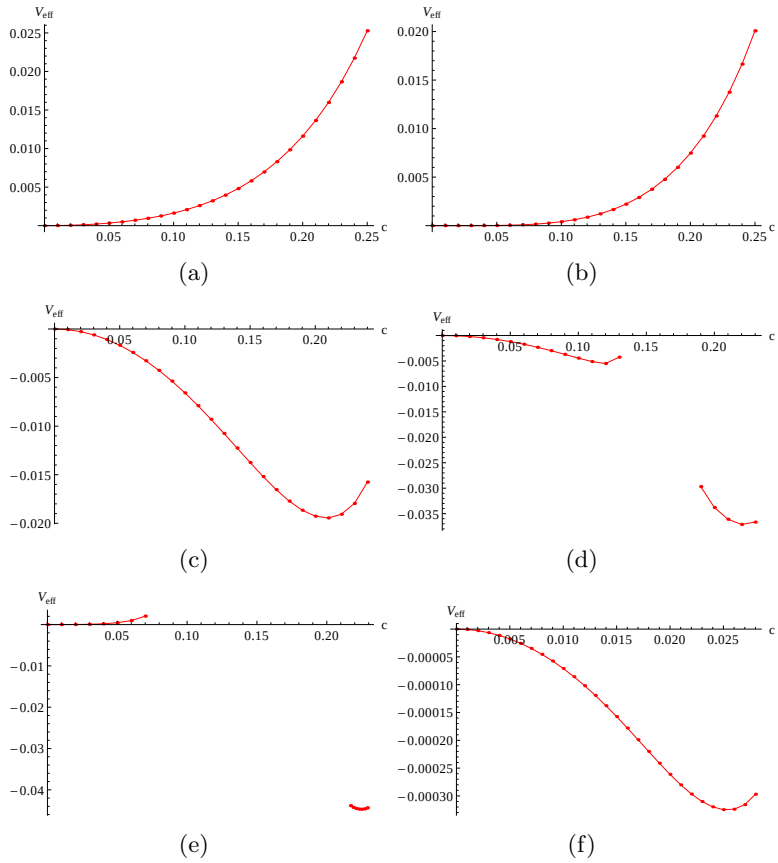

Figure 8.5: Plots of the Wilsonian effective potential for the quark condensate in the D3/D7 system with a world volume magnetic field ($B = 1$) at different values of the Wilsonian cut-off ϵ ($\epsilon = 0.5, 0.4686$(phase transition point)$, 0.3, 0.2, 0.15$ and 0.03 respectively). In (a)-(c) we see a second order transition from the unbroken to the broken phase. In (d)-(e) we see the IR potential degenerate as non-vacuum states are integrated out. In (f) we show the potential close to the origin at $\epsilon = 0.03$ displaying one of the metastable vacua, which corresponds to $c \sim 0.025$ also shown in Fig 8.3(b).

now proceed in this case with the single cut-off ϵ evaluating the action integrated from ϵ to infinity.

In Fig 8.5 we plot the potential as a function of ϵ for the D3/D7 system with magnetic field. When ϵ is large we are describing the UV lagrangian which has no preference for a quark condensate. As ϵ decreases we are "adding in" more of the strongly coupled quantum effects of the theory from lower scales to the bare potential. The first clear feature shown in Fig 8.5(a)-(c) is that there is a phase transition at the critical value $\epsilon_c = 0.4686 B^{1/2}$ to the chiral symmetry broken phase. This transition is our first main result. One can think of this transition as being in the spirit of a Coleman-Weinberg transition - at high energies the theory has no condensate but then strongly coupled loop effects enter in the IR and break the symmetry. We will return to the deep IR later but let us first explore this phase

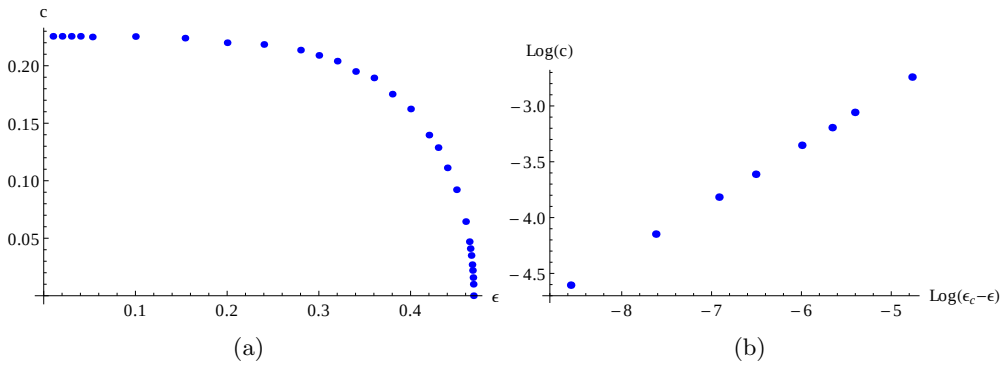

(a) (b)

Figure 8.6: (a) A plot of the quark condensate c against Wilsonian cut-off scale ϵ. (b) A log log plot of the same close to the transition point to show the mean field exponent.

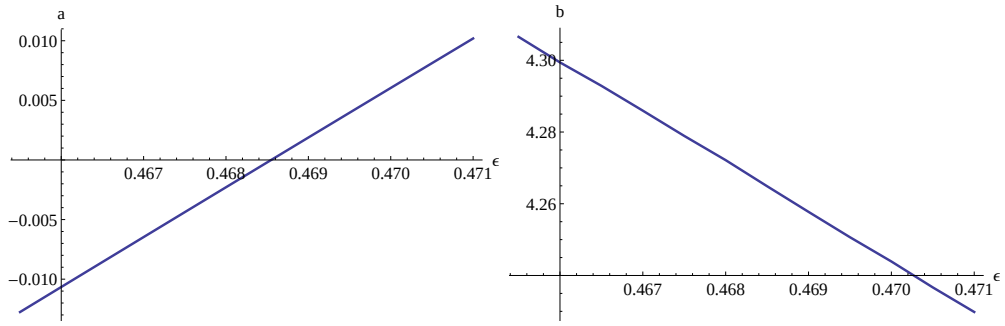

(a) (b)

Figure 8.7: Plots of the parameters (a) a and (b) b in our fitting potential in (8.11) against Wilsonian cut-off ϵ through the transition point.

transition in detail.

In Fig 8.6 we plot the quark condensate against ϵ showing that the transition is second order. We also plot $\log c$ vs $\log(\epsilon_c - \epsilon)$ near the transition point from which we can extract the critical exponent as $1/2$ - the transition is a mean field one.

In fact close to the transition we can perform a numerical fit to the potential we have derived of the form

$$V_{\text{eff}}(c; \epsilon, B) = ac^p + bc^q, \tag{8.11}$$

where a and b are functions of ϵ and B. Through the ϵ range $0.467 - 0.48$ the fit gives $p = 2$ and $q = 4$ to better than a percent.

The existence of such a potential (which is not present in the far UV theory at all) corresponds to the emergence of multi-trace operators in the spirit of the discussion in [138, 139]. We next plot the coefficients a, b against ϵ in Fig 8.7. a and b are

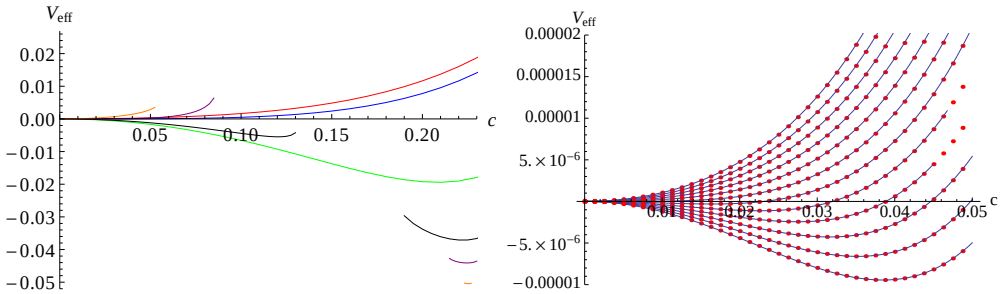

(a) (b)

Figure 8.8: (a) A summary plot of Fig 8.5 showing the Wilsonian potential at six different choices of ϵ on a single plot. (b) The potential and fit (solid line) close to the transition point - the dots are holographically determined data.

approximated as linear functions close to the transition. a is proportional to $(\epsilon - \epsilon_c)$ and b is always positive. This is all standard mean field expectations. In Fig 8.8(a) we plot the potential for different ϵ on a single plot. In Fig 8.8(b) we plot the potential for values of ϵ close to the transition, where the points are the numerical data whilst the solid curves are our fit potentials.

$$V_{\text{eff}}(c;\epsilon,B) = -4.17\left(0.4686 - \frac{\epsilon}{\sqrt{B}}\right)\frac{c^2}{B} + \left(-13.98\frac{\epsilon}{\sqrt{B}} + 10.81\right)\frac{c^4}{B^4}. \tag{8.12}$$

It is clear that the transition is well described by the expected mean field potential. We stress though that here we have derived this form holographically.

Another key feature is visible in Fig 8.5(d)-(e). When we impose a cut-off at $\rho = \epsilon$ we are excluding some range of condensates. In fact even for large ϵ, flows with very large c become complex in the UV before they reach the cut-off as we saw in the $\mathcal{N} = 2$ supersymmetric theory. Qualitatively it makes sense that if we write a Wilsonian effective model at low energies then large condensate values should be excluded from the theory since such states would be completely integrated out - they have an energy above the cut-off.

As we move to much lower ϵ, the deep IR, in addition some intermediate ranges of condensate also disappear from the effective description in the same fashion. This is why there are breaks in the potential plot for low ϵ. Again qualitatively these states have such high energy relative to the low cut-off scale of the effective theory that

they are integrated out.

If ϵ is strictly taken to zero only the regular flows corresponding to the turning points of the potential have finite action. This is clear from Fig 8.4(a). The effective potential we are computing therefore degenerates in the deep IR. In this Wilsonian language though this degeneration seems entirely appropriate - when we have integrated out anything above the vacuum energy it is no surprise we are left with only the vacuum state in our effective theory.

In addition to the vacuum state we have considered so far, in principle, at $\epsilon = 0$ there are an infinite number of meta-stable vacua near the flat embedding. This is shown in the self-similarity (spiral) structure in the c vs m plot in Fig 8.3(b). This self-similarity is realized in our Wilsonian context as follows. When ϵ is large $c = 0$ is the global minimum. As ϵ decreases it becomes a local maximum and a new ground state forms. This is shown in Fig 8.5(c). As ϵ decreases more, $c = 0$ becomes a local minimum Fig 8.5(e), which is preparing to produce a new meta-stable vacuum. As ϵ decreases yet further then $c = 0$ becomes a local maximum again Fig 8.5(f) leaving a meta stable vacuum. This process (from Fig 8.5(c) to Fig 8.5(f)) will continue as $\epsilon \to 0$ leaving more and more meta stable points. The first of these metastable vacua is visible in Fig 8.5(f) where we have focused near the origin at yet lower ϵ.

Finally here we should comment that the precise meaning of these phase transitions and absent regions will depend on the precise choice of cut-off. The cut-off in ρ seems natural in the D7 context but without a precise link between the holographic direction and the field theory RG scale there is some ambiguity. For example one could have chosen to make the cut-off at constant $r = \sqrt{\rho^2 + L^2}$ surface rather than constant ρ. Actually we find that particular choice unnatural because the true IR vacuum state would be missing from the $\epsilon = 0$ theory since the chiral symmetry breaking flow does not hit $r = 0$. Further at the point where the true vacuum disappears from the IR theory its vacuum energy remains above that of the flat embedding because the flat embedding has a missing contribution to its energy from where it extends below the cut off - we don't see the true vacuum emerge at

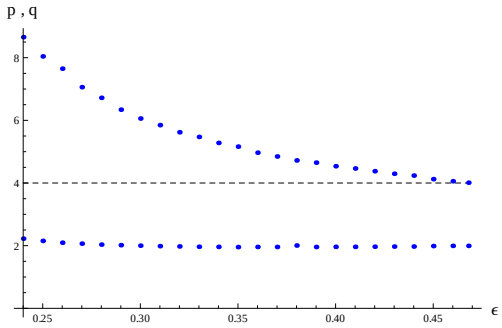

Figure 8.9: The fitting powers p, q in (8.11) as a function of Wilsonian cut-off ϵ below the second order transition.

any scale. This discussion shows though that the choice of cut-off could be dependent on the explicit flow. Although this identification remains an outstanding problem we believe the Wilsonian style description we have presented is very plausible and qualitatively helpful in understanding the holographic description.

8.3.2 Towards an on-shell IR effective potential

It is clear from our Wilsonian analysis above that the deep IR effective potential is highly degenerate. It is interesting though to track the form of the effective potential below the Wilsonian second order transition we described above. We can again fit the potential at varying ϵ to a potential of the form in (8.11). In Fig 8.9 we show the best fit values of the powers p, q with ϵ. Although p stays close to 2, q rises fast at values of ϵ below the second order transition. Of course this does not mean that the c^4 term is switching off but that the coefficients of $c^6, c^8, ..$ type terms are becoming large - one could in principle use a more complex potential fitting form to see this behaviour. At lower values of ϵ than those shown in Fig 8.9 the potential starts to become degenerate.

In the deep IR ($\epsilon = 0$) only the vacuum configuration with $c = 0.2255 B^{3/2}$ and $V = -0.05534 B^2$ is described holographically. If one wishes one can imagine (using dimensional analysis) an effective potential of the form

$$V_{\text{eff}} = \alpha \frac{c^2}{B} + \beta \frac{c^4}{B^4} \tag{8.13}$$

and fit for α and β. We find $\alpha = -2.17659$ and $\beta = 21.4014$.

It is important to stress though that the form of this potential is not fixed by the holographic flows - we could have included more terms with higher powers of c for example that would reproduce the computed values of c and V. Also there is no sense in which this potential is derived away from the minimum - it is an off-shell effective potential extrapolated from on-shell values. That is (8.13) is assumed to be true for off-shell c values so that the condition $\frac{\partial V}{\partial c} = 0$ makes sense. However, α and β are fixed only by on-shell data. In our off-shell method at finite ϵ above, α and β are determined by the off-shell data.

The on-shell action also describes a second order phase transition as $B \to 0$. For $B > 0$ the quark condensate grows as $B^{3/2}$ as it must on dimensional grounds. It is important to stress the difference between this transition and the holographic transition we found above with changing ϵ at fixed B.

8.3.3 B and perpendicular E

The pure B field theory is also very closely related to the theory with both a magnetic and perpendicular electric field present [69, 153, 155, 157]. The D7 action is

$$\mathcal{L} = -\rho^3\sqrt{(1+L'^2)}\sqrt{\left(1+\frac{R^4}{(L^2+\rho^2)^2}(B^2-E^2)\right)}. \tag{8.14}$$

Clearly this is little different from the previous case since we have an effective $\tilde{B} = \sqrt{B^2 - E^2}$. Indeed one can think of this system as a boosted version of the static case with just a B field. However, we find it a useful case to consider in this form because we can compare the magnitude of the condensate in units of the magnetic field with varying electric field value. It is interesting to have more than one scale in the problem.

One expects, since $\tilde{B}$ is the only scale in the DBI action that at small E values

$$c \sim (B^2 - E^2)^{3/4}. \tag{8.15}$$

In other words there should be a second order transition at $E = B$ with a non-mean field exponent.

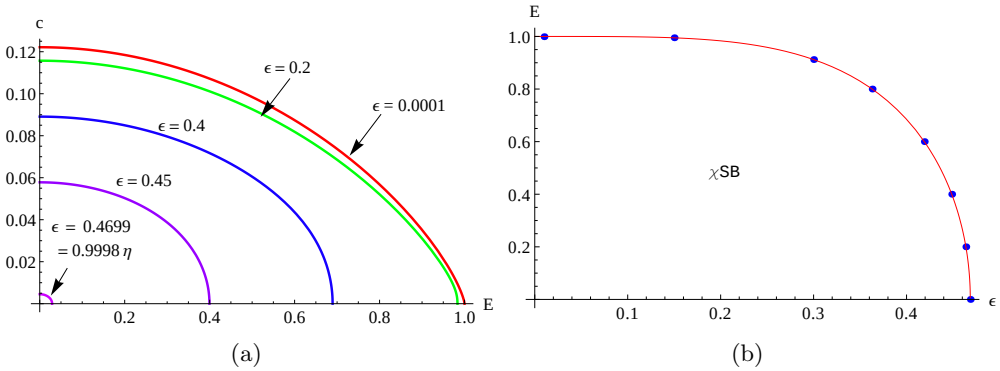

Figure 8.10: (a) Plot of the quark condensate against electric field (with a background perpendicular B field ($B = 1$)) at different values of ϵ. (b) Plot of the $E - \epsilon$ phase diagram - the points are derived from the holographic flows whilst the continuous curve is $E = \sqrt{1 - (\epsilon/\eta)^4}$

Above the transition the theory exhibits a singular surface where the DBI action naively turns complex. This can be resolved by introducing currents induced by the electric field. The theory becomes a conductor as well as chirally symmetric. We will not be exploring this high E phase here.

We can study the theory in our Wilsonian approach with a cut-off ϵ. The theory is equivalent to the analysis of our previous section but with B replaced by $\tilde{B}$. We can write the effective potential, valid close to the Wilsonian transition (8.12)

$$\frac{V_{\text{eff}}}{\tilde{B}^2} = \alpha \left(\frac{\epsilon}{\tilde{B}^{1/2}} - \eta \right) \frac{c^2}{\tilde{B}^3} + b \frac{c^4}{\tilde{B}^6}, \tag{8.16}$$

where

$$\eta = \frac{\epsilon_c}{\tilde{B}^{1/2}} = 0.4686, \quad \alpha = 4.17. \tag{8.17}$$

We can now hold ϵ fixed and vary E. This potential tells us the full E dependence of the theory near the transition point. In particular we can determine the transition point from where the mass term changes sign.

$$E_c^2 = B^2 - \frac{\epsilon^4}{\eta^4} \tag{8.18}$$

Further by writing $E = E_c + \delta E$ and expanding we find the effective mass squared depends on E as

$$m^2 = \frac{\alpha}{2} \frac{\eta^4}{\epsilon^4} \sqrt{B^2 - E^2} E_c (E - E_c). \tag{8.19}$$

In other words the transition is mean field as one moves in E as well as ϵ.

In Fig 8.10 we plot the condensate against E for various choices of ϵ and the phase diagram in the $E-\epsilon$ plane. It is important to realize that the transition for which we have found the effective potential is that at finite positive B^2-E^2 and finite ϵ close to the transition in ϵ. In other words our effective theory describes the $c-E$ plot only near the $c=0$ axis. We can see that the range of validity of our effective theory is only away from the point $\tilde{B}=0$ (i.e. away from $E=B$)

$$\sqrt{B^2-\frac{\epsilon^4}{\eta^4}}<E<B, \tag{8.20}$$

which clearly has no extent at $\epsilon=0$ The point $\epsilon=0$ on the E axis of the $c-E$ plot is distinct with a critical exponent of $3/4$ relative to the mean-field exponent along the rest of the axis. We can not compute the form of the effective potential for the transition at $\epsilon=0$ other than in the on-shell fashion described in the previous section.

8.4 Transitions with B-field and Density

The next models we will explore are the D3/D7 and the D3/D5 systems with magnetic field, to trigger chiral symmetry breaking, and density, d, which opposes chiral symmetry breaking. The phase structure of these theories has been explored in chapter 4 and [91] for the D3/D7 system that has a second order mean field transition with increasing density, and in chapter 5 and [92] for the D3/D5 system that displays a holographic BKT transition in which the condensate grows like an exponential of $-1/\sqrt{d_c-d}$. Our goal is again to use Wilsonian techniques to learn about these transitions and find the form of the effective potential responsible for the BKT transitions. This system is more complicated than the pure B system as we shall see but we will again enforce that all flows we compare have the same IR boundary conditions at the Wilsonian cut-off to give a concrete prescription. The outcome is a consistent Wilsonian picture of the theories and our ability to derive the effective potential for the condensate including a potential that generates the BKT behaviour. We will concentrate first on the D3/D7 system.

8.4.1 Density in the D3/D7 system

Density is introduced into the theory through a background value for the temporal gauge field of the $U(1)$ baryon number [55, 56, 75, 76]. The UV asymptotic form of the field is $\tilde{A}_t = 2\pi\alpha' A_t = \mu + d/\rho^2 + ..$ and describes the chemical potential μ and the quark density d. The probe D7 DBI action with $\tilde{A}_t$ is given by

$$\mathcal{L} = -\rho^3\sqrt{1 + L'^2 - \tilde{A}_t'^2}\sqrt{1 + \frac{B^2}{(\rho^2 + L^2)^2}}. \tag{8.21}$$

Since the action only depends on the derivative of $\tilde{A}_t$ there is a conserved charge density, d, defined as

$$d \equiv \frac{\partial \mathcal{L}}{\partial \tilde{A}_t'}. \tag{8.22}$$

We may Legendre transform the Lagrangian (8.21) to write the action in terms of density

$$\begin{aligned} \mathcal{L}_{\text{LT}} &= \mathcal{L} - \tilde{A}_t' d \\ &= -\sqrt{1 + L'^2}\sqrt{d^2 + \rho^6\left(1 + \frac{B^2}{(\rho^2 + L^2)^2}\right)}. \end{aligned} \tag{8.23}$$

For fixed B and d we can find solutions to the embedding equation of the D7 brane with UV behaviour $m + c/\rho^2$. We plot example flows in Fig 8.11(a). At first sight this system seems rather different from the $d = 0$ theory - solutions for a large range of c extended all the way to $\rho = 0$. One can naively evaluate the action of these curves and plot it as an effective potential against c - see Fig 8.11(b). This interpretation is though incorrect for several reasons.

Firstly, these flows all meet the L axis at different angles. This means that they have different IR boundary conditions and we should not compare their action in a standard Euler-Lagrange context. Further, since $L'(0) \neq 0$ these branes are actually kinked at $\rho = 0$, when $SO(4)$ rotated to provide the full D7 embedding.

Secondly, these flows have a non-zero gauge field on their surface that should be sourced. In [56] the authors argued that the correct source should be fundamental strings stretched between the D3 (or the origin) and the D7 branes. These would be

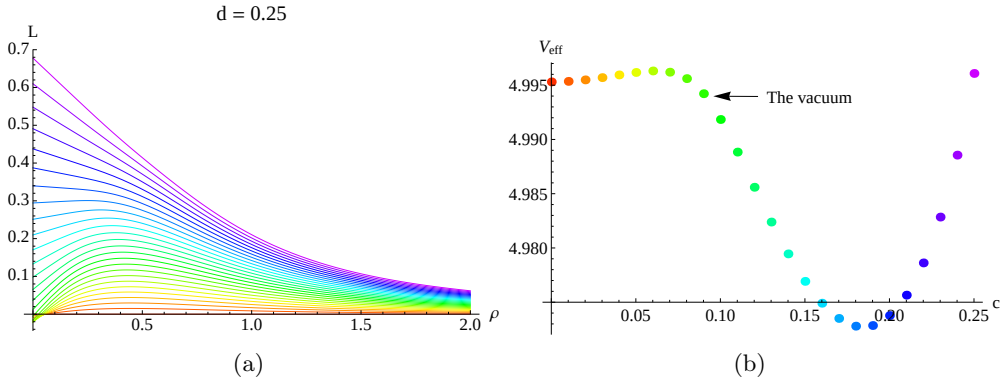

Figure 8.11: (a) D7 embeddings with a fixed B field ($B = 1$) and density ($d = 0.25$) but varying condensate c. (b) The incorrect effective potential derived by integrating over the action of the flows in (a) - the position of the true vacuum is marked.

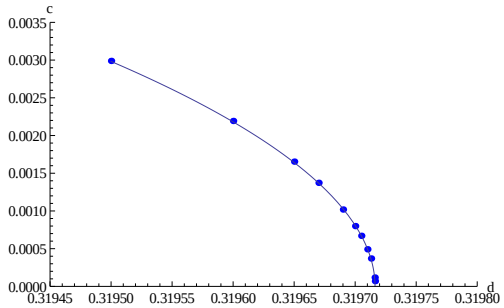

Figure 8.12: A plot of the quark condensate parameter c versus density in the D3/D7 system with a magnetic field $B = 1$.

explicitly the quarks corresponding to the density. Such a continuous distribution of fundamental strings can be absorbed into the D7 world volume and show up as the D7 brane spiking to the origin of the space. The authors of [56] argued in this way that only the embedding that ends at the origin was a "good" flow and it should represent the vacuum. This is now the standard interpretation and has provided a coherent picture across a wide range of problems including density.

Note that, with a naive choice of boundary condition shown in Fig 8.11(a), the vacuum flow for massless quarks is not the minimum of the potential (Fig 8.11(b)). This is no surprise since the other flows are not physical.

Using the "good" flow condition one can compute the quark condensate against density at fixed B (Fig 8.12). There is a phase transition at $d = d_c = 0.3198$. It is second order and mean field in nature ($c \sim \sqrt{d_c - d}$).

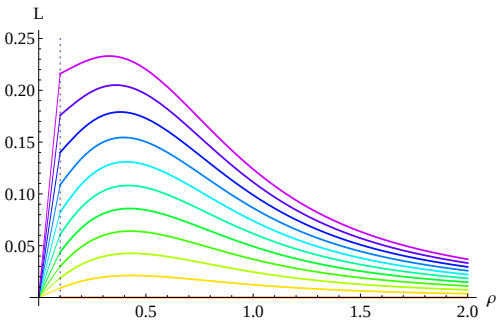

Figure 8.13: An example of matching UV flows to flows between the two cut-offs ϵ_+ and ϵ_- (here $\epsilon_- = 0$) which have $L(\epsilon_- = 0) = 0$.

8.4.2 Wilsonian Flows and Potentials

Our traditional analysis of the D3/D7 system with B, d has again left us with no consistent supergravity flows that describe off-shell quark condensate configurations. Let us try to use a Wilsonian cut-off to provide a hint as to how to proceed. To make progress we will again introduce a cut-off with structure consisting of two boundaries in ρ at ϵ_- and ϵ_+.

First consider the case when $\epsilon_- = 0$ but ϵ_+ is finite. For massless quarks, we shoot in from the UV, using a boundary condition of the form c/ρ^2, to the cut-off ϵ_+. These configurations must be unified to a single IR boundary condition at ϵ_-. They also have a non-zero A_t on their world volumes for which we must provide a source. Two of the flows, the true vacuum and the flat $L = 0$ embedding, have smooth extensions to $\epsilon_- = 0$ which end at the origin. These flows describe good vacuum states of the field theory and must be included. They, therefore, dictate what our choice must be for the ϵ_- boundary condition: we must have the flows satisfying $L(\epsilon_-) = 0$, so that we can correctly compare their actions. It is natural then to complete the off shell solutions with flows from $L(\epsilon_-) = 0$ to ϵ_+ that meet the UV flows. We show such flows in Fig 8.13.

We can explore the phase transition with changing density at fixed magnetic field using this cut-off prescription for the deep IR. In Fig 8.14 we show the effective potential for a range of d. Here we take $\epsilon_- = 0$ and $\epsilon_+ = 0.01$ so the cut-off is very thin. There is a second order transition as d is raised matching the previously derived critical value of d. Close to the transition point with changing d we can

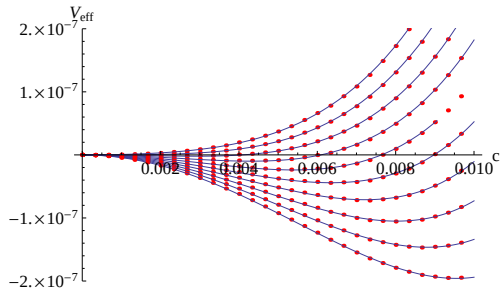

Figure 8.14: The effective potential with $\epsilon_- = 0$ and $\epsilon_+ = 0.01$. $B = 1$. Every curve is for a fixed density increasing from bottom to top. The red points are computed from the holographic flows, the blue lines are our fit potential.

perform a fit to the form of the potential and we find

$$V_{\text{eff}}(c; d) = -5.53(0.3198 - d)c^2 + 30.76c^4, \tag{8.24}$$

This is a mean field potential. In Fig 8.14 the points are holographically derived data whilst the curves are this fit potential. The coefficients of this mean field potential is a function of ϵ_+ in general, but a qualitative mean-field potential form is valid for all ϵ_+ near the phase transition.

Now we would again like to shrink ϵ_+ to ϵ_- to return to a single cut-off, which will fix our potential uniquely as a function of $\epsilon = \epsilon_- = \epsilon_+$. If we do that with $\epsilon_- = 0$ then the UV flows become those we had declared unphysical in Fig 8.11(a) but with an added length of D7 extending up the L axis from the origin. This suggests that that spike is the completion of the flows to make them physical. One can think of that spike as the fundamental strings that should source the A_t gauge field on the D7 world volume.

What then is the correct way to include the spike contribution at non-zero ϵ_-? The natural answer seems to be to maintain the condition $L(\epsilon_-) = 0$ at finite ϵ_-[2]. We must enforce the same boundary condition on all the flows at ϵ_- and that condition must smoothly map to the case $\epsilon_- = 0$. When we remove the structured cut-off by taking $\epsilon_+ \to \epsilon_- \equiv \epsilon$ we will again be left with a spike from the flow of Fig 8.11(a) to

[2]One could just evaluate the sum of the IR and UV contributions of the flows in Fig 8.13 for varying ϵ_+ and identifying $\epsilon = \epsilon_+$. If one does so then the vacuum flow is the minimum of the potential at all ϵ. This picture then does not match our previous analysis of the pure B theory - in the UV we expect to find a potential that is minimized at $c = 0$ representing the UV bare theory's unbroken symmetry. We have included too much IR information with such a prescription.

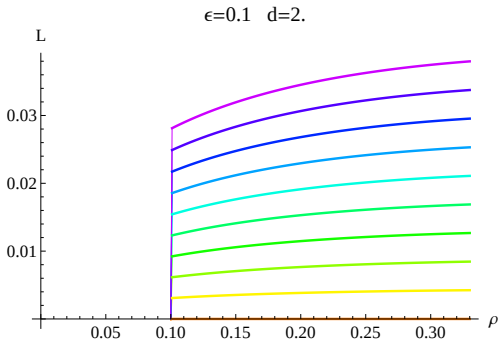

Figure 8.15: Our prescription for completing the flows of Fig 8.11(a) at non-zero Wilsonian cut off is to extended them with a spike lying along the cut-off down to the ρ axis as shown.

the ρ axis, but now at the scale ϵ as shown in Fig 8.15.

In a Wilsonian sense we would argue this is reasonable since the UV degrees of freedom should see all the IR physics compressed at the IR cut-off scale ϵ. In some sense the UV theory can not distinguish the origin from the point $(L = 0, \rho = \epsilon)$. Flows of the form shown in Fig 8.15 will then be our cut-off prescription away from $\epsilon = 0$.

The benefits of this configuration are that with a large cut-off the spike simply increases the action of non-zero c configurations and will leave $c = 0$ as the vacuum, whilst in the $\epsilon \to 0$ limit it will reproduce the known physical solution as the potential minimum. To compute the action of the spike we simply take a very thin limit of our two ϵ prescription - in particular below we will use $\epsilon_+ = \epsilon_- + 0.001$.

Taking this prescription we will now show that we get a sensible Wilsonian story including a derivation of an appropriate effective potential for both the D3/D7 and D3/D5 systems.

We first present results for the D3/D7 system. In Fig 8.16(a)-(c) we show the effective potential as a function of c for three choices of ϵ and various d. $B = 1$ is fixed. At large ϵ for all d we see that $c = 0$ is the preferred vacuum. As ϵ is decreased, provided $d < d_c \sim 0.32$, there is then a transition to a chiral symmetry broken phase. We show examples of values of the cut-off where this transition is first order and second order in Fig 8.16(b) and (c) respectively. We can summarize the full picture by drawing the $d - \epsilon$ phase diagram which we show in Fig 8.16(d). Note that the $d = 0$ transition point matches that we found above. The $\epsilon = 0$

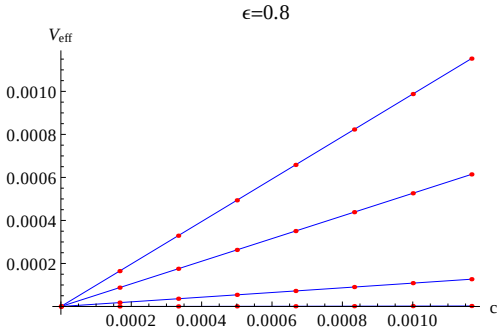

(a) $\epsilon = 0.8$. $d = 0.001, 0.1, 0.5, 1$ from bottom. The theory is always in the chiral phase.

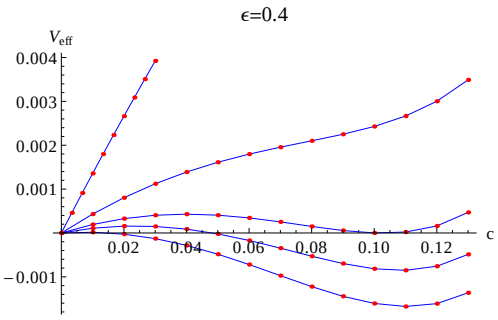

(b) $\epsilon = 0.4$. $d = 1/300, 1/100, 1/62$(transition point),$1/30, 1/10$ from bottom. There is a first order transition

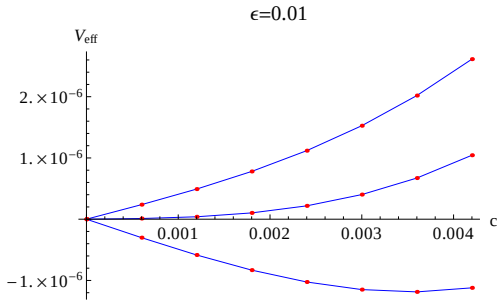

(c) $\epsilon = 0.01$. $d = 0.3085, 0.30879$(transition point),0.309. There is a second order transition

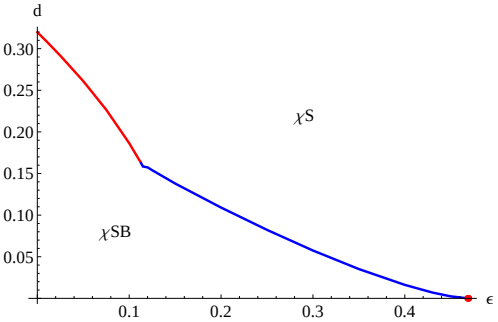

(d) The d-ϵ phase diagram. The blue colour corresponds to a first order transition and the red to second order.

Figure 8.16: The D3/D7 system d-ϵ phase diagram ($B = 1$).

transition point reproduces our potential fit in (8.24). The red line is a mean-field second order transition, while the blue lie is a first order transition.

The insertion of the quark spike with ϵ has therefore provided a believable Wilsonian picture. In fact though as presented so far the IR diverges from the story we told at $d = 0$. In particular we argued that the potential should degenerate as $\epsilon \to 0$ as all states other than the vacuum are integrated from the low energy Wilsonian theory. We simply don't observe the embeddings that shoot in from the UV becoming complex in this system with density for embeddings with condensate values of order d (very large choices of c do still go complex). We've not been able to find a simple resolution. Most likely the effective potential we are deriving here is equivalent to that we produced in the pure $\mathcal{N} = 2$ theory freezing and retaining the potential value at the point where the embeddings go complex - see Fig 8.2(b). We leave this issue for future thought.

8.4.3 BKT transitions in the D3/D5 system

The D3/D5 system with magnetic field and density displays a (holographic) BKT transition [92]. The reason it is distinct from the D3/D7 case is that both B and d are dimension 2 in 2+1 dimension and they can be tuned against each other in the deep IR to force the embedding scalar mode of the theory to violate the Breitenlohner Freedman bound of the effective IR AdS_2. The result is that a BKT transition occurs with an exponential growth of the order parameter (quark condensate) for d below $d_c = \sqrt{7}B$ ($c \sim e^{-1/\sqrt{d_c - d}}$). This is discussed in detail in [92] and chapter 5. Our goal here is to derive an effective potential for a BKT transition.

The probe D5 brane is embedded in the t and two x directions of the D3 brane coordinates so that the quarks live on a 2+1 dimensional defect in the $\mathcal{N} = 4$ gauge theory [94–97]. The D5 brane also extends in three directions perpendicular to the D3 brane. The probe D5 brane DBI action with $\tilde{A}_t$ and B present is given by

$$\mathcal{L} = -\rho^2 \sqrt{1 + L'^2 - \tilde{A}_t'^2} \sqrt{1 + \frac{B^2}{(\rho^2 + L^2)^2}}. \tag{8.25}$$

We may Legendre transform to write the action in terms of density (8.22)

$$\begin{aligned} \mathcal{L}_{\text{LT}} &= \mathcal{L} - \tilde{A}_t' d \\ &= -\sqrt{1 + L'^2} \sqrt{d^2 + \rho^4 \left(1 + \frac{B^2}{(\rho^2 + L^2)^2}\right)}. \end{aligned} \tag{8.26}$$

For fixed B and d we can find solutions to the embedding equation of the D7 brane with UV behaviour $m + c/\rho$.

Following the last section we will introduce a cut-off at the scale ϵ and complete the UV flows with a spike down the cut-off to the ρ axis (we again fix $\epsilon_+ = \epsilon_- + 0.001$ to generate the spike's action) - see Fig 8.15. We can determine the phase diagram of the theory in the $d - \epsilon$ space at fixed B which is shown in Fig 8.17. The transition is first order at large ϵ (the blue line) then becomes a mean field second order transition at small ϵ before finally ending on a BKT transition at $\epsilon = 0$. The cut-off

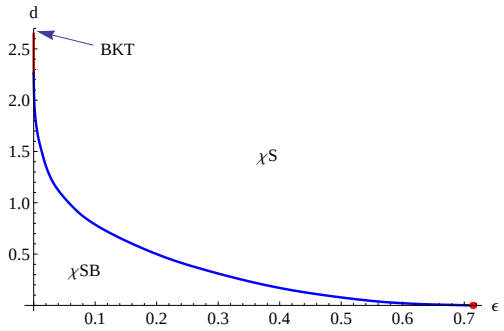

Figure 8.17: The D3/D5 system d-ϵ phase diagram ($B = 1$). The blue colour corresponds to a first order transition, the red to a second order and the end point BKT transition is labelled.

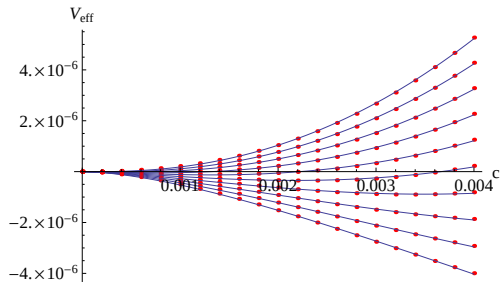

Figure 8.18: The potential with the cut-off $\epsilon = 0$ for the condensate in the D3/D5 system at fixed B ($B = 1$) and finite density close to the transition. Every curve is for a fixed density increasing from bottom to top. Red points are holographic data and the blue curves are the fitted potential in (8.28).

behaves like temperature which has already been observed to convert the BKT transitions to second order with the introduction of any non-zero temperature [92].

We plot the $\epsilon \to 0$ potential for varying choices of d in Fig 8.18. This potential can not be well fitted by a mean field potential. Instead if we fit to

$$V_{\text{eff}} = ac^2 + bc^2(\log c)^2, \tag{8.27}$$

we find a good fit - see Fig 8.18. The fitting potential in Fig 8.18 is

$$V_{\text{eff}}(c;d) = (0.74d^2 - 4.72)c^2 + (0.016d^2 - 0.12)c^2(\log c)^2. \tag{8.28}$$

This potential form implies that the condensate near the phase transition is

$$c \sim e^{-\frac{\sqrt{-4a+b}}{2\sqrt{b}}} \sim e^{\frac{-3.29}{\sqrt{2.77-d}}} . \tag{8.29}$$

Note that to numerically extract this data one needs to work at extremely high

accuracy near the transition where the condensate is exponentially small. The data shown are the best we have managed. In fact the form of the condensate is known analytically to be given by [92]

$$c \sim e^{\frac{-3.86}{\sqrt{2.65-d}}}. \tag{8.30}$$

Although we have not reproduced this perfectly our numerics support this form. We consider it a considerable success to have derived the potential for the BKT transition in the holographic setting.

8.5 Conclusions

We have analyzed the phase structure of a number of theories that break chiral symmetry and have a holographic dual using a Wilsonian cut-off. Including a cut-off allows us to consider off-shell states, i.e. configurations with a value of the quark condensate different from that in the true vacuum. We believe that the results give an improved intuitive understanding of the holographic description and we have been able to derive low energy effective actions for the phase transitions in these models including a potential for a BKT transition. The precise identification of our cut-offs in the holographic description and the equivalent cut-off structure in the gauge theory remains inexact but the spirit seems correct.

We first studied the D3/D7 system (the $\mathcal{N} = 4$ gauge theory with quark hypermultiplets in 3+1d). This theory has $\mathcal{N} = 2$ supersymmetry and does not generate a quark condensate. We nevertheless can in principle plot an effective potential for the condensate that should be minimized at zero. The D7 embedding encodes the quark condensate and in Fig 8.1(a) we display the Euler Lagrange solutions for the theory with different condensate values. In Fig 8.1(b) we insert a cut-off at a finite value of ρ - here we give the cut-off some finite width and use that width to match all of the solutions to solutions of the Euler Lagrange equations with the same IR boundary condition at the lower cut-off. In this case as one shrinks the width of the cut-off, the UV action returns to that of just the UV flow. In Fig 8.2 we plot the Wilsonian potential, evaluated from the action of the D7 brane above

the cut-off, in the theory as a function of cut-off value. The Wilsonian potential is indeed minimized at zero condensate at all energy scales. There is a finite extent of the potential in the quark condensate because the embeddings become complex (which we showed analytically in (8.7). We interpret the removal of large condensate configurations from the low energy effective actions as representing those configurations having too high energy to appear in the low energy theory.

The same system with an applied magnetic field has chiral symmetry breaking. We display the Euler Lagrange solutions for the D7 branes with different condensate values in Fig 8.4(a). We introduced a cut off at finite ρ as in the pure $\mathcal{N} = 2$ theory. In Fig 8.5 we plot the resulting Wilsonian potential as a function of cut-off value. The UV of the theory preserves chiral symmetry. The system then shows a second order mean field transition to the broken phase at intermediate cut-offs in the spirit of a Coleman Weinberg transition. The form of the potential near the transition can be extracted numerically and is displayed in (8.12). Finally in the deep IR non-vacuum configurations begin to be integrated out of the IR effective theory because they can not be accessed with the IR theory's energy and the effective potential again degenerates.

We translated these results to the theory with a magnetic field and perpendicular electric field. This theory shares the same DBI action as the pure B theory but our results enlarge to describe the phase diagram in the electric field versus cut-off plane, which we show in Fig 8.10.

We then added a constant quark density into the D3/D7 theory with magnetic field. The density opposes chiral symmetry breaking. In Fig 8.11 we show the D7 embeddings for different values of the quark condensate which are again ill determined because they end at the IR axis in a kinked configuration. The true vacuum is the embedding that ends at the origin. Introducing a cut-off with width as in Fig 8.13 allows us to define non-vacuum configurations that all end at the origin. If we take that cut-off to zero then the embeddings are completed by a spike to the origin. For a generic value of the Wilsonian cut-off we have suggested that such a spike should be introduced along the cut-off as shown in Fig 8.15. Using this

prescription we have determined the phase structure in the density, cut-off plane at fixed magnetic field, see Fig 8.16. Here we see first order transitions with changing Wilsonian scale as well as mean field cases. The IR transitions are mean field and the effective potential is of the form given in (8.24) (in units of B).

Finally we looked at the D3/D5 system describing the $\mathcal{N} = 4$, 3+1 dimensional theory with quarks introduced on a 2+1 dimensional defect. Here with a magnetic field and density the zero temperature theory exhibits a holographic BKT transition. We have again determined the phase diagram in the density cut-off plane at fixed magnetic field in Fig 8.17. As the cut-off is lowered the transition changes from first to second order before becoming a BKT transition in the deep IR. We have been able to derive an effective potential for the BKT transition in the IR given by (8.28).

The Wilsonian style analysis therefore allows one to see strongly coupled versions of Coleman Weinberg like symmetry breaking transitions. It also allows us to derive the low energy effective action in these theories by defining off-shell configurations. The effective potential for the BKT transition is a new result derived here.

A number of problems remain to be analyzed in these settings including introducing finite temperature and looking at the non-mean field transitions that lie between mean field and BKT transitions [111]. We hope to study these in the future. These methods will hopefully also be of use away from the probe limit where even simple deformations of AdS are typically singular and hard to interpret [74, 158].

Chapter 9

Discussion

In this thesis holographic methods where employed to study strongly coupled field theories. Of particular interest throughout this work were chiral phase transitions. Various phase diagrams where produced regarding chiral phase transitions and in some cases confinement/deconfinement transitions. The underlying purpose of all studies performed was to investigate theories which are in the spirit of QCD and exhibit QCD-like characteristic, with the hope that these theories would provide an insight into how QCD and strongly coupled theories could potentially behave e.g perhaps give a hint for the existence of new phases in the phase diagram.

In chapter 4 a D3/D7 system was studied which is the dual description of a 3+1d $\mathcal{N} = 2$ SYM strongly coupled field theory with fundamental matter. To introduce chiral symmetry breaking a magnetic field was turned on in the D3/D7 system, which provided the scale for the chiral symmetry breaking. The purpose of the chapter was the exploration of the phase diagram of the theory and therefore the study was performed at finite temperature and chemical potential. A confinement / deconfinement phase transition was studied as well. It should be made clear though that bound states in this setup are more in the spirit of atomic bound states rather than QCD bound states. The reason for this is that firstly the $\mathcal{N} = 4$ background does not induce linear confinement and secondly the presence of any temperature leads to screening of the quarks at the length scale of the inverse temperature.

The phase diagram produced was rich with first and second order phase transitions

connected by a tricritical point and with the chiral transition and confinement/deconfinement transition been separated for the most part of the phase diagram. Also, the order of the chiral transition was found to be first order with temperature and second order with chemical potential. Our phase diagram does not match the standard picture of the QCD phase diagram but the real phase diagram of QCD is not known. Many different scenarios are possible and some of them qualitatively match our chiral transition phase diagram. Another element that distinguishes our phase diagram from the standard picture of QCD is the existence of a phase with chiral symmetry broken and finite density, in some part of the phase diagram, created by the confinement/deconfinement transition when this transition is separated from the chiral transition. This phase and the separation of the two different transitions could potentially exist in QCD. Therefore, although our phase diagram might not describe true QCD, a very rich structure arose which develops our intuition about strongly coupled field theories.

In chapter 5 the same analysis was performed as in chapter 4, but this time for a D3/D5 brane system. This setup corresponds to a 2+1d $\mathcal{N} = 2$ SYM strongly coupled field theory with fundamental matter. The phase diagram calculated has the same structure as that of chapter 4, apart from the zero temperature chiral transition. At zero temperature a BKT transition was present as opposed to the mean field transitions present in other regions of the diagram. This type of transition is relatively new in holography and it could potentially be of interest in condense matter physics, where such transitions are known to exist.

In chapter 6 a D3/D7 system was explored again for finite temperature and chemical potential. The new element of this chapter was the introduction, by hand, of a running dilaton (instead of the magnetic field used in the previous chapters) in order to induce chiral symmetry breaking. Some parameters in the dilaton profile were free to be dialed and the purpose was to explore all the possible phase diagrams that can arise using holography for different parameters of the running coupling. The purpose was achieved since a plethora of phase diagrams were produced for different running couplings, among them a diagram matching the standard picture of QCD. Therefore, the analysis done in this chapter clearly proves

that holography can very easily model many different phase diagrams and at the same time gives a hint on how the profile of the running coupling can affect the form of the phase diagram.

The analysis performed in the chapters 4,5,6 included bound states of mesons or a quark-gluon plasma phase but no baryons at all. The QCD phase diagram is known to have a baryon phase transition in low temperatures and for increasing chemical potential, which is first order for zero temperature and second order for some range of temperatures. In chapter 7 a baryon vertex was introduced in the field theory by introducing a wrapped D5 brane in the gravity description. The rest of the setup remained the same as in chapter 6. The analysis of the baryon vertex revealed that, at least for some dilaton profiles, a baryon phase can exist in our holographic phase diagram in the area of the phase diagram expected from QCD. The phase transition is second order for all temperatures up to some critical temperature where the phase ceases to exist. The order of the transition found in our study is different from that expected in QCD for the zero temperature case but that could be because the interactions between the nucleons, which result in the first order transition, are not included in the D3/D7 system.

Furthermore, Wilson loops where used to explore the possibility that baryon formation and their presence in the phase diagram can be related, in a loose way, to confinement in the geometry. Indeed, according to our analysis, the potential between the quark-antiquark pairs became linear at the same values of dilaton parameters that gave rise to baryons as preferable configurations in the phase diagram, giving a qualitative consistent picture.

In chapter 8 the idea of Wilsonian renormalisation approach in holography was applied. The aim was to understand chiral phase transitions for different Wilsonian cutoffs and to holographically produce effective potentials for the quark condensate near the transition points. D3/D7 and D3/D5 brane setups where considered, whose phase structure was known. Wilsonian (energy) cutoffs where imposed in order to split the embedding solutions in two pieces, the high energy(UV) regime and low energy(IR) regime . The UV part of the solution was integrated out so that

a Wilsonian description would emerge. Effective potentials where succefully derived using this holographic method, giving examples of first, second (mean-field or not) and BKT transitions.

In this chapter a clear picture of phase transitions in Wilsonian language was been achieved. Some problems remain unsolved like the the choice of the cutoff, whose choice might seem a bit naive since it does not give a clear picture of the field theory cutoff. Also what was used as energy scale in our holographic models does not have a precise matching in the field theory side. Nevertheless, the results derived are consistent with the expectations of the Wilsonian description and provide a qualitative holographic way of understanding chiral phase transitions. .

Finally, in this thesis many different studies of strongly coupled field theories where performed by using gauge /gravity duality. The strongly coupled field theories used are considerably different than QCD (superpartners, large N e.t.c) but manage to captures many characteristics of QCD. The holographic analysis is considerably easier than attempting to calculate strongly coupled phenomena using other methods and at the same time it does provide a very rich picture that could be useful to understand strongly coupled field theories.

Bibliography

[1] D.J. Gross and F. Wilczek , *" Ultraviolet Behavior of Non-Abelian Gauge Theories, "* Phys. Rev. Lett. **30**, 13431346 (1973)

[2] H. Politzer, *" Reliable Perturbative Results for Strong Interactions?, "* Phys.Rev.Lett. 30 (1973) 13461349.

[3] S. Weinberg , *" Non-Abelian Gauge Theories of the Strong Interactions, "* Phys. Rev. Lett. **31**, 494497 (1973)

[4] H. Fritzsch, M. Gell-Mann, H. Leutwyler , *" Advantages of the color octet gluon picture, "* Phys. Lett. B **47**, 365 (1973)

[5] K.G. Wilson, J. Kogut, *" The renormalization group and the ϵ expansion, "* Phys. Rep. **12** 2 75199 (1974)

[6] M. Gell-Mann, Y. Neeman, *" The Eightfold Way, "* (Benjamin, New York, 1964)

[7] M. Gell-Mann, *" A Schematic Model of Baryons and Mesons, "* Phys.Lett. **8** (1964) 214215.

[8] G. Zweig, *" An $SU(3)$ model for strong interaction symmetry and its breaking, "* CERN-TH-401 ;CERN-TH-412

[9] P.W. Higgs, *" Broken Symmetries and the Masses of Gauge Bosons, "* Phys. Rev. Lett. **13**, 508509 (1964)

[10] F. Englert, R. Brout *" Broken Symmetry and the Mass of Gauge Vector Mesons, "* Phys. Rev. Lett. **13**, 321323 (1964)

[11] G.S. Guralnik, C.R. Hagen, T.W.B. Kibble , *" Global Conservation Laws and Massless Particles, "* Phys. Rev. Lett. **13**, 585587 (1964)

[12] Y. Nambu, *" Axial Vector Current Conservation in Weak Interactions, "* Phys. Rev. Lett. **4**, 380 (1960)

[13] J. Goldstone, *" Axial Vector Current Conservation in Weak Interactions, "* Nuovo Cim. **19**, 154 (1961)

[14] S. Scherer,M.R. Schindler, *"A Chiral Perturbation Theory Primer,"* [arXiV:hep-ph/0505265].

[15] M. E Peskin, D. V. Schroeder, *" An Introduction to Quantum Field Theory, "* WestView Press 1995.

[16] I. J. Aitchison, A. V. Hey, *" Gauge Theories in Particle Physics Vol.II: QCD and the Electroweak Theory, "* Graduate Student Series in Physics, Third Edition (2004).

[17] T. Schaefer , *"Phases of QCD ,"* [arXiv:hep-ph/0509068]

[18] K. Rajagopal and F. Wilczek, *"The Condensed Matter Physics of QCD ,"* [arXiv:hep-ph/0011333].

[19] M. Stephanov , *"QCD phase diagram: an overview ,"* PoS **LAT2006** (2006) 024 [arXiv:hep-lat/0701002].

[20] Owe Philipsen , *"Towards a determination of the chiral critical surface of QCD ,"* [arXiv:0910.0785 [hep-ph]].

[21] W. Weise , *"Nuclear Chiral Dynamics and Phases of QCD ,"* [arXiv:1201.0950 [nucl-th]].

[22] M. Cheng et al., Phys. Rev. D **77** (2008) 014511 ; Phys. Rev. D **81** (2010) 054510

[23] S. Borsanyi et al. , *"Is there still any T_c mystery in lattice QCD? Results with physical masses in the continuum limit III ,"* JHEP **1009**, 073 (2010) [arXiv:1005.3508 [hep-lat]] .

[24] A. Bazanov, P. Petreczky , *"Deconfinement and chiral transition with the highly improved staggered quark (HISQ) action ,"* PoS **LAT2009**, 163 (2009) [arXiv:1005.1131 [hep-lat]]

[25] Y. Aoki, Z. Fodor, S.D. Katz, K.K. Szabo , *"The QCD transition temperature: Results with physical masses in the continuum limit ,"* Phys. Lett. B **643** (2006) 46 [arXiv:hep-lat/0609068]

[26] K. Becker, M. Becker, J.H. Schwarz, *"String theory and M-theory,"* Cambridge University Press (2007).

[27] M.B. Green, J.H. Schwarz, E. Witten, *"Superstring Theory, Volume 1,"* Cambridge University Press (1987).

[28] Clifford V. Johnson, *"D-Branes,"* Cambridge University Press (2003)

[29] R.J. Szabo, *"An introduction to String theory and D-brane dynamics,"* 2nd edition, Imperial College Press.

[30] B. Swiebach, *"A first course in String theory,"* Cambridge University Press (2004).

[31] G. t'Hooft, *"A Planar Diagram Theory for Strong Interactions,"* Nucl. Phys. B **72** (1974) 461.

[32] O. Aharony, S.S. Gubser, J. Maldacena, H. Ooguri, Y. Oz, *"Large N Field Theories, String Theory and Gravity,"* Phys.Rept. **323**, 183-386 (2000) [arXiV:hep-th/9905111].

[33] G. Horowitz, J. Polchinski, *"Gauge/Gravity duality,"* [arXiv:gr-qc/0602037].

[34] G.T. Horowitz, A. Strominger, *"Black strings and P-branes ,"* Nucl. Phys. **B360** (1991) 197209

[35] E. D'Hoker, D.Z. Freedman, *"Supersymmetric Gauge Theories and the AdS/CFT Correspondence,"* [arXiv:hep-th/0201253].

[36] J. Maldacena, *"TASI 2003 Lectures on AdS/CFT, "* [arXiv:hep-th/0309246]

[37] J. Casalderrey-Solana, Hong Liu, D. Mateos, K. Rajagopal, U.A. Wiedemann *"Gauge/String Duality, Hot QCD and Heavy Ion Collisions, "* [arXiv:1101.0618 [hep-th]].

[38] Y. Kim, I.J. Shin, T. Tsukioka, *"Holographic QCD: Past, Present and Future, "* [arXiv:1205.4852 [hep-th]].

[39] J. Erdmenger, N. Evans, I. Kirsch, E. Threlfall, *"Mesons in Gauge/Gravity Duals - A Review, "* Eur. Phys. J. A **35** (2008) 81 [arXiv:0711.4467 [hep-th]].

[40] A.W. Peet, J. Polchinski *"UV/IR Relations in AdS Dynamics, "* Phys.Rev. D **59** 065011 (1999) [arXiv:0711.4467 [hep-th]].

[41] L. Martucci, J. Rosseel, D. Van den Bleeken, and A. Van Proeyen, *"D-branes on backgrounds with fluxes, "* Class. Quant. Grav. **22** (2005) 2745-2764 [hep-th/0504041]

[42] T. Sakai and S. Sugimoto, *"Low energy hadron physics in holographic QCD,"* Prog. Theor.Phys. **113** (2005) 843-882 [hep-th/0412141]

[43] T. Sakai and S. Sugimoto, *"More on a holographic dual of QCD,"* Prog. Theor. Phys. **114** (2006) 1083-1118 [hep-th/0507073]

[44] Edward Witten *" Anti de Sitter Space,Transition, and confinement in gauge theories, "* Adv.Theor.Math.Phys. **2** 505-532,1998 [arXiv:hep-th/9803131]

[45] Horatiu Nastase, *" Introduction to AdS-CFT, ",* [arXiv:0712.0689 [hep-th]]

[46] J. Maldacena *"The Large N Limit of Superconformal Field Theories and Supergravity, "* Adv. Theor. Math. Phys. **2**, 231 (1998) Int. J. Theor. Phys. **38**, 1113 (1999) [arXiv:hep-th/9711200].

[47] Edward Witten, *" Anti De Sitter Space And Holography, "* Adv. Theor. Math. Phys. **2** (1998) 253 [arXiv:hep-th/9802150].

[48] S.S. Gubser, I.R. Klebanov and A.M. Polyakov, *" Gauge Theory Correlators from Non-Critical String Theory, "* Phys. Lett. B **428** (1998) 105 [arXiv:hep-th/9802109].

[49] P. Breitenlohner and D. Z. Freedman, *" Positive Energy in anti-De Sitter Backgrounds and Gauged Extended Supergravity, "* Phys. Lett. B **115** (1982) 197

[50] P. Breitenlohner and D. Z. Freedman, *" Stability in Gauged Extended Supergravity "* Ann. Phys. **144** (1982) 249

[51] A. Karch and E. Katz, *"Adding flavor to AdS/CFT, "* JHEP **0206**, 043 (2002) [arXiv:hep-th/0205236].

[52] M. Grana and J. Polchinski, *"Gauge-gravity duals with holomorphic dilaton,"* Phys. Rev. **D65** (2002) 126005, [arXiv: hep-th/0106014].

[53] M. Bertolini, P. Di Vecchia, M. Frau, A. Lerda and R. Marotta, *"N = 2 gauge theories on systems of fractional D3/D7 branes,"* Nucl. Phys. B **621**, 157 (2002) [arXiv:hep-th/0107057].

[54] M. Kruczenski, D. Mateos, R. C. Myers and D. J. Winters, *"Meson spectroscopy in AdS-CFT with flavor,"* JHEP **0307** 049, 2003 [arXiv:hep-th/0304032].

[55] S. Nakamura, Y. Seo, S. J. Sin and K. P. Yogendran, *"A new phase at finite quark density from AdS/CFT,"* J. Korean Phys. Soc. **52**, 1734 (2008) [arXiv:hep-th/0611021].

[56] S. Kobayashi, D. Mateos, S. Matsuura, R. C. Myers and R. M. Thomson, *"Holographic phase transitions at finite baryon density,"* JHEP **0702**, 016 (2007) [arXiv:hep-th/0611099].

[57] S. Nakamura, Y. Seo, S. J. Sin and K. P. Yogendran, *"Baryon-charge Chemical Potential in AdS/CFT,"* Prog. Theor. Phys. **120**, 51 (2008) [arXiv:0708.2818 [hep-th]].

[58] A. Karch and A. O'Bannon, *"Holographic Thermodynamics at Finite Baryon Density: Some Exact Results,"* JHEP **0711**, 074 (2007) [arXiv:0709.0570 [hep-th]].

[59] D. Mateos, S. Matsuura, R. C. Myers and R. M. Thomson, *"Holographic phase transitions at finite chemical potential,"* JHEP **0711** (2007) 085 [arXiv:0709.1225 [hep-th]].

[60] K. Ghoroku, M. Ishihara and A. Nakamura, *"D3/D7 holographic Gauge theory and Chemical potential,"* Phys. Rev. D **76**, 124006 (2007) [arXiv:0708.3706 [hep-th]].

[61] K. Peeters, J. Sonnenschein and M. Zamaklar, *"Holographic melting and related properties of mesons in a quark gluon plasma,"* Phys. Rev. D **74** (2006) 106008 [arXiv:hep-th/0606195].

[62] C. Hoyos-Badajoz, K. Landsteiner and S. Montero, *"Holographic Meson Melting,"* JHEP **0704** (2007) 031 [arXiv:hep-th/0612169].

[63] J. Erdmenger, M. Kaminski and F. Rust, *"Holographic vector mesons from spectral functions at finite baryon or isospin density,"* Phys. Rev. D **77**, 046005 (2008) [arXiv:0710.0334 [hep-th]]

[64] J. Erdmenger, C. Greubel, M. Kaminski, P. Kerner, K. Landsteiner and F. Pena-Benitez, *"Quasinormal modes of massive charged flavor branes,"* arXiv:0911.3544 [hep-th].

[65] V. G. Filev, C. V. Johnson, R. C. Rashkov and K. S. Viswanathan, *"Flavoured large N gauge theory in an external magnetic field,"* JHEP **0710**, 019 (2007) [arXiv:hep-th/0701001]

[66] T. Albash, V. G. Filev, C. V. Johnson and A. Kundu, *"Finite Temperature Large N Gauge Theory with Quarks in an External Magnetic Field,"* JHEP **0807**, 080 (2008) [arXiv:0709.1547 [hep-th]].

[67] V. G. Filev, *"Criticality, Scaling and Chiral Symmetry Breaking in External Magnetic Field,"* JHEP **0804**, 088 (2008) [arXiv:0706.3811 [hep-th]]

[68] V. G. Filev, C. V. Johnson, *"Universality in the Large N_c Dynamics of Flavour: Thermal Vs. Quantum Induced Phase Transitions,"* JHEP **0810**, 058 (2008) [arXiV:0805.1950 [hep-th]]

[69] J. Erdmenger, R. Meyer and J. P. Shock, *"AdS/CFT with Flavour in Electric and Magnetic Kalb-Ramond Fields,"* JHEP **0712**, 091 (2007) [arXiv:0709.1551 [hep-th]].

[70] A. V. Zayakin, *"QCD Vacuum Properties in a Magnetic Field from AdS/CFT: Chiral Condensate and Goldstone Mass,"* JHEP **0807** (2008) 116 [arXiv:0807.2917 [hep-th]].

[71] V. G. Filev, C. V. Johnson and J. P. Shock, *"Universal Holographic Chiral Dynamics in an External Magnetic Field,"* JHEP **0908**, 013 (2009) [arXiv:0903.5345 [hep-th]]

[72] V. G. Filev, *"Hot Defect Superconformal Field Theory in an External Magnetic Field,"* JHEP **0911**, 123 (2009) [arXiv:0910.0554 [hep-th]].

[73] S. S. Gubser, *"Dilaton-driven confinement,"* arXiv:hep-th/9902155.

[74] L. Girardello, M. Petrini, M. Porrati and A. Zaffaroni, *"The supergravity dual of N = 1 super Yang-Mills theory,"* Nucl. Phys. B **569** (2000) 451 [arXiv:hep-th/9909047].

[75] K. Y. Kim, S. J. Sin and I. Zahed, *"Dense hadronic matter in holographic QCD,"* arXiv:hep-th/0608046

[76] K. Y. Kim, S. J. Sin and I. Zahed, *"The Chiral Model of Sakai-Sugimoto at Finite Baryon Density,"* JHEP **0801**, 002 (2008) [arXiv:0708.1469 [hep-th]];

[77] J. Babington, J. Erdmenger, N. J. Evans, Z. Guralnik and I. Kirsch, *"Chiral symmetry breaking and pions in non-supersymmetric gauge / gravity duals,"* Phys. Rev. D **69** (2004) 066007 [arXiv:hep-th/0306018].

[78] R. Apreda, J. Erdmenger, N. Evans and Z. Guralnik, *"Strong coupling effective Higgs potential and a first order thermal phase transition from AdS/CFT duality,"* Phys. Rev. D **71** (2005) 126002 [arXiv:hep-th/0504151].

[79] T. Albash, V. G. Filev, C. V. Johnson and A. Kundu, *"A topology-changing phase transition and the dynamics of flavour,"* Phys. Rev. D **77** (2008) 066004 [arXiv:hep-th/0605088].

[80] D. Mateos, R. C. Myers and R. M. Thomson, *"Holographic phase transitions with fundamental matter,"* Phys. Rev. Lett. **97** (2006) 091601 [arXiv:hep-th/0605046].

[81] D. Mateos, R. C. Myers and R. M. Thomson, *"Thermodynamics of the brane,"* JHEP **0705**, 067 (2007) [arXiv:hep-th/0701132].

[82] S. Nakamura, *"Comments on Chemical Potentials in AdS/CFT,"* Prog. Theor. Phys. **119**, 839 (2008) [arXiv:0711.1601 [hep-th]].

[83] Y. Seo, J. P. Shock, S. J. Sin and D. Zoakos, *"Holographic Hadrons in a Confining Finite Density Medium,"* arXiv:0912.4013 [hep-th].

[84] P. de Forcrand and O. Philipsen, *"The chiral critical point of Nf=3 QCD at finite density to the order $(mu/T)^4$,"* JHEP **0811** (2008) 012 [arXiv:0808.1096 [hep-lat]].

[85] P. de Forcrand and O. Philipsen, *"The chiral critical line of $N_f = 2 + 1$ QCD at zero and non-zero baryon density,"* JHEP **0701** (2007) 077 [arXiv:hep-lat/0607017].

[86] J. Langelage and O. Philipsen, *"The deconfinement transition of finite density QCD with heavy quarks from strong coupling series,"* arXiv:0911.2577 [hep-lat].

[87] S. Kim, Ph. de Forcrand, S. Kratochvila and T. Takaishi, *"The 3-state Potts model as a heavy quark finite density laboratory,"* PoS **LAT2005** (2006) 166 [arXiv:hep-lat/0510069].

[88] E. D'Hoker and P. Kraus, *"Magnetic Brane Solutions in AdS,"* JHEP **0910**, 088 (2009) [arXiv:0908.3875 [hep-th]];

[89] E. D'Hoker and P. Kraus, *"Charged Magnetic Brane Solutions in AdS_5 and the fate of the third law of thermodynamics,"* JHEP **1003**, 095 (2010) [arXiv:0911.4518 [hep-th]];

[90] E. D'Hoker and P. Kraus, *"Holographic Metamagnetism, Quantum Criticality, and Crossover Behavior,"* JHEP **1005**, 083 (2010) [arXiv:1003.1302 [hep-th]].

[91] K. Jensen, A. Karch and E. G. Thompson, *"A Holographic Quantum Critical Point at Finite Magnetic Field and Finite Density,"* JHEP **05**(2010)015 arXiv:1002.2447 [hep-th].

[92] K. Jensen, A. Karch, D. T. Son and E. G. Thompson, *"Holographic Berezinskii-Kosterlitz-Thouless Transitions,"* Phys. Rev. Lett. **105**, 041601 (2010) arXiv:1002.3159 [hep-th].

[93] N. Iqbal, H. Liu, M. Mezei and Q. Si, *"Quantum phase transitions in holographic models of magnetism and superconductors,"* Phys. Rev. D **82**, 045002 (2010) arXiv:1003.0010 [hep-th].

[94] A. Karch and L. Randall, *"Open and closed string interpretation of SUSY CFT's on branes with boundaries,"* JHEP **0106** (2001) 063 [arXiv:hep-th/0105132]

[95] O. DeWolfe, D. Z. Freedman and H. Ooguri, *"Holography and defect conformal field theories,"* Phys. Rev. D **66** (2002) 025009 [arXiv:hep-th/0111135]

[96] J. Erdmenger, Z. Guralnik and I. Kirsch, *"Four-Dimensional Superconformal Theories with Interacting Boundaries or Defects,"* Phys. Rev. D **66** (2002) 025020 [arXiv:hep-th/0203020]

[97] R. C. Myers and M. C. Wapler, *"Transport Properties of Holographic Defects,"* JHEP **0812**, 115 (2008) [arXiv:0811.0480 [hep-th]]

[98] M. C. Wapler, *"Holographic Experiments on Defects,"* Int. J. Mod. Phys. A **25**, 4397 (2010) [arXiv:0909.1698 [hep-th]]

[99] M. C. Wapler, *"Thermodynamics of Holographic Defects,"* JHEP **1001**, 056 (2010) [arXiv:0911.2943 [hep-th]]

[100] M. C. Wapler, *"Massive Quantum Liquids from Holographic Angel's Trumpets,"* JHEP **1005**, 019 (2010) [arXiv:1002.0336 [hep-th]].

[101] V. L. Berezinskii, Zh. Eksp. Theo. Fiz **59**, 907 (1970);
J. M. Kosterlitz and D. J. Thouless, *"Ordering, metastability and phase transitions in two-dimensional systems,"* J. Phys. C C **6** (1973) 1181.

[102] D. B. Kaplan, J. W. Lee, D. T. Son and M. A. Stephanov, *"Conformality Lost,"* Phys. Rev. D **80**, 125005 (2009) [arXiv:0905.4752 [hep-th]].

[103] K. Y. Kim and J. Liao, *"On the Baryonic Density and Susceptibilities in a Holographic Model of QCD,"* Nucl. Phys. B **822**, 201 (2009) [arXiv:0906.2978 [hep-th]].

[104] K. Rajagopal, *"Mapping the QCD phase diagram,"* Nucl. Phys. A **661** (1999) 150 [arXiv:hep-ph/9908360].

[105] O. DeWolfe, S. S. Gubser and C. Rosen, *"A holographic critical point,"* Phys. Rev. D **83** (2011) 086005 [arXiv:1012.1864 [hep-th]].

[106] M. Kruczenski, D. Mateos, R. C. Myers and D. J. Winters, *"Towards a holographic dual of large N(c) QCD,"* JHEP **0405** (2004) 041 [arXiv:hep-th/0311270].

[107] K. Ghoroku and M. Yahiro, *"Chiral symmetry breaking driven by dilaton,"* Phys. Lett. B **604** (2004) 235 [arXiv:hep-th/0408040].

[108] R. Alvares, N. Evans, A. Gebauer and G. J. Weatherill, *"Holographic integral equations and walking technicolour,"* Phys. Rev. D **81** (2010) 025013 [arXiv:0910.3073 [hep-ph]].

[109] J. Erlich, E. Katz, D. T. Son and M. A. Stephanov, *"QCD and a holographic model of hadrons,"* Phys. Rev. Lett. **95**, 261602 (2005) [arXiv:hep-ph/0501128].

[110] L. Da Rold and A. Pomarol, *"Chiral symmetry breaking from five dimensional spaces,"* Nucl. Phys. B **721** (2005) 79 [arXiv:hep-ph/0501218].

[111] N. Evans, K. Jensen, and K.-Y. Kim, *Non Mean-Field Quantum Critical Points from Holography*, *Phys. Rev.* **D82** (2010) 105012, `arXiv:1008.1889`.

[112] N. Evans, A. Gebauer, and K.-Y. Kim, E, B, μ, T *Phase Structure of the D3/D7 Holographic Dual*, *JHEP* **05** (2011) 067, `arXiv:1103.5627`.

[113] N. Evans, K. Y. Kim and J. P. Shock, *"Chiral phase transitions and quantum critical points of the D3/D7(D5) system with mutually perpendicular E and B*

fields at finite temperature and density," JHEP **09** (2011) 021 arXiv:1107.5053 [hep-th].

[114] N. Evans, T. Kalaydzhyan, K. y. Kim and I. Kirsch, *"Non-equilibrium physics at a holographic chiral phase transition,"* JHEP **1101** (2011) 050 [arXiv:1011.2519 [hep-th]].

[115] D. E. Kharzeev and H. U. Yee, *"Chiral helix in AdS/CFT with flavor,"* Phys. Rev. D **84**, 125011 (2011) arXiv:1109.0533 [hep-th].

[116] B. Gwak, M. Kim, B.-H. Lee, Y. Seo, and S.-J. Sin, *"Holographic Instanton Liquid and chiral transition,"* Phys. Rev. D **86**, 026010 (2012) `arXiv:1203.4883`.

[117] K. Ghoroku, T. Sakaguchi, N. Uekusa and M. Yahiro, *"Flavor quark at high temperature from a holographic model,"* Phys. Rev. D **71** (2005) 106002 [arXiv:hep-th/0502088].

[118] B. Holdom, *"Raising the Sideways Scale,"* Phys. Rev. D **24** (1981) 1441.

[119] N. Evans, J. French and K. Y. Kim, *"Holography of a Composite Inflaton,"* JHEP **1011** (2010) 145 [arXiv:1009.5678 [hep-th]].

[120] F. Bigazzi, A. L. Cotrone, J. Mas, D. Mayerson and J. Tarrio, *"D3-D7 Quark-Gluon Plasmas at Finite Baryon Density,"* JHEP **1104**, 060 (2011) [arXiv:1101.3560 [hep-th]].

[121] S.-J. Rey and J.-T. Yee, *"Macroscopic strings as heavy quarks in large N gauge theory and anti-de Sitter supergravity ,"* *Eur.Phys.J.* **C22** (2001) 379–394 [arXiV:hep-th/9803001].

[122] J. M. Maldacena, *"Wilson loops in large N field theories ,"* *Phys.Rev.Lett.* **80** (1998) 4859–4862, [arXiV:hep-th/9803002].

[123] G. Policastro, D. Son, and A. Starinets, *"The Shear viscosity of strongly coupled N=4 supersymmetric Yang-Mills plasma,"* *Phys.Rev.Lett.* **87** (2001) 081601 [arXiV:hep-th/0104066].

[124] V. G. Filev and R. C. Raskov, *"Magnetic Catalysis of Chiral Symmetry Breaking. A Holographic Prospective, "* *Adv.High Energy Phys.* **2010** (2010) 473206 [arXiv:1010.0444[hep-th]].

[125] E. Witten, *"Baryons and branes in anti-de Sitter space"*, *JHEP* **9807** (1998) 006 [arXiV:hep-th/9805112].

[126] J. Callan, Curtis G., A. Guijosa, K. G. Savvidy, and O. Tafjord, *"Baryons and flux tubes in confining gauge theories from brane actions, "* *Nucl.Phys.* **B555** (1999) 183–200 [arXiV:hep-th/9902197].

[127] Y. Seo and S.-J. Sin, *"Baryon Mass in medium with Holographic QCD, "* *JHEP* **0804** (2008) 010 [arXiv:0802.0568[hep-ph]].

[128] Y. Kim, Y. Seo, I. J. Shin, and S.-J. Sin, *"Holographic meson mass in asymmetric dense matter, "* [arXiv:1108.2751[hep-ph]].

[129] K. Jo, M. Rho, Y. Seo, and S.-J. Sin, *"The Dropping of In-Medium Hadron Mass in Holographic QCD, "*, *JHEP* **1107** (2011) 008 [arXiv:1104.2362[hep-ph]].

[130] O. Bergman, G. Lifschytz, and M. Lippert, *"Holographic Nuclear Physics, "* *JHEP* **0711** (2007) 056 [arXiv:0708.0326[hep-th]].

[131] S. Aoki, K. Hashimoto, and N. Iizuka, *"Matrix Theory for Baryons: An Overview of Holographic QCD for Nuclear Physics, "* [arXiv:1203.5386[hep-th]].

[132] S.-J. Rey, S. Theisen, and J.-T. Yee, *"Wilson-Polyakov loop at finite temperature in large N gauge theory and anti-de Sitter supergravity"*, *Nucl.Phys.* **B527** (1998) 171–186 [arXiV:hep-th/9803135].

[133] A. Brandhuber, N. Itzhaki, J. Sonnenschein, and S. Yankielowicz, *"Wilson loops in the large N limit at finite temperature"*, *Phys.Lett.* **B434** (1998) 36–40 [arXiV:hep-th/9803137].

[134] D. Bak, A. Karch, and L. G. Yaffe, *"Debye screening in strongly coupled N=4 supersymmetric Yang-Mills plasma"*, *JHEP* **0708** (2007) 049, [arXiv:0705.0994[hep-th]].

[135] R. Alvares, N. Evans, and K.-Y. Kim, *"Holography of the Conformal Window, "* Phys.Rev. D**86** (2012) 026008 [arXiv:1204.2474[hep-ph]].

[136] I. Bredberg, C. Keeler, V. Lysov, and A. Strominger, *"Wilsonian Approach to Fluid/Gravity Duality"*, *JHEP* **1103** (2011) 141, [arXiv:1006.1902[hep-th]].

[137] D. Nickel and D. T. Son, *"Deconstructing holographic liquids, "* New J. Phys. **13** 075010 [arXiv:1009.3094[hep-th]].

[138] I. Heemskerk and J. Polchinski, *"Holographic and Wilsonian Renormalization Groups, " JHEPA,1106,031.2011* **1106** (2011) 031 [arXiv:1010.1264[hep-th]].

[139] T. Faulkner, H. Liu, and M. Rangamani, *"Integrating out geometry: Holographic Wilsonian RG and the membrane paradigm, "* JHEP **08** (2011) 051 [arXiv:1010.4036[hep-th].

[140] M. R. Douglas, L. Mazzucato, and S. S. Razamat, *"Holographic dual of free field theory, " Phys.Rev.* **D83** (2011) 071701 [arXiv:1011.4926[hep-th]].

[141] S.-J. Sin and Y. Zhou, *"Holographic Wilsonian RG Flow and Sliding Membrane Paradigm, " JHEP* **1105** (2011) 030 [arXiv:1102.4477[hep-th]]. .

[142] S.-S. Lee, *"Holographic description of quantum field theory, " Nucl.Phys.* **B832** (2010) 567–585 [arXiv:0912.5223].

[143] S.-S. Lee, *"Holographic description of large N gauge theory, " Nucl.Phys.* **B851** (2011) 143–160 [arXiv:1011.1474].

[144] E. T. Akhmedov, *"A Remark on the AdS / CFT correspondence and the renormalization group flow, " Phys.Lett.* **B442** (1998) 152–158, [arXiV: hep-th/9806217].

[145] E. T. Akhmedov, *"Notes on multitrace operators and holographic renormalization group, "* [arXiV:hep-th/0202055].

[146] J. de Boer, E. P. Verlinde, and H. L. Verlinde, *"On the holographic renormalization group, " JHEP* **0008** (2000) 003, [arXiV:hep-th/9912012].

[147] J. de Boer, *"The Holographic renormalization group, " Fortsch.Phys.* **49** (2001) 339–358 [arXiV:hep-th/0101026].

[148] A. Lewandowski, M. J. May, and R. Sundrum, *"Running with the radius in RS1, " Phys.Rev.* **D67** (2003) 024036 [arXiV:hep-th/0209050].

[149] A. Lewandowski, *"The Wilsonian renormalization group in Randall-Sundrum 1, " Phys.Rev.* **D71** (2005) 024006 [arXiV:hep-th/0409192].

[150] L. Susskind and E. Witten, *"The Holographic bound in anti-de Sitter space, "* [arXiV:hep-th/9805114].

[151] A. W. Peet and J. Polchinski, *"UV / IR relations in AdS dynamics, " Phys.Rev.* **D59** (1999) 065011, [arXiV:hep-th/9809022].

[152] N. Evans, T. R. Morris, and O. J. Rosten, *"Gauge invariant regularization in the AdS/CFT correspondence and ghost D-branes, " Phys.Lett.* **B635** (2006) 148–150 [arXiV:hep-th/0601114].

[153] A. Karch and A. O'Bannon, *"Metallic AdS/CFT, "*, *JHEP* **09** (2007) 024, `arXiv:0705.3870`.

[154] S. R. Coleman and E. J. Weinberg, *"Radiative Corrections as the Origin of Spontaneous Symmetry Breaking, " Phys.Rev.* **D7** (1973) 1888–1910.

[155] A. O'Bannon, *"Hall Conductivity of Flavor Fields from AdS/CFT, " Phys. Rev.* **D76** (2007) 086007 [arXiv:0708.1994[hep-th]].

[156] K.-Y. Kim, J. P. Shock, and J. Tarrio, *"The open string membrane paradigm with external electromagnetic fields, "* [arXiv:1103.4581[hep-th]].

[157] T. Albash, V. G. Filev, C. V. Johnson, and A. Kundu, *"Quarks in an External Electric Field in Finite Temperature Large N Gauge Theory, " JHEP* **08** (2008) 092 [arXiv:0709.1554[hep-th]].

[158] S. S. Gubser, *"Curvature singularities: The Good, the bad, and the naked, " Adv.Theor.Math.Phys.* **4** (2000) 679–745 [hep-th/0002160].